

The University of Nottingham

**Evaluation of AChE inhibitors and dual AChE/GSK3- β
inhibitor as Alzheimer's disease treatment**

Giuseppe Uras, MSc
(Experimental and Applied Biology)

Thesis submitted to the University of Nottingham for the degree of
Doctor of Philosophy

Publications

Discovery of Novel Tacrine-Pyrimidone Hybrids as Potent Dual AChE/GSK-3 β Inhibitors for the Treatment of Alzheimer's disease – Submitted to Journal of Medicinal Chemistry (2020)

Pengfei Zhang & Giuseppe Uras, Hong Yao, Shengtao Xu, Shuai Qin, Qi Gong, Haiyan Zhang, Zheyang Zhu, and Jinyi Xu,

Therapeutic potential of a newly synthesized AChE-I in a Drosophila Melanogaster model of Alzheimer's disease – Submitted Neurobiology of Disease (2020)

Giuseppe Uras, Alessia Manca, Marco Bo, Pengfei Zhang, Zsuzsa Markus, Natalie Mack, Stephanie Allen, Shengtao Xu, Jinyi Xu, Marios Georgiou and Zheyang Zhu

Conferences

Podium Presentation - 10th APS PharmSci Conference, Greenwich London, UK (2019)

Newly synthesized AChE inhibitor reduces amyloid aggregation in Drosophila Alzheimer's Disease model.

Uras G., Manca A., Georgiou M., Allen S., Zhu Z.

Podium presentation - 39° SISC congress, Sassari, Italy (2019)

Testing the effectiveness of Alzheimer's Disease current therapies on Drosophila Melanogaster transgenic model

Manca A. & Uras G., Pantaleo A., Zhu Z.

[European Journal of Histochemistry 2019; 63:s3]

Poster presentation - 92° SIBS congress, Sassari, Italy (2019)

Testing the effectiveness of a new promising acetylcholinesterase inhibitors for Alzheimer's Disease treatment.

Manca A. & Uras G., Georgiou M., Allen S., Panataleo A., Zhu Z.

[Journal of Biological Research 2019; 92:s2]

Seminar invited speaker – University of Sassari, Sassari, Italy (2018)

Alzheimer's disease: current models, therapies and future perspective.

Uras G.

Author's Declaration

The research work presented in this Thesis entitled “*Evaluation of AChE inhibitors, and dual AChE/GSK3- β inhibitor as Alzheimer's disease treatment*” has been entirely performed by myself unless otherwise cited and acknowledged. I hereby declare that this work is original and has not been submitted in part, or full, for any other degree or diploma at any other University or Institution. All contributions of others are indicated in references to the literature.

Acknowledgments

I wish to thank my supervisor Dr. Zheyang Zhu for giving me the opportunity to work on this amazing project. Her guidance and constant support have facilitated my period in the lab, and improved me both personally and professionally. You have always been available for me, and supported through difficult times. I will always be grateful that I had the chance to work under your supervision.

I want to thank my other supervisors Prof. Stephanie Allen and Dr. Marios Georgiou for the patience in guiding me through this research project. Their critical thinking and suggestions led me to obtain better results and to improve as a scientist. Thank you for being patience with me when results were not good and for supporting me.

I would like to thank Prof. Jinyi Xu and Dr. Pengfei Zhang, from CPU, for the collaboration established and the compound provided. The constant updates and feedbacks we shared improved the quality of our work together. Thank you.

A huge thank you goes to my colleagues Alexandra, Zsuzsa, Robert, and Alessia. No words can describe what you have done for me. I was alone in Nottingham, with no friends and far from home, but I had you all around me and that was more than enough to forget about the rest. Thank you so much for being my friends, this is an honour for me.

A big thank you to Xinuo, it is not easy to make work together between a biologist and a chemist, but we did a great job and achieved great results!! Thank you so much for everything, always friends.

I want to thank my family for supporting me through this incredible journey. A special mention to my friends in Sardinia, for keeping me up despite being distant, you are my brothers.

Lastly, I want to thank Giorgia. I met you mid-way of this journey, and since then everything has changed. Thank you for making everyday special.

Contents

<i>Publications</i>	i
<i>Conferences</i>	i
<i>Author's Declaration</i>	ii
<i>Acknowledgments</i>	ii
<i>List of figures</i>	6
<i>List of Tables</i>	4
<i>Abbreviations</i>	4
<i>Abstract</i>	6
1 Introduction	7
1.1 History of AD	8
1.2 Alzheimer's disease fundamental features	9
1.2.1 Amyloid Precursor Protein.....	9
1.2.2 Amyloid plaques	10
1.2.3 Tau protein	12
1.2.4 Neurofibrillary tangles	13
1.2.5 Cholinergic network.....	15
1.2.6 Cholinergic system in AD pathogenesis	16
1.2.7 Neuroinflammation in AD	18
1.2.8 NMDA receptors and excitotoxicity	19
1.3 Models to study AD	20
1.3.1 <i>Drosophila melanogaster</i> as model of AD	21

1.3.2	Cell culture models of AD	23
1.3.3	Mouse models of AD	24
1.4	AD therapies	26
1.4.1	AD therapy selection.....	27
1.4.2	AChE inhibitors	27
1.4.3	NMDAR antagonist	28
1.4.4	Future perspectives.....	29
1.4.5	Novel compounds	31
1.5	Thesis aim and hypothesis.....	33
2	Materials and methods	34
2.1	Reagents	34
2.2	<i>Drosophila melanogaster</i> strains and cross schemes	34
2.3	<i>Drosophila</i> food preparation	35
2.4	Rough Eye Phenotype Experiment.....	36
2.5	Lifespan Assay	36
2.6	Climbing assay	37
2.7	<i>Drosophila melanogaster</i> brain immunostaining.....	37
2.8	Confocal microscopy.....	38
2.9	Images analysis.....	38
2.10	Western Blot	39
2.11	Quantification of AChE-induced A β 42 aggregation	40
2.12	SH-SY5Y culture and neuronal differentiation	41

2.13	Glyceraldehyde (GA) induced Tau hyperphosphorylation.....	42
2.14	AChE activity assay (Ellman’s method).....	42
2.15	Cell viability assay.....	42
2.16	pTAU quantification.....	43
2.17	Immunostaining cell culture.....	43
2.18	Morphological analysis of SH-SY5Y derived neurons.....	44
2.19	Data analysis.....	44
3	Drosophila model development and characterisation.....	46
3.1	Introduction.....	46
3.1.1	Experimental aim.....	48
3.1.2	Experimental procedures.....	48
3.2	Results.....	49
3.2.1	Expression of human Tau and mutant APP protein lead to reduced lifespan and locomotive defects.....	49
3.2.2	Ommatidia neurodegeneration in A β_{arc} and Tau transgenic flies.....	52
3.2.3	Characterisation of transgenic A β_{arc} flies and Tau flies brain.....	54
3.3	Discussion.....	56
4	XJP-1 treatment ameliorates amyloid-induced symptomatology in Aβ_{arc} flies	58
4.1	Introduction.....	58
4.1.1	Experimental aim.....	59
4.1.2	Experimental procedures.....	60

4.2	Results	60
4.2.1	XJP-1 treatment improves life expectancy in A β_{arc} flies	60
4.2.2	XJP-1 treatment improves locomotive functions in A β_{arc} flies.....	63
4.2.3	XJP-1 reduces the number of amyloid plaques in the brain.....	65
4.2.4	XJP-1 reduces amyloid aggregation via AChE inhibition	72
4.3	Discussion	73
5	AChE inhibition by XJP-1 treatment does not result in reduction of Tau phosphorylation in <i>Drosophila melanogaster</i> AD model	77
5.1	Introduction	77
5.1.1	Experimental aim	78
5.1.2	Experimental procedures.....	78
5.2	Results	80
5.2.1	XJP-1 treatment improves Tau flies lifespan, but does not result in improved locomotive functions	80
5.2.2	Tau hyperphosphorylation in Tau <i>Drosophila</i> cannot be prevented, or reduced, by XJP-1 treatment.....	83
5.2.3	XJP-1 treatment does not rescue REP induced by human Tau expression and hyperphosphorylation.....	86
5.3	Discussion	88
6	Development and characterization of neuron-like model of AD and screening of novel AChE and dual AChE/GSK3-β inhibitors	90
6.1	Introduction	90

6.1.1	Experimental aim	92
6.1.2	Experimental procedures.....	92
6.2	Results	94
6.2.1	GA treatment induces abnormal Tau phosphorylation and axon degeneration in SH-SY5Y-differentiated neurons	94
6.2.2	Novel compounds inhibit AChE enzyme activity in SH-SY5Y differentiated neurons.....	97
6.2.3	AChE inhibition prevents GA-induced Tau phosphorylation on S396, but not on S199.	100
6.2.4	Dual AChE/GSK3- β inhibitor 16g modulates Tau phosphorylation on S199 and S396	105
6.2.5	Efficacy of AChE inhibitors in preventing hyperphosphorylated Tau-induced neurodegeneration	110
6.2.6	Treatment with compound 16g prevents Tau-induced neurodegeneration 113	
6.2.7	Increased cell viability following novel AChE inhibitor treatment...	116
6.2.8	Compound 16g prevents neuronal cell death.....	119
6.2.9	Novel AChE inhibitors and dual AChE/GSK3- β inhibitor reduce AChE-induced amyloid aggregation rate	122
6.3	Discussion	123
7	Final Discussion	126
7.1	Inhibition of AChE enzyme by XJP-1 results in amelioration of amyloid-induced symptomatology	128

7.2	Inhibition of AChE enzyme does not result in a clear anti-Tau effect.....	131
7.3	Dual inhibition of GSK3- β and AChE enzymes modulates Tau phosphorylation in neuron-like model of AD and improves cognitive functions in mice	134
8	Final Conclusions	136
9	Limitations and future perspectives	137
10	Supplementary figures	140
	Bibliography.....	144

List of figures

Figure 1.	Novel compounds structure	33
Figure 2.	Transgenic AD <i>Drosophila</i> lifespan.....	50
Figure 3.	Evaluation of different <i>Drosophila</i> AD genotypes locomotive functions ..	51
Figure 4.	REP development by expressing different AD transgene	53
Figure 5.	Effects of Tau and A β_{arc} -peptides expression on CNS.....	55
Figure 6.	A β_{arc} flies lifespan under different treatment.....	62
Figure 8.	Amelioration of amyloid spots in A β_{arc} flies CNS after 10 days of treatment.	67
Figure 9.	Representative images of cholinergic neurons network in <i>Drosophila Melanogaster</i> brain obtained from the Virtual Fly Observatory	69
Figure 10.	Amelioration of amyloid spots in A β_{arc} flies CNS after 20 days of treatment.....	71
Figure 11.	Reduction of AChE-induced A β -peptide aggregation rates in the presence of AChE Inhibitors.....	73

Figure 12. Tau flies lifespan under different treatment.....	81
Figure 13. Treated Tau flies climbing assay	82
Figure 14. CNS analysis of Tau hyperphosphorylation after 10 days of treatment...	84
Figure 15. CNS analysis of Tau hyperphosphorylation after 20 days of treatment...	85
Figure 16. Treated REP images	87
Figure 17. Initial characterization of novel AD model	95
Figure 18. AChE inhibition by novel compounds at different concentration in 0.7mM GA exposed SH-SY5Y-derived neurons	98
Figure 19. AChE inhibition by novel compounds at different concentration in 1mM GA exposed SH-SY5Y-derived neurons	99
Figure 20. Tau S199 phosphorylation levels in 0.7mM GA exposed neurons after treatment with novel AChE inhibitors	101
Figure 21. Tau S199 phosphorylation levels in 1mM GA exposed neurons after treatment with novel AChE inhibitors	102
Figure 22. Tau S396 phosphorylation levels in 0.7mM GA exposed neurons after treatment with novel AChE inhibitors	103
Figure 23. Tau S396 phosphorylation levels in 1mM GA exposed neurons after treatment with novel AChE inhibitors	104
Figure 24. Reduction of Tau S199 phosphorylation after 16g treatment in 0.7mM GA exposed neurons	106
Figure 25. Reduction of Tau S199 phosphorylation after 16g treatment in 1mM GA exposed neurons	107
Figure 26. Reduction of Tau S396 phosphorylation after 16g treatment in 0.7mM GA exposed neurons	108

Figure 27. Reduction of Tau S396 phosphorylation after 16g treatment in 1mM GA exposed neurons	109
Figure 28. Morphological analysis of 0.7mM GA exposed neurons after different AChE inhibitors treatment	111
Figure 29. Morphological analysis of 1mM GA exposed neurons after different AChE inhibitors treatment	112
Figure 30. Dose-dependent amelioration of neurite morphology by compound 16g in 0.7mM GA exposed neurons	114
Figure 31. Amelioration of neurite morphology by compound 16g in 1mM GA exposed neurons	115
Figure 32. Cell viability quantification of 0.7mM GA exposed SH-SY5Y differentiated neurons after treatment with different AChE inhibitor	117
Figure 33. Cell viability quantification of 1mM GA exposed SH-SY5Y differentiated neurons after treatment with different AChE inhibitors	118
Figure 34. Prevention of 0.7mM GA-induced cell death by compound 16g treatment	120
Figure 35. Prevention of 1mM GA-induced cell death by compound 16g treatment	121
Figure 36. Reduction of amyloid peptides aggregation rate by inhibition of AChE enzyme	123
Supplementary figure 1. Dosage screening.....	140
Supplementary figure 2. Comparisons between combined therapies and monotherapies on A β_{arc} flies.....	141
Supplementary figure 3. Amyloid peptides quantity in A β_{arc} flies' heads	142
Supplementary figure 4. Effects of compound 16g on scopolamine treated mice...	143

List of Tables

Table 1. <i>Drosophila melanogaster</i> strains.....	24
Table2. Cell culture media for SH-SY5Y neuronal differentiation.....	30
Table3. UAS-Gal4 system.....	47

Abbreviations

AChE – Acetylcholinesterase

AD – Alzheimer’s disease

APP – Amyloid precursor protein

A β -peptide – Amyloid- β -peptide

ASC specks - Apoptosis-associated speck-like protein containing CARD

BACE1 - β -site amyloid precursor protein cleaving enzyme 1

BBB – Blood brain barrier

BDNF - brain derived neurotrophic factor

BuChE – butyrylcholinesterase

CAS – Catalytic active site

CNS – Central nervous system

DUB – Deubiquitinase

EOAD – Early onset Alzheimer’ disease

FDA – Food and Drug Administration

GSK3- β - Glycogen synthase kinase 3 beta

GA - Glyceraldehyde

IC₅₀ - Half-maximal inhibitory concentration

LTP – Long term potentiation

MAP – Microtubule associated protein

MTT - Methylthiazolyldiphenyl-tetrazolium bromide

NBM – Nucleus basalis of Meynert

NGS – Normal goat serum

NMDAR - N-methyl-D-aspartate receptor

NFTs – Neurofibrillary tangles

PAS – Peripheral anionic site

PFA - Paraformaldehyde

PBS - Phosphate-buffered saline

PBS-T – PBS-Tween20

PCD – Protein-conformational disease

PHF – Paired helical filaments

RA – Retinoic acid

ROS – Reactive oxygen species

RT – Room temperature

sAPP α – Soluble ectodomain APP

SF – Straight filaments

ThT - Thioflavin T

TGN – Trans Golgi Network

UAS – Upstream activating sequence

Abstract

Since the first patient affected by Alzheimer's disease was reported in 1907, it became the worldwide leading cause of dementia. The disease is characterised by an initial accumulation of amyloid plaques, neurofibrillary tangles, along with cholinergic markers depletion. The currently available therapies for Alzheimer's disease provide an amelioration of the cognitive symptomatology for a limited period, without altering the disease progression and outcome. Thus, a number of research projects are currently underway in order to find a therapy able to modify the disease course. For this, we evaluated the efficacy of different acetylcholinesterase inhibitors (XJP-1, SAD-2, SAD-6, and FAD), along with a dual acetylcholinesterase/Glycogen synthase kinase 3 β (16g), as potential Alzheimer's disease treatment.

To assess the efficacy of novel compounds we exploited two different Alzheimer's models: *Drosophila melanogaster*, expressing either toxic amyloid peptides or hyperphosphorylated Tau protein, and differentiated SH-SY5Y cells treated with glyceraldehyde to induce Tau abnormal phosphorylation.

The initial investigation on *Drosophila* Alzheimer's models, carried out on XJP-1 only, showed contradictory results, proving beneficial effects, on both symptomatology and protein deposition, in fruit flies expressing amyloid peptides, but not in those flies presenting an hyperphosphorylated Tau protein.

Subsequent testing of the novel cholinesterase inhibitors on differentiated SH-SY5Y model presenting an hyperphosphorylated Tau protein confirmed a not homogenous response to this class of compounds, in any of the assessed parameters, despite a similar level of inhibition of acetylcholinesterase enzyme.

Conversely, inhibition of both AChE and GSK3- β enzymes resulted in an overall improvement of the GA induced defects. In particular, phosphorylation levels on

residues S199 and S396 of Tau protein were reduced following 16g administration. Other than that, 16g administration rescued the neuronal-like morphology and prevented neuronal cell death in this particular model, which are fundamental parameters when treating Alzheimer's disease. In summary, this work shows that the limited beneficial effects of cholinesterase inhibition for Alzheimer's treatment, mainly on the amyloid-derived pathology, can be enhanced by dual-inhibition of both AChE and GSK3 β , which resulted in a significant improvement of the hyperphosphorylated Tau-induced defects along with reduction of amyloid peptides aggregation.

1 Introduction

Alzheimer's disease (AD) is a protein-conformational disease (PCD), characterised by a severe progressive neurodegeneration, accumulation of amyloid plaques, and presence of neurofibrillary tangles (NFTs) (Tiwari *et al.* 2019).

AD is currently recognized as the worldwide leading cause of dementia in elderly people, with about 6 million patients reported in the United States, with this figures expected to be at least doubled by 2050 (Association 2019).

The disease is characterised by an array of cognitive symptoms, such as memory impairment, learning disabilities, behavioural changes, which lead to a progressive loss of independency in routinely tasks by the affected patients (Merriam *et al.* 1988). In addition to this, the poor efficacy of the currently available to therapies, results in increased financial costs, and social issues, for the patients' families (El-Hayek *et al.* 2019).

A missing triggering mechanism, the lack of an early diagnosis biomarker, along with an effective therapy yet to be discovered, turned AD into the fifth cause of death (Heron 2019). Thus, the development of an AD therapy, able to modify the course of the disease is a crucial step to improve patients' life, and the socioeconomic burden experienced by their families and carers.

1.1 History of AD

AD was firstly described by Alois Alzheimer in 1907, in Munich, after an autopsy on a 55-year-old woman named Auguste Deter, who died after a progressive cognitive disorder. Alzheimer was able to highlight the presence of two different pathologies in the woman's brain: abnormal intercellular aggregates and the presence of miliary foci surrounded by a special substance in the cortex (Alzheimer 1907; Stelzmann *et al.* 1995). The special substance was later characterized in 1984 by Glenner and Wong to be a 4.2kDa peptide formed of 40-42 amino acids (Glenner *et al.* 1984). They also speculated that this peptide was originated from the cleavage of a longer precursor, which was then identified in 1987, and subsequently named Amyloid Precursor Protein (APP), while their peptide is now known as amyloid- β peptide ($A\beta$ peptide) (Kang *et al.* 1987).

On the other hand, the intercellular aggregates were later shown to be formed of hyperphosphorylated and shorter forms of the microtubule associated protein (MAP) Tau (Goedert *et al.* 1988).

Through the years, a number of different AD triggering mechanisms have been suggested, but none of them was clearly demonstrated. However, familial forms, with an early onset of Alzheimer's disease (EOAD), are characterised by the presence of different mutations in crucial genes. Genetic screenings have identified a number of

mutation in genes, such as *APP*, *PSEN1*, and *PSEN2*. Patients with an EOAD, present a clear pathogenic mechanisms, often derived by the accumulation of A β peptides, as it happens in cases presenting the Arctic mutation of the APP gene. The latter is a substitution of the glutamate on residue 693 with a glycine, which in turn leads to the formation of toxic 42aa long A β peptides (Kamino *et al.* 1992).

Despite EOAD have a clear etiopathogenesis of AD, they account for only 1% of the total patients. Thus, the vast majority of patients are affected by a late-onset Alzheimer's disease (LOAD), which main risk factor is aging (Sala Frigerio *et al.* 2019). However, several causative agents have been proposed, such as amyloid cascade, NFTs formation, and the cholinergic hypothesis.

1.2 Alzheimer's disease fundamental features

1.2.1 Amyloid Precursor Protein

APP is a single pass transmembrane glycoprotein with a large extracellular domain, and it plays a role in cell motility, neurite growth and cell survival (Oh *et al.* 2009). In Neurons APP is found in the axon and somatodentric areas, and its functions are implicated in multiple pathways. Its role in cell signalling it can be divided into two categories: interactions with APP family members or interactions with other receptors (Müller *et al.* 2017). In the first scenario two APP proteins from two neurons interact together (trans-dimer), they promote synaptogenesis, and synapsis stability (Baumkötter *et al.* 2012). When two APP of same cell form a dimer (cis-dimer) they promote APP processing. When a sAPP α interact with an APP in the membrane, they promote cell survival and neuroprotection (Isbert *et al.* 2012). In interaction with other receptors, APP binds to protein such as Death receptor 6 (DR6) it triggers neuronal outgrowth (trans-signalling).

APP can also have a receptor-like role in multiple pathways. In neurite outgrowth, membrane APP co-localize with FE65, which in turn activates RAC1. This enzyme is able to regulate actin dynamics and, therefore, drive morphological changes (Müller *et al.* 2017).

1.2.2 Amyloid plaques

The amyloid cascade hypothesis gives to amyloid plaques deposition a central role in AD pathogenesis (Selkoe 1991).

It is during the APP processing where the A β peptides formation takes place. However, APP proteolysis can follow multiple different pathways and not all of them lead to the production of A β peptides. The most important steps of APP proteolysis occur at the cell surface and in the Trans-Golgi-Network (TGN). In a process mediated by clathrin-associated vesicles, APP can be transported from the TGN either to the cell surface or to an endosomal compartment. On the cell surface APP can undergo to a series of cleavages, mediated by α -secretase first, and γ -secretase then, which do not generate β amyloid peptides, but generates soluble ectodomain APP α (sAPP α) instead (also known as non-amyloidogenic pathway) (O'Brien *et al.* 2011). Conversely, in the amyloidogenic pathway APP from the TGN can be directed to an endosomal compartment containing the β -site amyloid precursor protein cleaving enzyme 1 (BACE1, also known as β -secretase). The latter cleaves APP, between +1 and +11, releasing the sAPP β ectodomain, while the APP C-terminal fragment becomes substrate of the endosomal γ -secretase, which cleaves it in a number of sites from +40 to +44, generating β -peptides of different length, with A β -40 and A β -42 being the most commonly produced (Nalivaeva *et al.* 2013).

The lack of sAPP α , which promotes neurite growth and neurite plasticity, can result in toxic effect, playing a role in AD pathogenesis as well (Gralle *et al.* 2009).

However, the accumulation of A β peptides exert the most toxic effect in AD pathogenesis. In particular, the A β peptides aggregates have the most cytotoxic effect, which results in the activation of oxidative stress pathway, aberrant activation of kinases, most likely resulting in neuronal cell-death (Leong *et al.* 2020).

A β peptides increase the expression of DKK1, and LRP6 inhibitor, therefore impairing the Wnt-signalling and further shifting the APP processing towards the amyloidogenic pathway, and establishing a pathological positive-feedback loop (Norwitz *et al.* 2019). Moreover, GSK3 β also phosphorylates Tau protein on multiple residues, causing Tau dissociation from the microtubules, causing cytoskeletal defects, impaired axonal transport, and aggregation of the protein Tau into NFTs, which are known to be neurotoxic (Llorens-Martín *et al.* 2014).

In addition to this, mutation in APP protein, such as the Arctic mutation, result in a higher aggregation rate of A β monomers, into aggregates first, in A β protofibrils then, and finally into amyloid plaques (Johansson *et al.* 2006). Furthermore, A β protofibrils have proven to be synaptotoxic, therefore damaging the neuronal connectivity (O'Nuallain *et al.* 2010).

According to the amyloid hypothesis, the accumulation of A β peptides results in an improper activation of kinases, such as Glycogen synthase kinase 3 beta (GSK3- β), which then increase the phosphorylation levels of the Tau protein, ultimately resulting in the formation of NFTs, the other fundamental hallmark of AD (Hardy *et al.* 1992; Götz *et al.* 2001).

1.2.3 Tau protein

Tau is a microtubule-associated protein (MAP) that exists in 6 different isoforms in the human brain which are all generated from alternative splicing of the same pre-mRNA (Himmler *et al.* 1989; Goedert *et al.* 1989).

Each of the six isoforms differs in the number of microtubule binding sites at the carboxyl terminal half (three or four sites named 3R and 4R respectively) and in the number of amino terminal inserts: one (1N), two (2N) and zero (0N). As a result, the alternative splicing generates 3 different forms of 3R Taus (0N3R, 1N3R and 2N3R) and 3 different forms of 4R Taus (0N4R, 1N4R and 2N4R) with the isoform 2N4R being the largest in size in human brain (Götz *et al.* 2019).

The distribution of different Tau isoform is developmentally controlled, with Tau isoforms -3R and -4R having a 1:1 ratio in adults' neurons (Götz *et al.* 2019).

Tau functions are multiple, from stabilization of the microtubule architecture, to axonal transport, neuronal polarity, and axon stability (Ittner *et al.* 2011; Dubey *et al.* 2008; Goedert *et al.* 1990).

In the neurons Tau can be either associated to the microtubule or to the membrane. Phosphorylated Tau is mainly present in the somatodendritic area, whilst dephosphorylated Tau is mainly present in the axon terminal (Avila *et al.* 2004). Tau main function is tubuline stabilization in microtubule architecture. It also promotes neurite outgrowth, as seen in non-neuronal cells where its ectopic expression resulted in the formation of long cytoplasmatic extension (Weingarten *et al.* 1975). In addition to this, it is proposed a role for Tau in axonal transport since its microtubule binding domain overlaps with the molecular motor kinesin (Combs *et al.* 2019).

Tau protein also play a role in synapsis stabilization and long term potentiation (LTP). Tau protein is translocated from the dendritic shaft to the synaptic compartment, upon

synapsis activation. At the same time, kinase Fyn, in the synaptic compartment, phosphorylate NMDAR to facilitate NMADR and PSD-95 interaction, which is crucial for a proper LTP (Frاندemiche *et al.* 2014). The de-association of the Tau/Fyn/PSD-95/NMDAR complex is equally important to maintain proper stabilization of NMDAR and correct LTP, which is disrupted in AD pathology (Marttinen *et al.* 2018).

1.2.4 Neurofibrillary tangles

NFTs are found in the neuronal cytoplasm of AD patients, and are composed of abnormally phosphorylated Tau protein. In addition to this, Tau protein can be subject to a number of different post-translational modifications, with the majority of them having a physiological function. However, abnormal phosphorylation of Tau protein can results in a loss of affinity toward tubulin, resulting in a jeopardized microtubule architecture (Martin *et al.* 2011).

A total of 85 residues can be subject of phosphorylation on Tau isoform 2N4R, resulting in either physiological, or pathological, effects (Tapia-Rojas *et al.* 2019). In particular, Serine (S) 199 and S396 residues, were found to be hyperphosphorylated in AD mice models (Foidl *et al.* 2018). Whilst, Threonine (T) 205 phosphorylation was found to have protective effects, against A β peptides-induced toxicity (Ittner *et al.* 2016).

Tau hyperphosphorylation is the result of the aberrant activation of either kinases, or phosphatases enzymes. One of the most studied kinase, responsible of phosphorylation on Tau protein at multiple residues, is GSK3- β .

GSK3- β is ubiquitously expressed in the central nervous system (CNS), and is activated by a number of different pathways, which are often linked to AD (Beaulieu

2012; Chu *et al.* 2017; Hernandez *et al.* 2013; Hooper *et al.* 2008; Li, Lv, *et al.* 2012b). Moreover, phosphorylation performed by GSK3- β on Tau results in a loss of affinity to microtubules and promotion of Tau self-aggregation (Jackson *et al.* 2002; Hernández *et al.* 2010).

In AD, as well as in other tauopathies, the aberrant phosphorylation process that occurs on Tau triggers its assembly in paired helical filaments (PHF) and straight filaments (SF) which leads to the development of NFTs (Farias *et al.* 2011).

AD is considered a secondary tauopathy, due to the contemporaneous presence of NFTs and amyloid plaques, and it is well known the strict link between these two fundamental hallmarks of AD (Götz *et al.* 2019).

Studies in mice have demonstrated that, A β increases the NFTs presence in the surrounding areas of the brain. Moreover, it was shown that hyperphosphorylated Tau is required to trigger amyloid toxicity in vivo, with prevention of cognitive defects, neuronal death, synaptotoxicity, along with reduction of mortality, in Tau knockout mice despite the presence of amyloid plaques (Roberson *et al.* 2007; Leroy *et al.* 2012). Tau phosphorylation is a major issue when treating AD, the lack of a clear triggering mechanism, and the multiple toxic effect because of Tau aberrant phosphorylation make this challenge even more difficult. Evidence about the involvement of the cholinergic network in Tau phosphorylation, along with beneficial effects of the cholinergic replacement therapy, were not confirmed in patients, leaving space for an unmet clinical target (Hempel *et al.* 2018; Noh *et al.* 2009; Yoshiyama *et al.* 2010; Tayeb *et al.* 2012).

1.2.5 Cholinergic network

The cholinergic network is well known to play a role in cognitive functions, forming those crucial connections implicated in the memory and learning abilities (Hampel *et al.* 2018). The number of different cholinergic pathways mainly depends on the type of acetylcholine receptor expressed by the examined neuron. In the human brain, acetylcholine binds to two different categories of receptor: nicotinic or muscarinic.

The nicotinic receptors are an ion channel heteropentamer, composed of two alpha subunit, one delta, one gamma and one beta subunit. The receptor structure can be found in two status, closed or open, and the shift from a closed status to an open status depends on the binding of acetylcholine (or other agonists)(Albuquerque *et al.* 2009). In addition to this, the composition of the nicotinic receptor is complicated by the presence of different types of alpha subunits, known as alpha-like, which further differentiate the properties of the nicotinic receptor (Albuquerque *et al.* 2009).

The stoichiometry of the different subunits characterize the receptor subtypes. The $\alpha 7$ nicotinic receptor can be activated by both acetylcholine and choline, and it is permeable to both Na^+ and Ca^{2+} ions. Conversely, the $\alpha 2\beta 4$ and $\alpha 3\beta 4$ receptors are only activated by acetylcholine, and are only permeable to Na^+ . This differences in permeability and ligand affinity confer the various receptor subtypes the ability, or not, to generate action potential by themselves, as it happens for the $\alpha 2\beta 4$ and $\alpha 3\beta 4$ receptors, without needing the activation of other receptors (i.e. NMDA receptors) (Khiroug *et al.* 2002). The location of the nicotinic receptor further influence their function in the human brain. Pre-terminal $\alpha 2\beta 4$ and $\alpha 3\beta 4$ receptors located in the CA1 interneurons in the hippocampus, one of the most affected brain areas in AD, regulate GABA release and, therefore, inhibitory signalling toward the postsynaptic neurons. The presence of $\alpha 4\beta 2$ in myelinated axons has been shown to modulate axon

excitability and LTP. $\alpha 7$ nicotinic receptor found in the somatodendritic area of neurons are responsible of Ca^{2+} currents, which is required for neuron desensitization, especially in hippocampal GABA neurons (Albuquerque *et al.* 2009).

Differently from the nicotinic receptors, the muscarinic receptors is a class of G-coupled receptors. Five different subtypes of this class of Ach receptors exists, M1-M5, with the M1 making up 60-90% in the human brain. This subtype is of peculiar important as upon Ach binding, it activates the PKC, which in turn phosphorylates GSK3- β , therefore inactivating it, preventing potential Tau phosphorylation (Jiang *et al.* 2014) .

1.2.6 Cholinergic system in AD pathogenesis

The mechanisms underlying AD pathogenesis are multiple, and the connection among them not yet fully understood. These include amyloid deposition, NFTs, neuroinflammation, insulin resistance, and depletion of cholinergic markers accompanied by a loss of cholinergic neurons.

In particular, the cholinergic system attracted the attention after multiple reports regarding its involvement in cognitive networks, and the severe neurodegeneration of cholinergic neurons during AD progression (Whitehouse *et al.* 1981). Despite the cholinergic hypothesis, which place the cholinergic lesion as central triggering mechanism, is not fully demonstrated and accepted, the involvement of the cholinergic network on multiple pathways involved in AD progression, and symptoms exacerbation is clear. The cholinergic depletion seen in AD patients is typically pre-synaptic, with the axons of the neurons projecting from the Nucleus basalis of Meynert (NBM) to the cortex undergoing a severe neurodegeneration (Hampel *et al.* 2018). In addition to this, the post-synaptic neurons present changes in acetylcholine receptors

during AD progression, with either muscarinic and nicotinic receptors being less expressed or dysfunctional (Schröder *et al.* 1991; Jiang *et al.* 2014b). This is of great relevance, since different subtypes of acetylcholine receptors can have a role in AD pathogenic pathways. In particular, $\alpha 7$ nicotinic receptor activation result in a downregulation of GSK3- β enzyme, which is responsible of Tau abnormal phosphorylation and shifting APP processing towards the amyloidogenic pathway (Beaulieu 2012) (Hooper *et al.* 2008; Chu *et al.* 2017). Moreover, activation of $\alpha 7$ receptor, result in a reduced neuroinflammation, which plays an important role in neuronal damage during AD (Kalkman *et al.* 2016).

Nicotinic $\alpha 2\beta 4$, the major component of nicotinic receptors, is also severely depleted in AD brain. This is of particular relevance given its function in GABA release, which suggests a possible role for cholinergic depletion in excitotoxicity observed in AD brains (Albuquerque *et al.* 2009).

In addition to this, activation of muscarinic receptors were reported to shift the APP processing towards the non-amyloidogenic pathway (Cisse *et al.* 2011; Welt *et al.* 2015). Activation of M1 muscarinic receptor inhibits GSK3- β via PKC pathway. Depletion of ACh, as observed in AD patients results in reduced activation of M1 receptor, and subsequent over-activation of GSK3- β , which not only phosphorylates Tau protein, but also shift APP process towards amyloidogenic cleavage by phosphorylating APP protein. Moreover, activation of M1 receptors, stabilizes beta-catenin, by inhibition of GSK3- β , and induces the expression of *engrailed* and *Cyclin-D1* genes (involved in cell survival processes). In AD, it has been found that patients present uncoupled G-protein from muscarinic receptor M1. It is suggested that amyloid peptides may induce such uncoupling, activating a further mechanism to increase amyloidogenic pathway (Norwitz *et al.* 2019; Jiang *et al.* 2014a).

Animal experiments, further strengthened the involvement of the cholinergic network, by demonstrating that cholinergic lesions, or deficit, result in amyloid deposition, Tau phosphorylation, and pro-inflammatory pathways activation (Ramos-Rodriguez *et al.* 2013; Field *et al.* 2012).

Studies on healthy patients have confirmed the role of cholinergic networks in cognitive processes, with anti-cholinergic therapies resulting learning and cognitive impairments (Sittironnarit *et al.* 2011). Other than that, anti-cholinergic treatment exacerbated cognitive symptomatology in patients at risk of AD, especially in those already presenting amyloid plaques (Lim *et al.* 2015).

Conversely, therapies that improve cholinergic connectivity, such as acetylcholinesterase (AChE) inhibitors, were found to improve the cognitive functions in AD patients, and are now the most represented class of molecules for AD therapy approved by the FDA (Summers *et al.* 1986; Cavedo *et al.* 2016; Cavedo *et al.* 2017; Hampel *et al.* 2018).

1.2.7 Neuroinflammation in AD

In AD pathogenesis, neuroinflammation is primarily caused by microglial cells. A β peptides activate microglial cells, which in turn secrete pro-inflammatory cytokines and chemokines. The aggregation of amyloid peptides results in a chronic activation of microglial cells. Chronic production of pro-inflammatory cytokines, triggers the assembly of the apoptosis-associated speck-like protein containing CARD (ASC specks) (Mandrekar-Colucci *et al.* 2010). The ASC specks are known to promote the formation amyloid plaques, prevent amyloid clearance, and promote their spreading, further aggravating the neuroinflammatory scenario (Venegas *et al.* 2017). In addition to this, microglia are well known for their role in synapsis pruning. The constant

activation of microglial cells increases microglial-mediated synaptic loss, aggravating the neurodegeneration in AD (Heneka *et al.* 2015).

TREM-2 expressing microglia have a physiological role in synapsis pruning during development. Multiple ligands can physiologically activate TREM-2, such as phospholipids, lipoprotein, phosphoglycan. In AD, TREM-2 amyloid oligomers are capable of activating TREM-2, which further aggravates the inflammatory status in the brain (Gratuzze *et al.* 2018).

1.2.8 NMDA receptors and excitotoxicity

NMDA receptor are Ca^{2+} and Na^+ channels, activated by the major excitatory neurotransmitter in the human brain, glutamate. Under physiological condition glutamate activates NMDAr, which in turn allows the influx of Ca^{2+} and Na^+ generating depolarization and axon potential. This mechanisms is finely regulated to generate as LTP, a crucial mechanism for neuronal plasticity, generation of novel networks, memory and learning functions (RIEDEL *et al.* 1996).

However, improper activation of NMDAr can lead to uncontrolled Ca^{2+} , resulting in cellular toxicity by disrupting mitochondrial functioning, and therefore inhibiting proper metabolism (Wang *et al.* 2017). The stimulation of glutamate receptor induces changes in concentration of Ca^{2+} , Ca^{2+} , and H^+ ions in the cells. It is suggested as well that other ion channels such as TRP1 may play a role in increased Ca^{2+} levels under oxidative stress and excitotoxicity conditions. In addition to this, glutamate-induced Ca influx activate mitochondrial PARP-1, which in turn lead to decreased NADH levels, resulting in profound mitochondrial depolarization, and bioenergetics failures.

A β peptides increase Long-term depression, via excitotoxicity mechanisms, as a result of post-synaptic NMDAr desensitization, and overstimulation of extrasynaptic NMDAr (Rush *et al.* 2014).

1.3 Models to study AD

Experimental models are a crucial tool to study the fundamental mechanistic biology of every disease, as well as the efficacy of potential therapies. The complexity of AD has frequently limited the realism of experimental models, which often resulted in contradictive results.

AD models are vary, such as mice, *Drosophila melanogaster*, cells (either cell lines, or patients derived), and *Caenorhabditis elegans* (Drummond *et al.* 2017). The majority of them exploit the transgenic expression of either A β peptides, or human Tau, in order to study amyloid plaques derived pathology and Tau hyperphosphorylation respectively (Busche *et al.* 2019; Smith *et al.* 1998). However, different approaches have been used, such as cholinergic denervation in mice, to study the cognitive defects described in AD (Lim *et al.* 2015).

Despite the large number of different models available to study AD, none of them represent the real scenario of a human patient. This fundamental limit often results in a failure during clinical trials of potential AD therapies, since the results in pre-clinical studies are not confirmed in patients. As a result, since 2003 the 100% of drug candidates for AD treatment have failed in clinical trial (Cummings *et al.* 2019b). Thus, the development of a reliable model, able to recapitulate the complexity of the human clinical scenario of AD, remain an open challenge.

1.3.1 *Drosophila melanogaster* as model of AD

The common fruit fly has served as model organism for many decades, to study both mechanisms underlying a certain phenotype, and for drug screening purposes. *Drosophila melanogaster* allows the simultaneous study of hundreds of animals without special adjustment to manage them. In addition to this, analysis of the fruit fly genome has showed that 77% of disease-causing genes in humans are present in *Drosophila* as well, therefore allowing the study of multiple pathways linked to a particular disease (Reiter *et al.* 2001).

However, in some diseases, such as AD, the genes related to the pathogenesis may harbour some differences. For instance, the *APPl* gene in *Drosophila*, orthologue of the *APP* human gene, does not present the β domain, therefore preventing any A β peptide generation. Moreover, in *Drosophila* dBACE1 enzyme, the equivalent of the human BACE1, has little to no activity raising further problems to study the human amyloidogenic pathway and its product A β peptides (Bilen *et al.* 2005; Nichols 2006). To overcome this problem, a number of research groups have exploited the UAS/Gal4 system to drive the expression of AD human genes in the fruit fly (Duffy 2002).

The UAS/Gal4 is a binary system composed of the Upstream activating sequence (UAS), which works as gene promoter, and the Gal4 protein, which binds to UAS and recruit the transcription machinery. By placing the gene of interest under the control of the UAS promoter, researchers have developed a multitude of different *Drosophila* models. The expression of the Gal4 can be spatially limited to a particular area, for instance CNS, to further optimize the fruit fly model (Chakraborty *et al.* 2011).

Other aspects of *Drosophila melanogaster* have been exploited to model diseases, for instance the compound eye.

The fruit fly eye is composed of hundreds of repetitive units called ommatidia, and each one of them is connected to 8 photoreceptor neurons (Katz *et al.* 2009). The defined eye structure, and neuronal connection, have been used to develop the Rough eye phenotype (REP), in which a transgene expression is driven toward the compound eye (Zhong *et al.* 2019). The subsequent transgene expression results in a jeopardized morphology and a REP (Wolff *et al.* 1991). The REP has been extensively used to study AD neurodegeneration, and therapies able to prevent it (Zhong *et al.* 2019).

In addition to a reduced lifespan as a result of AD-related gene expression, the fruit fly offers a number of assays to study behaviour and memory as well, and how these parameters are affected by the AD gene expression through a certain period (Pham *et al.* 2018). The simple climbing assay can be used to assess the locomotive functions of a *Drosophila* under different AD treatment for instance (Zhang, Li, *et al.* 2016). Also, the fruit fly memory phases can be used to study the fly cognitive functions after the expression of AD related genes (Chakraborty *et al.* 2011; Miyazaki *et al.* 2019).

To date a number of different genotypes have been generated by driving the expression of the human *APP*, *BACE1*, and *MAP* genes, either alone or together. These models have served as drug screening platforms to study different type of therapies, such as plant-derived compound, peptides, and radiation (Hwang *et al.* 2019; Miyazaki *et al.* 2019; Zhong *et al.* 2019).

Thus, *Drosophila melanogaster* can be modelled to recapitulate the human AD scenario, and exploited for mechanistic and drug screening experiments.

1.3.2 Cell culture models of AD

Cell culture models have been developed to study different mechanisms of AD. The controlled environment and media gives a great advantage to point to a particular component the subsequent effect.

Among different cell lines, SH-SY5Y cells, derived from bone marrow neuroblastoma, have been extensively exploited to study A β peptides induced toxicity and cell deaths, the mechanisms behind it, and several compounds to prevent it (Agholme *et al.* 2010; Huang *et al.* 2015; Wang *et al.* 2009; Zhang, Yu, *et al.* 2010). Moreover, SH-SY5Y have been used to model Tau abnormal phosphorylation either by adding chemical compounds, such as glyceraldehyde and okadaic acid, or by exploiting hypothermia (Zhang and Simpkins 2010; Bretteville *et al.* 2012; Koriyama *et al.* 2015).

Despite the utility of using SH-SY5Y cell line as AD model, it harbours some crucial limitations, such as active division, poor neurite density, and poor neurite outgrowth. To overcome this problem, a differentiation protocol of SH-SY5Y exploiting retinoic acid (RA) and brain derived neurotrophic factor (BDNF) was developed to achieve neuronal differentiation (Agholme *et al.* 2010; Constantinescu *et al.* 2007; Shipley 2016).

The SH-SY5Y-derived neurons well recapitulated the human neuronal characteristics, with long projection neurons, a G0 phase, and high neurite density. This neuron-like cells have been used to study different aspects of AD (Krishtal *et al.* 2017).

Despite differentiated SH-SY5Y cells offer a more realistic model of AD, they do not form a proper neuronal network architecture, due to the limitation of a 2D cell culture type. Thus, novel approaches relying of 3D cell culture have been recently developed. These model offer to study not only neurons in a proper, brain-like architecture, but as well they offer the possibility to study a complex structure such as the blood brain

barrier (BBB) (Choi *et al.* 2014; Kwak *et al.* 2020; Papadimitriou *et al.* 2018) (Shin *et al.* 2019) .

Other cell line models used to model AD include HEK293T cells, derived from the human embryo kidney (Lessard *et al.* 2005). This type of cells has been extensively exploited to perform Crispr genome editing on crucial AD genes, such as *BACE1*, *ADAM10*, and *PSNI* (Giau *et al.* 2018). However, the realism of a kidney cells used to model a complex neurodegenerative disease as AD is limited (Drummond *et al.* 2017)

In addition to this, some 3D cell culture models have exploited patient derived iPSC to model AD, despite some limitations due to epigenetic heterogeneity that may differ from patient to patient, and the fact that the subsequent neuronal differentiation result in a non-adult neuron (Zhang *et al.* 2014; Drummond *et al.* 2017).

1.3.3 Mouse models of AD

The generation of more complex AD models that better recapitulate the human scenario has mainly relied on the exploitation of mouse models. Through the year, the majority of mouse models have been generated using autosomal dominant forms of AD. Despite this form of AD account for a very small minority of the human patients, they share some similarities with sporadic AD (Hall *et al.* 2012). The majority of genetic AD mice models express transgenic human APP, harbouring defined mutations, such as the Arctic, Swedish, or London (Cheng *et al.* 2004). These models showed accumulation of A β peptides, resulting in memory and learning deficit. In addition to this, they presented a characteristic synaptotoxicity, but failed to show any neurodegeneration, the main hallmark of AD. Moreover, this type of mouse model

only presents amyloid plaques, but not NFTs another crucial aspect in AD pathogenesis and symptoms exacerbation (Hall *et al.* 2012).

Apart from amyloid, genetic Tau mice models have also been developed. The latter exploit mutated forms of human Tau, which are the primary cause of fronto-temporal dementia. Despite recapitulating the typical Tau hyperphosphorylation, and derived defects, none of these mutant Tau variants has been linked to AD, posing a crucial limit on the validity of mice models to study AD (Hall *et al.* 2012).

Other strategies to model AD in mice have exploited selective neuronal damage to recapitulate the cognitive dysfunction observed in the patients. The usage of scopolamine, a muscarinic antagonist, is used to block the cholinergic network and induce memory and learning defects in mice (Bhuvanendran *et al.* 2018) . However, this method has the main limitation of affecting only the cholinergic system selectively, whilst human patients experience a broader and less specific neuronal dysfunction (Drummond *et al.* 2017).

Despite a number of differences between mice AD models and the human scenario, they still are an efficient model for a crucial aspect of AD drug development: the presence of a functional BBB. This structure in drug development cannot be assessed in other models such as *Drosophila melanogaster*, *C. elegans*, and cell culture, therefore inserting a crucial limitation on the data reality.

1.4 AD therapies

Treatment of AD and related dementias remains an open challenge for a number of research groups around the world. This invalidating disease not only creates pathological issues in the affected patients, but has social and economic consequences for the patients' families as well (El-Hayek *et al.* 2019).

The available therapies do not show any disease modifying effect, with a temporary benefit only on the psychiatric symptomatology that is soon reversed by the disease progression.

So far, a number of different drug candidates have been proposed as potential AD therapy, but eventually failed during clinical trials. These included anti-amyloid agents, anti-Tau agents, monoclonal antibodies, and further psychiatric therapies (Cavedo *et al.* 2016). The lack of a proper AD model to study the drug effects, an early diagnosis biomarker still missing, and difficulties in recruiting patients for clinical tests, are the major contributors for clinical testing failures.

Despite difficulties, the search of a therapy able to stop the progression, or at least delay, the disease is necessary. It is estimated that we could have 9.2 million less cases per year, just by delaying the disease onset of 12 months (Brookmeyer *et al.* 2007).

Currently, two class of molecules are approved for AD treatment: AChE inhibitors and NMDAR antagonists. In addition to this, a combination of both AChE inhibitor and NMDAR antagonist is used in severe AD cases (Graham *et al.* 2017).

Unfortunately, none of these molecules showed disease-modifying effects. Thus, improvement of the already available therapies or research for new drug candidates remain an open challenge.

1.4.1 AD therapy selection

The choice of treatment made by the clinician mainly depends on two factors: stage of AD, and patient compliance.

AD progression is divided into three stages: mild, moderate, and severe, which take into account different psychiatric symptoms, and ability to perform daily tasks. In order to discriminate between different phases of AD, the clinician perform a psychiatric assessment, i.e. Mini-Mental state examination, during which the patient performance on multiple cognitive tasks are given a quantitative score. The score obtained on such tests will determine the AD stage of the patient (Galasko *et al.* 1990). Subsequently, the choice of the AD therapy will be based on the stage of the disease. Usually Rivastigmine and Glantamine are the primary choices in patients with mild to moderate AD, whilst severe cases of AD are routinely treated with Memantine or Donepezil, or both (Buschert *et al.* 2010).

Patient compliance in AD therapy selection is another aspect for clinicians, as often patients find difficult to get tablets, especially at multiple times during the day (i.e. Donepezil). For this, Rivastigmine available in patches is often a golden route for patient with poor compliance.

1.4.2 AChE inhibitors

AChE inhibitors are the first class of molecules approved by the Food and Drug Administration (FDA) in 1993, after Tacrine was cleared to be administrated to patients. However it was subsequently retired due to severe side-effects (Knapp *et al.* 1994).

Currently, three different AChE inhibitors are available for AD treatment: Donepezil (Arcipet), Galantamine (Razadyne), and Rivastigmine (Exelon) (Birks *et al.* 2009).

AChE inhibitors therapy, also known as cholinergic replacement therapy, aims to increase the acetylcholine levels, by inhibiting AChE enzyme, and improve the cholinergic connectivity, crucial in memory and learning functions.

Soon after AD diagnosis the AChE inhibitor therapy start, with dosage increased along with disease progression.

Donepezil is initially administrated at 5mg per day, and subsequently at 10mg after few weeks. However, 23mg dosage is available, despite increased side effects (Farlow *et al.* 2010).

Rivastigmine is usually prescribed as 1.5mg twice a day, and increased to 6mg after few weeks (Birks *et al.* 2009).

Galantamine therapy is initiated at 4mg twice a day, and subsequently increased to 12mg. Despite some differences in dosages, and mechanism, none of these therapies resulted to have increased efficacy when compared to each other (Tayeb *et al.* 2012). Study in placebo controlled trials showed as well that improvement of the psychiatric symptomatology was modest, with effects lasting up to two years (Giacobini 2000; Hansen *et al.* 2008). Furthermore, none of these therapies prevented the progressive decline of cognitive functions in long term study (Courtney *et al.* 2004).

Despite the controversy about the efficacy of AChE inhibitor therapy, it was proven that such molecule at least delayed the nursing home placement of AD patients of one year (Wattmo *et al.* 2011). AChE inhibitor therapy, reduced caregiver stress, and behavioural symptomatology (Adler *et al.* 2014).

1.4.3 NMDAR antagonist

The second class of molecules approved by the FDA as AD therapy is NMDAR antagonist. In an attempt to prevent excitotoxicity resulting from glutamate, and Tau

phosphorylation, NMDAR antagonist Memantine, is currently administrated to AD patients (Folch *et al.* 2018).

Increased levels of A β peptides can increase the activity of NMDAR, leading to an uncontrolled Ca²⁺ uptake, which in turn impairs the mitochondrial functions and, therefore, triggering the release of reactive oxygen species (ROS) which are cytotoxic (Lipton 2007).

In particular, among various NMDAR subtypes, Memantine main targets are extrasynaptic NMDAR, located in the dendrites, and not those located in the synapsis (Lipton 2005; Folch *et al.* 2018). This is of peculiar importance, since extrasynaptic NMDAR are implicated in A β production and toxicity (Tackenberg *et al.* 2013; Rush *et al.* 2014).

Memantine significantly ameliorated the cognitive functions of AD patients, administrated either alone, or as combination with AChE inhibitor (Dantoine *et al.* 2006; Gauthier *et al.* 2008).

Despite beneficial effects on psychiatric symptomatology, and the involvement of NMDAR over-activation with the pathogenesis of AD, Memantine treatment did not modify the progression of the disease (Tayeb *et al.* 2012).

1.4.4 Future perspectives

The unmet clinical need of an effective therapy to stop the disease progression on AD patients continue to stimulate the research of novel drug candidates. Currently, there are 121 drugs under clinical trial, at various phases, as potential AD therapy (Cummings *et al.* 2020).

In phase III of clinical trials there are 29 agents under study, with 40% of them targeting the psychiatric symptomatology, whilst the remaining 60% are potential disease-modifying pharmaceutical (Cummings *et al.* 2020).

Therapies with disease-modifying effects exploit different targets and approaches to interfere with AD pathogenesis. Targeting A β peptides aggregation, and prevention of oligomer formation, by using monoclonal antibodies is a common strategy, despite a number of clinical trials have failed to show any significant amelioration on AD patients, further highlighting the raising doubts about the amyloid hypothesis (Panza *et al.* 2019).

A different target is the neuroinflammation, which represents 20% of the clinical trial target of disease-modifying molecules (Cummings *et al.* 2020). It is clear that neuroinflammation plays a major role in AD pathogenesis, being the ultimate actor responsible of neuronal damage and death, thus its prevention, or modulation, may be an effect AD therapy (Heneka *et al.* 2015).

Aberrant autophagy is a raising mechanism that could trigger AD pathogenesis, with an aberrant persistence of impaired mitochondria as result of deubiquitinase (DUB) enzyme activity. Thus, a potential therapy based on DUBs inhibitors is currently under investigation, not only for AD, but also for other neurodegenerative diseases such as Parkinson's disease (Van Bulck *et al.* 2019) (Das *et al.* 2020).

Another aspect involving AD progression is neuronal cells death. The lack of an active division in neurons result in the incapacity of this cell type to be replaced upon cell death. As a result, neuronal network and connectivity can be jeopardized resulting in

cognitive and memory deficit in AD patients. The development of a cell therapy aimed to replace the dead cells by using stem cells transplants could reverse the psychiatric symptomatology by restoring the neuronal architecture (Derakhshankhah *et al.* 2020).

There are a number of potential targets that could modify the progression of AD and alter the usual outcome. However, the complexity and multifactorial nature of the disease could prevent the success of a single-target drug as universal AD therapy. Thus, the development of a multi-targeted strategy could result in an effective way to treat AD.

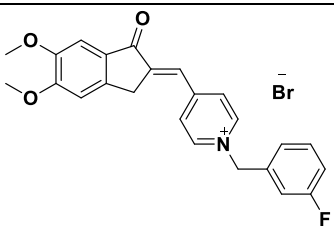
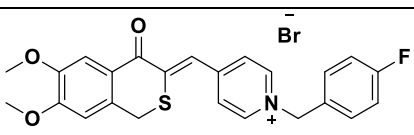
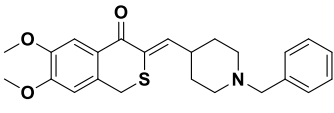
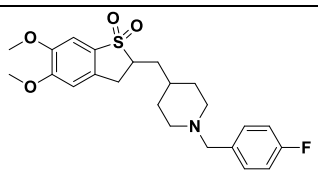
1.4.5 Novel compounds

The compounds tested in this work were kindly provided by Prof. Jinyi Xu (China Pharmaceutical University – Nanjing). The novel drugs structure is derived from the (\pm)-7,8-Dihydroxy-3-methylisochroman-4-one [(\pm)-XJP] compound, which was initially isolated from the *Musa sapientum* L (Wang *et al.* 2015). This compound was then added with an N- N-benzyl pyridinium moiety, reported to have AChE inhibitory properties, with different –R group. Compound with 4-F as R group, 1-(4-fluorobenzyl), named XJP-1 (Fig.1 A) was shown to have the lowest AChE half-maximal inhibitory concentration (IC₅₀) of 8.93nM (Wang *et al.* 2015). Docking studies also showed that XJP-1 is able to bind both sites of AChE enzyme, peripheral anionic site (PAS), and the catalytic active site (CAS), which confers XJP-1 a higher specificity for AChE enzyme, over butyrylcholinesterase (BuChE). This is an important details, since many of the side effects reported by commercial AChE inhibitor Tacrine, were reported to be a consequence of aberrant BuChE inhibition

(Sharma 2019). Following the design and synthesis of compounds XJP-1, novel AChE inhibitors were from XJP-1 structure, named SAD-2, SAD-6 and FAD (Fig.1 B-D).

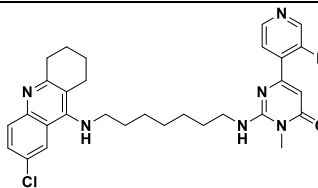
In addition to this, given the relevance and central role of GSK3- β enzyme in multiple pathways during AD pathogenesis, Prof. Xu research group designed and synthesized a novel dual AChE/GSK3- β inhibitor, named 16g (Fig.1 E) (data not yet published). The latter is a Tacrine-pyrimidone hybrid derivate, with an IC_{50} for AChE and GSK3- β of 50nM, and 89nM respectively (data not yet published).

All compounds have a *in silico* predicted BBB penetration, and are water soluble (data not published yet).

No.	Compd.	Structures
A	XJP-1	 <p>Name: (E)-4-((5,6-dimethoxy-1-oxo-1,3-dihydro-2H-inden-2-ylidene)methyl)-1-(3-fluorobenzyl)pyridin-1-ium bromide</p>
B	SAD-2	 <p>Name: (Z)-4-((6,7-dimethoxy-4-oxoisothiochroman-3-ylidene)methyl)-1-(4-fluorobenzyl)pyridin-1-ium bromide</p>
C	SAD-6	 <p>Name: (Z)-3-((1-benzylpiperidin-4-yl)methylene)-6,7-dimethoxyisothiochroman-4-one</p>
D	FAD	

Name: 2-((1-(4-fluorobenzyl)piperidin-4-yl)methyl)-5,6-dimethoxy-2,3-dihydrobenzo[b]thiophene 1,1-dioxide

E **16g**



Name: 2-((7-((6-chloro-1,2,3,4-tetrahydroacridin-9-yl)amino)heptyl)amino)-6-(3-fluoropyridin-4-yl)-3-methylpyrimidin-4(3H)-one

Figure 1. Novel compounds structure

AChE inhibitors and dual AChE/GSK3- β inhibitors structure and IUPAC name. **A)** XJP-1. **B)** SAD-2. **C)** SAD-6. **D)** FAD. **E)** 16g.

1.5 Thesis aim and hypothesis

AD is a neurodegenerative disease affecting millions of people around the world. The multiple pathways involved, and the unclear triggering mechanism, are currently limiting the discovery of any effective therapy able to modify the progression of this disease.

Our hypothesis proposes a series of novel AChE inhibitors, and AChE/GSK3- β dual target inhibitor as potential AD therapy.

We believe that a higher specificity, of the newly synthesized compounds, for the AChE over BuChE could enhance their efficacy in slowing the AD progression, or improve the cognitive functions for a longer period. We also speculated that inhibition of both AChE and GSK3- β enzymes would results in disease modifying effects, particularly preventing GSK3- β induced Tau hyprophosphorylation.

In order to test our hypothesis, we firstly aimed to generate an AD model, using *Drosophila melanogaster*, with measurable AD-like defects. Secondly, we tested the available compounds on the fruit fly models, highlighting the limitation of the current compounds, which resulted in an improvement of the initial AChE inhibitor into a dual

AChE/GSK-3 β inhibitor. Lastly, we tested the best compound developed within this project on a novel neuron-like model we generated to study Tau aberrant phosphorylation.

2 Materials and methods

2.1 Reagents

AChE inhibitors Donepezil, Galantamine and Rivastigmine were purchased from Sigma-Aldrich Ltd. NMDAR antagonist Memantine was purchased from Sigma-Aldrich Ltd. Drug candidates XJP-1, SAD-2, SAD-6, FAD, and 16g were gifted by Prof. Jinyi Xu (CPU – Nanjing).

All drug were dissolved in ddH₂O to make a stock with a final concentration of 1mM.

2.2 *Drosophila melanogaster* strains and cross schemes

List of *Drosophila melanogaster* strains are outlined in Table 1.

Flies were kept at 25°C in 25mL plastic vials containing 5ml of standard fly food, or standard fly food containing the appropriate drug concentration. To obtain A β _{arc} flies, 20 *elav*-Gal4 (Ref. M19 – kindly provided by Dr. Georgiou – University of Nottingham) virgin females were crossed with 5 UAS-APPE693G males (Ref. 33774 – Bloomington Indiana *Drosophila* stock centre). To obtain Tau flies, 20 *elav*-Gal4 virgin females were crossed with 5 UAS-Tau males (Ref.51363 - Bloomington Indiana *Drosophila* stock centre). To obtain TBA flies, 20 *elav*-Gal4 virgin females were crossed with 5 UAS – MAPT - BACE1 – APP males (Ref. 33799 - Bloomington Indiana *Drosophila* stock centre). To obtain A β ₄₂ flies 20 *elav*-Gal4 virgin females were crossed with 5 UAS – Abeta₁₋₄₂ males (Ref. 32037 - Bloomington Indiana

Drosophila stock centre). The female progeny of each cross scheme was used for all the assays (except REP experiments). *Elav*-Gal4 flies were used as a wild type (WT) control.

In REP experiments, *gmr*-Gal4 flies were used to drive the expression of the transgene of interest in the *Drosophila* compound eye. Thus, to obtain A β _{arc} flies, 20 *gmr*-Gal4 (Ref. M572 – kindly provided by Dr. Georgiou – University of Nottingham) virgin females were crossed with 5 UAS-APPE693G males (Ref. 33774 – Bloomington Indiana *Drosophila* stock centre). To obtain Tau flies, 20 *gmr*-Gal4 virgin females were crossed with 5 UAS-Tau males (Ref.51363 - Bloomington Indiana *Drosophila* stock centre). To obtain TBA flies, 20 *gmr*-Gal4 virgin females were crossed with 5 UAS – MAPT - BACE1 – APP males (Ref. 33799 - Bloomington Indiana *Drosophila* stock centre). To obtain A β ₄₂ flies 20 *gmr*-Gal4 virgin females were crossed with 5 UAS – A β ₁₋₄₂ males (Ref. 32037 - Bloomington Indiana *Drosophila* stock centre).

Table 1. *Drosophila Melanogaster* strains

Different Alzheimer’s disease genotype exploited to generate fruit fly AD models.

<i>Drosophila Melanogaster</i> genotype	Reference Number
w[*]; P{w[+mC]=GAL4-ninaE.GMR}12	M572
P{w[+mW.hs]=GawB}elav{C155}	M19
w[1118]; P{w[+mC]=UAS-APP.Abeta42.E693G.VTR}8	33774
w[1118]; P{w[+mC]=UAS-Tau.wt}7B	51363
w[1118]; P{w[+mC]=UAS-BACE1.Exel}7b, P{w[+mC]=UAS-APP.695.Exel}1/TM6B, Tb[1]	33797
w[*]; P{w[+mC]=UAS-Abeta1-42.G}3	32037

2.3 *Drosophila* food preparation

Flies were fed using the standard fly food recipe containing (quantity for 1 litre): 70.62ml of golden syrup, 15.87g of yeast, 9.12g of soya flour, 67g of cornmeal, 5.25g

of agar, and 711.25ml of water. To add the drug of interest into the food, an aliquot of the drug stock solution was dissolved in a volume of water evenly to a 1/5th of the total food volume and mixed on the magnetic stirrer for 2 minutes. Subsequently, when the food was cooling down (Temperature < 80°C), the diluted drug was added and mixed it homogenously. Food containing drugs was then stored at +4° C up to three weeks.

2.4 Rough Eye Phenotype Experiment

The cross scheme for REP experiments is described in section 2.2. Flies were crossed on standard fly food or on drug containing food. Female progeny was analysed within 24 hours after eclosion and after 10 days of respective drug treatment. Prior the eye imaging, the flies are anesthetized on CO₂ pads, and the transferred under the Leica MZ10 F microscope (Leica) for the live imaging. All the eye pictures were taken using a 4x magnification and an exposure time of 15ms. All images have been acquired using the Qcapture software (Qimaging).

2.5 Lifespan Assay

Newly emerged flies aged 0-24 hours were collected and placed into fresh food vials containing 5mL of fly food. Each vial contained a group of maximum 20 flies. At least 100 flies per genotype were analysed. Food vials containing the flies were kept horizontally in order to avoid the deaths due to sticky food. Food replacement occurred 3 times a week, number of dead flies was counted at that time. Lifespan assay was performed until all flies into a vial have died. Flies that flew away, died in the food or trapped in the cotton lid were not taken in to account.

2.6 Climbing assay

Wild type and transgenic *Drosophila* locomotive functions were measured by performing the climbing assay. Flies aged 0-24 hours were collected and placed into fresh food vials containing the appropriate treatment. Each food vial contained up to 10 flies. Food was replaced 3 times a week, for a total of three weeks, and at this time the climbing performances were recorded as follow: flies were moved into an empty 50ml falcon tube, flies were then gently tapped down and allowed to climb. The number of flies above the three cut off lines (40ml, 30ml and 20ml) were counted after 20 seconds. The results are then calculated using the following formula:

$$\begin{aligned} \text{Climbing Index} = & (\text{percentage of total flies above the 40ml line}) \times 1 \\ & + (\text{percentage of total flies between the 30ml and 40ml lines}) \times 0.75 \\ & + (\text{percentage of total flies between the 20ml and 30ml lines}) \times 0.50. \end{aligned}$$

2.7 *Drosophila melanogaster* brain immunostaining

Adult flies were firstly anesthetized with CO₂, and subsequently euthanized in pure ethanol. Brains were dissected in Phosphate Buffered Saline (PBS) and then fixed in 4% paraformaldehyde (PFA) for 20 minutes at room temperature (RT). Tissues were then washed three times in 1% PBS-Tween 20 (PBS-T) for 2 minutes, and subsequently placed in 5% Normal Goat Serum (NGS) in PBS-T for 2 hours at room temperature. After removing the 5% NGS-T the rabbit anti-A β ₄₂ primary antibody (#ab2539, Abcam plc.) was added at a final concentration of 1:200 in 5% NGS-T and left to incubate overnight at +4° C. The primary antibody was then washed with 1%

PBS-T for three times and subsequently the goat – anti rabbit secondary antibody was added to a final 1:250 concentration. The sample was allowed to incubate for 1 hour at room temperature. Goat anti-Rabbit 488 Alexa Fluor secondary antibody (#A-11034; ThermoFisher Scientific) was then washed with 1% PBS-T for three times. Brain samples were then mounted for confocal imaging exploiting a “bridge” structure to avoid any sample damage cause by the coverslip. Two 0.1mm thin coverslips were attached to the glass slide at approximately 5mm distance to each other. Subsequently, 20µl of mounting media (90% PBS and 10% glycerol) were added in the gap between the two coverslips. Samples were then placed into the mounting media, and an additional cover slip to bridge the gap between the two “pylons” coverslips. Samples were analysed by confocal microscopy within 24 hours from mounting.

2.8 Confocal microscopy

All brain images were acquire using the Zeiss880 Confocal Microscope. Laser power was set up at 2.5%, gain at 520. Digital offset was set at 200. Acquiring speed at 1.03s averaging 2 times per slice. Cells images were acquired using Zeiss880 Confocal Microscope (Zeiss). Laser power was set at 4%, gain 650. Digital offset at 350. Acquisition speed was set at 1.3m averaging 2 times per image. Z-stack images at distance of 5µm were acquired.

2.9 Images analysis

A macro was created in ImageJ (Fiji) to identify and measure Amyloid spots in the images scanned at with the confocal microscope. The processing and analysis was carried out following the steps: raw, 16 bit confocal images were imported into ImageJ;

maximum projection, focus stack flattening, was applied and we created a copy of this image; the copy will be used for object identification and creation of the mask; a Gaussian blur filter was applied to the image to smooth the noise pixels; a threshold of 14850-61890 was used to separate the plaques signals from the rest of the image and from the background; the lower value of thresholding 14850 was determined by using negative control and non-stained areas of the brain; top value we set just below the maximum to avoid occasionally appearing large clumps of overexposed areas; a mask was created based on the thresholded areas; particle analysis was carried out on the mask while fluorescent intensity measurements were done by redirecting the measure function to the original image; the particle analysis was carried out to generate size, intensity and shape measurements of the plaques.

2.10 Western Blot

For *Drosophila Melanogaster* samples, a total of 50 fly heads for each sample were dissected and frozen overnight at -80°C . Samples were then homogenized on ice in RIPA buffer (0.22% Beta glycerophosphate, 10% Tergitol-NP40, 0.18% Sodium orthovanadate, 5% Sodium deoxycholate, 0.38% EGTA, 1% SDS, 6.1% Tris, 0.29% EDTA, 8.8% Sodium chloride, 1.12% Sodium pyrophosphate decahydrate) (#89901, ThermoFisher Scientific) containing 1X protease inhibitor cocktails (AEBSF, aprotinin, bestatin, E-64, leupeptin, and pepstatin A) (#201119, Abcam plc.). Subsequently, samples were centrifuged at 16000G for 15 minutes at 4°C . The supernatant was then transferred into a fresh clean vial. Protein were quantified as described by Bradford (Au - Ernst *et al.* 2010). Following quantification, equal amount of samples were mixed with 4X Nu-Page LDS Sample Buffer (Invitrogen) and loaded into Nu-Page 4-12% Bis-Tris Gel (Invitrogen). Protein were then transferred

on 0.2 μ M nitrocellulose membrane (Bio-Rad) via Trans-Blot Turbo (Bio-Rad) semi-dry apparatus. The membrane was then incubated for 1 hour at room temperature in 5% skim milk in TBS-T, and subsequently incubated overnight at 4°C with the appropriate primary antibody at a final concentration of 1:2500, either loading control rabbit polyclonal anti-Actin antibody (#ab1801, Abcam plc.), or rabbit monoclonal anti-amyloid₁₋₄₂ antibody (#ab180956, Abcam plc). Each membrane was then washed three times with TBS-T and then incubated for 1 hour at room temperature with HRP conjugated secondary antibody at a final concentration of 1:5000. Membranes were then imaged using LAS-4000 (Fujifilm), and imaged analysed using ImageJ software (Fiji).

2.11 Quantification of AChE-induced A β 42 aggregation

Measurements of AChE-induced amyloid aggregation were taken following the protocol reported by (Jiang *et al.* 2019). Briefly, hexafluoroisopropanol (HFIP)-treated E22G A β peptides (# SP-Ab-11_0.1, JPT – Innovative Peptide Solution) were dissolved in DMSO to reach a final 200 μ M stock. The dissolved peptides were subsequently centrifuged at 13500g for 10 minutes, the supernatant was then transferred into a fresh vial used for the following experiments. To evaluate the aggregation rate in presence of AChE inhibitors, 2 μ L of the compound of interest (at the appropriate concentration) were added into each vial, followed by 2 μ L of 200 μ M A β peptides stock, 20 μ L AChE enzyme (#C3389-500UN, Sigma-Aldrich Ltd) (2U/mL, in 1X PBS at pH 8.0), and 76 μ L of 1X PBS pH 8.0. The reaction was then incubated at RT for 24 hours. Subsequently, 100 μ L of 5 μ M Thioflavin T (ThT) were added into each vial. After one-hour incubation at RT, fluorescence emission was recorded at 490nm with an excitation wavelength of 450nm using a Tecan Spark microplate

reader. Results were then processed as done by Jiang and colleagues (Jiang *et al.* 2019) using the subsequent formula: $(F_i - F_b)/(F_o - F_b) \times 100$. Where F_i correspond to amyloid aggregation in presence of peptides, AChE, AChE inhibitors and ThT; F_o represents the amyloid aggregation in presence of peptides, AChE and ThT; F_b corresponds to blank control containing ThT only.

2.12 SH-SY5Y culture and neuronal differentiation

SH-SY5Y cells were cultured on different types of media, described in Table N.2, and differentiated as described by Shipley with some modifications (Shipley 2016). Briefly, SH-SY5Y were plated with Basic Growth media and allowed to reach 70% confluency. Subsequently, media was changed to Differentiation media #1 and replaced every 48 hours for the following 7 days. Cells were then split 1:1 and moved into fresh flasks/dishes and Differentiation Media # 2 was added. Differentiation Media #2 was then replaced every 48 hours for the following 4 days. Subsequently, media was changed with Differentiation media #3 and replaced every 48 hours for the following 7 days. After this period SH-SY5Y derived neurons were used for the subsequent assays and analysis.

Table 2. Cell culture media for SH-SY5Y neuronal differentiation

Breakdown of different cell culture media used for SH-SY5Y differentiation protocol

Basic Growth Media	Differentiation media #1	Differentiation media #2	Differentiation media #3
EMEM	EMEM	EMEM	Neurobasal
15% hiFBS	2.5% hiFBS	1% FBS	20mM KCl
1x Pen/Strep	1x Pen/Strep	1x Pen/Strep	1x Pen/Strep
2mM Glutamine	2mM Glutamine	2mM Glutamine	2mM Glutamax
	10 μ M RA	10 μ M RA	10 μ M RA
			50ng/ml BDNF

2.13 Glyceraldehyde (GA) induced Tau hyperphosphorylation

In order to induce Tau hyperphosphorylation, differentiated SH-SY5Y were treated with either 0.7mM or 1mM GA for 24 hours as previously described (Koriyama *et al.* 2015). After 24 hours treatment with GA, cells were used for downstream analysis.

2.14 AChE activity assay (Ellman's method)

Acetylcholinesterase activity was assessed using acetylcholinesterase assay kit (#ab138871, Abcam plc.) following the manufacturer instruction. A total of 10^5 per well were seeded into a clear 96-well plate. After appropriate differentiation and treatment, cell culture media was removed, and 100 μ l of lysis buffer were added into each well and left to incubate for 15 minutes at room temperature (RT). Subsequently, 50 μ l of acetylthiocholine reaction mixture (1X assay buffer, 1X DTNB stock solution, 1X acetylthiocholine stock solution) were added to each well and samples were left to incubate for 30 minutes at room temperature. Samples were then analysed using a 96-well microplate reader at OD= 410 ± 5 nm. In order to avoid false positive given by butyrylcholinesterase activity, the specific AChE inhibitor Donepezil hydrochloride was used as control.

2.15 Cell viability assay

A total of 10^5 per well were seeded into a 96-well plate. After SH-SY5Y differentiation, cells were treated with either 0.7mM or 1mM GA respectively. Along with GA treatment, appropriate concentration of the compounds to be tested was added. After 24 hours, 25 μ l of 5mg/ml Methylthiazolyldiphenyl-tetrazolium bromide (MTT) (#M2128-100MG, Sigma-Aldrich) were added into each well without

removing cell culture media and incubated at 37°C with 5% CO₂ for 2 hours. Subsequently, 100µl of lysing buffer (50% SDS solution, 25% DMF, 25% Demineralised water) were added. After an overnight incubation (20hrs) at 37°C, the optical densities at 490nm were measured using 96-well plate reader. The medium/MTT/lysing buffer incubated under the same conditions was used as the control.

2.16 pTAU quantification

Phosphorylation levels of Tau protein on Serine 199 and S396 were quantified using Enzyme Linked Immunosorbent Assay methodology. Following the manufacturer recommended protocol, ELISA kits KHB7041, KHB7031, and KHB0041 (ThermoFisher Scientific) were used to quantify phosphorylated Tau S199, phosphorylated S396, and total Tau respectively. Phosphorylation percentage was obtained, for the analysed residues, by normalization against total Tau.

2.17 Immunostaining cell culture

SH-SY5Y cells and differentiated SH-SY5Y cells were fixed in 4% PFA for 10 minutes at minutes at room temperature. Each sample was then washed three times with 0.1% PBS-T for 2 minutes. Following fixation, cells were incubated at room temperature for 2 hours in 5% NGS-T blocking solution, and incubated overnight at +4° C with the mouse monoclonal anti-tubulin III primary antibody (#ab179513, Abcam plc.) at a final concentration of 1:1000. Primary antibody was then removed, and each sample was washed three times with 0.1% PBS-T. Rabbit anti-mouse secondary antibody Alexa Fluor 488 (#ab150113, Abcam plc.) was then added at a

final 1:2000 concentration, and left to incubate at RT for 1 hour. Secondary antibody was then removed, and each sample was washed three times with 0.1% PBS-T. Samples were then mounted on to glass slide, using FluoroGel Mounting media (Genetex). Samples were then imaged by confocal microscopy within 24 hours.

2.18 Morphological analysis of SH-SY5Y derived neurons

Analysis of confocal images was performed using ImageJ plug-in NeuronJ. Three or more random areas were analysed. A threshold mask was applied to visualize the axon only and not the cell body. Subsequently measurement of the axon length were taken, and distance between coordinates measured with NeuronJ.

2.19 Data analysis

All statistical analysis is performed using GraphPad Prism 9 software. Data obtained was firstly tested for normality using the Shapiro-Wilk test. Kaplan-Meier test was used to compare different survival curves. Kruskal-Wallis test followed by Dunn's post-hoc was used to compare the differences between three or more groups in non-normally distributed data. ANOVA test was used to compare the differences between three or more groups of normally distributed samples. ANOVA repeated measures analysis of variance followed by Dunn's post-hoc test was used to analyse the differences between three or more groups in the climbing assay. Each experiment has been performed in triplicate and all results are presented as mean \pm standard error of the mean, or mean \pm standard deviation.

Results with a P-value <0.05 were considered as significant. * $P<0.05$; ** $P<0.01$; *** $P<0.001$; **** $P<0.0001$. *n* indicates the number of independent experiment performed for performed procedure.

3 *Drosophila* model development and characterisation

3.1 Introduction

AD and related dementias are characterised by numerous different symptoms, triggered by an array of multiple pathways. To investigate either the basic biological mechanisms underlying the disease progression, or potential treatments, the development, and choice, of a reliable model is always necessary. Since the first-case report by Alois Alzheimer in 1907 a number of different AD models have been developed (Tue *et al.* 2020). Generating an AD model has mainly relied on the usage of genetic tools to knockout selected genes, or to deliver the expression of mutant proteins, involved in either the amyloidogenic cascade, or Tau hyperphosphorylation (Duyckaerts *et al.* 2008). The AD models so far developed include mice, 2D cells, 3D organoids, *Zebrafish*, and *Drosophila Melanogaster* (Papadimitriou *et al.* 2018; Newman *et al.* 2014; Coleman *et al.* 2017; Koriyama *et al.* 2015; Sivanantharajah *et al.* 2019). In particular, the fruit fly has been recognised as important tool to study both AD mechanisms and potential therapies (Tue *et al.* 2020). The development of *Drosophila* AD models has mainly relied on the overexpression of the human genes involved in either amyloidogenic pathway, or the human Tau protein (both mutant and wild type) by exploiting the UAS/Gal4 system to overcome the lack of functional AD-related genes (Table 3) (Duffy 2002).

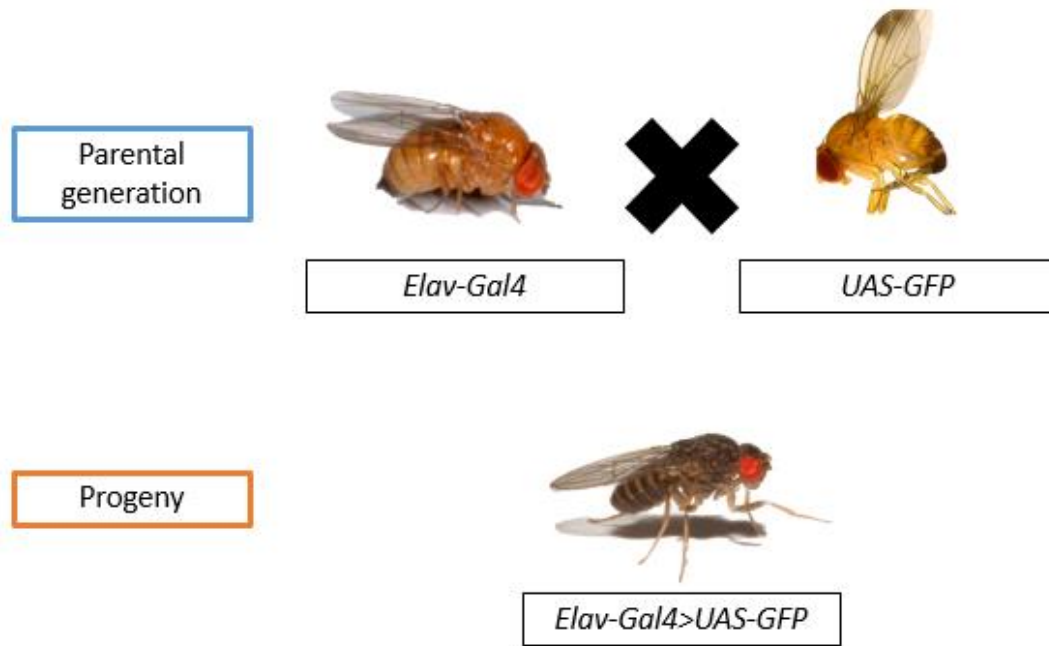


Table 3. UAS-Gal4 system representation.

The parental generation harbour either the *elav-Gal4* gene, or the *UAS-GFP* gene, preventing the expression of the GFP protein. After crossing the parental lines, the progeny is able to express the *GFP* gene as it harbour both element of the UAS-Gal4 system.

Among the various transgenic AD flies, the most widely used have been strains expressing A β peptides, the BACE1/APP proteins, and human Tau protein (either wild type or mutant) (Hwang *et al.* 2019; Cornelison *et al.* 2019; Miyazaki *et al.* 2019; Zhong *et al.* 2019; Higham *et al.* 2019; Pham *et al.* 2018; Zhang, Li, *et al.* 2016; Sandin *et al.* 2016; Chakraborty *et al.* 2011). In addition to this, reports of familial AD forms, where patients harbour a mutant gene, for instance the APP Arctic mutation, have further extended the AD models developed exploiting *Drosophila melanogaster*.

In addition to this, induced REP by expression of the AD toxic protein in the developing eye has served as quick model to study neuronal defects. The REP has been used to study amyloid and tau derived neurotoxicity by quantifying, or simply

visualizing, the eye size and ommatidia architecture, and to identify potential AD treatment by screening for those therapies able to revert the induced REP (Zhong *et al.* 2019; Zhang, Li, *et al.* 2016).

Drosophila AD models have been employed in drug screening projects, involving plant derived products as well (Ali *et al.* 2019; Hwang *et al.* 2019; Miyazaki *et al.* 2019; Zhong *et al.* 2019; Pham *et al.* 2018; Zhang, Li, *et al.* 2016; Sandin *et al.* 2016; Mhatre *et al.* 2014).

3.1.1 Experimental aim

Despite a large number of *Drosophila Melanogaster* AD models have been developed, often different results are reported on the recorded symptomatology. (Ogunsuyi *et al.* 2020; Liu *et al.* ; Kizhakke P *et al.* 2019).

In the work presented below, we evaluated different *Drosophila* AD models expressing A β ₄₂-peptides, Tau/APP/BACE1 proteins, Tau 2N4R, and mutant APP E693G (Arctic mutation) protein. For each genotype, we characterised different symptomatology induced by the transgene expression in the CNS. We also exploited the REP model to investigate whether AD derived neurodegeneration can be studied in the *Drosophila* developing eye, and use it for further drug screening purposes.

3.1.2 Experimental procedures

This chapter describes the data collected using 4 experimental procedures as follows:

- 1- Characterisation of transgene expression effects on *Drosophila Melanogaster* lifespan.
- 2- Investigation on locomotive functions in different AD genotypes.
- 3- Screening for different transgene expression in developing a Rough Eye Phenotype

4- Characterization of Tau and A β_{arc} flies CNS at multiple time points.

3.2 Results

3.2.1 Expression of human Tau and mutant APP protein lead to reduced lifespan and locomotive defects

To investigate the effects of pan-neuronal expression of AD-related transgenes on *Drosophila melanogaster* survival time, a lifespan assay was performed (Fig.2). Among the transgenic *Drosophila* expressing the human AD proteins, flies carrying the mutant E693G APP protein (hereafter referred to as A β_{arc} flies), and transgenic Tau-2N4R *Drosophila* (hereafter referred to as Tau flies), recorded an almost halved survival time when compared to the wild type control (Fig.2 A, B). Further to this, transgenic flies expressing Tau 2N4R, BACE1 enzyme, and APP protein (hereafter referred to as TBA flies) showed a significant drop in life expectancy, with similar results recorded for transgenic *Drosophila* expressing the amyloid- β_{1-42} peptide (hereafter referred to as A β_{42} flies) (Fig.2 A, B). To address whether the expression of transgenic AD protein would affect the fruit fly locomotive functions as well, we performed a climbing assay. Locomotive activity measurements were recorded for 21 days, and showed a significant time-dependant drop in climbing scores for A β_{arc} *Drosophila*, with transgenic flies showing a significant reduction at each time point analysed (Fig.3 A). On the other hand, Tau flies showed fluctuant climbing scores, with significant locomotive defects being recorded for the first 14 days of analysis, with the exception of day 7, but not during the last week of analysis (Fig. 3B). Other than that, both TBA and A β_{42} flies did not show any progressive locomotive defects, with climbing scores being significantly lower than the wild type at three time points only (Fig.3 C, D).

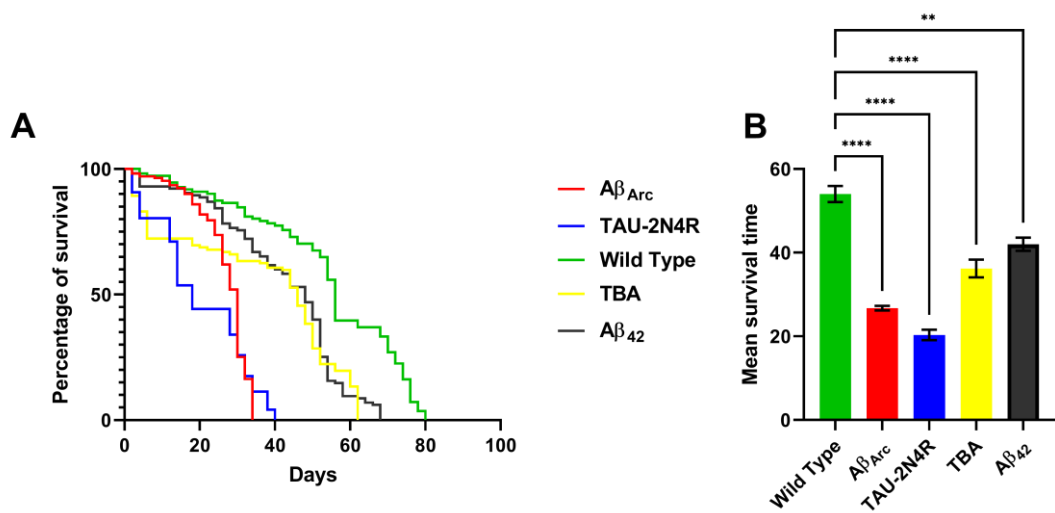


Figure 2. Transgenic AD *Drosophila* lifespan

A) Kaplan-Meier survival trajectories of different *Drosophila* AD genotypes. **B)** Mean survival time of transgenic AD flies. Kuskar-Wallis test followed by Dunn's post-hoc was used to compare the differences between different groups. Data are expressed as mean \pm SEM, n = 3 (number of independent experiments, each experiment, with a minimum of 10 animals per treatment). P<0.05 was considered as significant. * P<0.05; **P<0.01; *** P<0.001; ****P<0.0001.

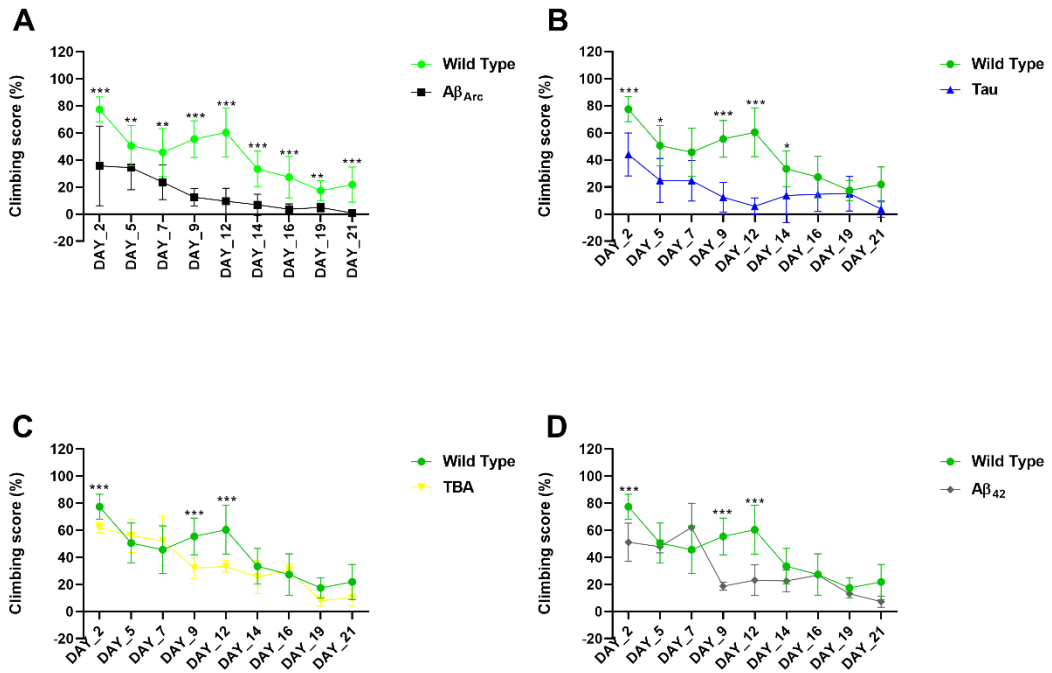


Figure 3. Evaluation of different Drosophila AD genotypes locomotive functions

Data shows the climbing performance trends over a 21 day period. Data generated from the climbing index was processed as a percentage of the total. In order to compare vials with a different number of flies, repeated measures analysis of variance was used to compare climbing scores between treated and untreated groups. **A)** Climbing assay of Aβ_{Arc} flies. **B)** Climbing assay of Tau flies. **C)** Climbing assay of TBA flies. **D)** Climbing assay of Aβ₄₂ flies.

Data is presented in the figure as the mean ± SD. *n* = 3 (number of independent experiments, each experiment, with a minimum of 10 animals per treatment). P<0.05 was considered as significant. * P<0.05; **P<0.01; *** P<0.001; ****P<0.0001.

3.2.2 Ommatidia neurodegeneration in A β _{arc} and Tau transgenic flies

In order to investigate the effects of AD-related proteins at neuronal levels, the *gmr-Gal4* was exploited to drive the expression within the *Drosophila* developing eye. This methodology exploits the architecture of compound eye of the fruit fly, composed by hundreds of ommatidia, each one presenting 8 photoreceptor neurons. Eyes of the flies expressing AD-related proteins were analysed within 24 hours post eclosion. Among transgenic *Drosophila*, only Tau flies showed a clear REP, whilst A β _{arc}, TBA, and A β ₄₂ did not show any visible difference compared to the wild type control (Fig.4 A). To understand whether a REP would be detectable at more advanced stage of *Drosophila* adulthood, we analysed again transgenic AD flies after 7 days post eclosion, Once again, among all genotypes analysed only Tau flies showed a visible REP, while the other AD flies showed an eye morphology identical to the wild type (Fig.4 B). In addition to this, we hypothesized that the expression of the AD-related transgene might have been affected by the flies growing temperature of 25°C. Thus, in an attempt to increase the transgene expression, transgenic AD flies were grown at 29°C and analysed within 24 hours post-eclosion. Tau and A β _{arc} flies showed a visible REP compared to the wild type, whilst no differences were recorded for TBA and A β ₄₂ flies (Fig.4 C). The minimal effects recorded in TBA and A β ₄₂ flies in the REP analysis, and previous carried out analysis suggests that these transgene are not suitable to induce AD in *Drosophila melanogaster*, for this reasons they were not exploited further for AD drug testing purposes.

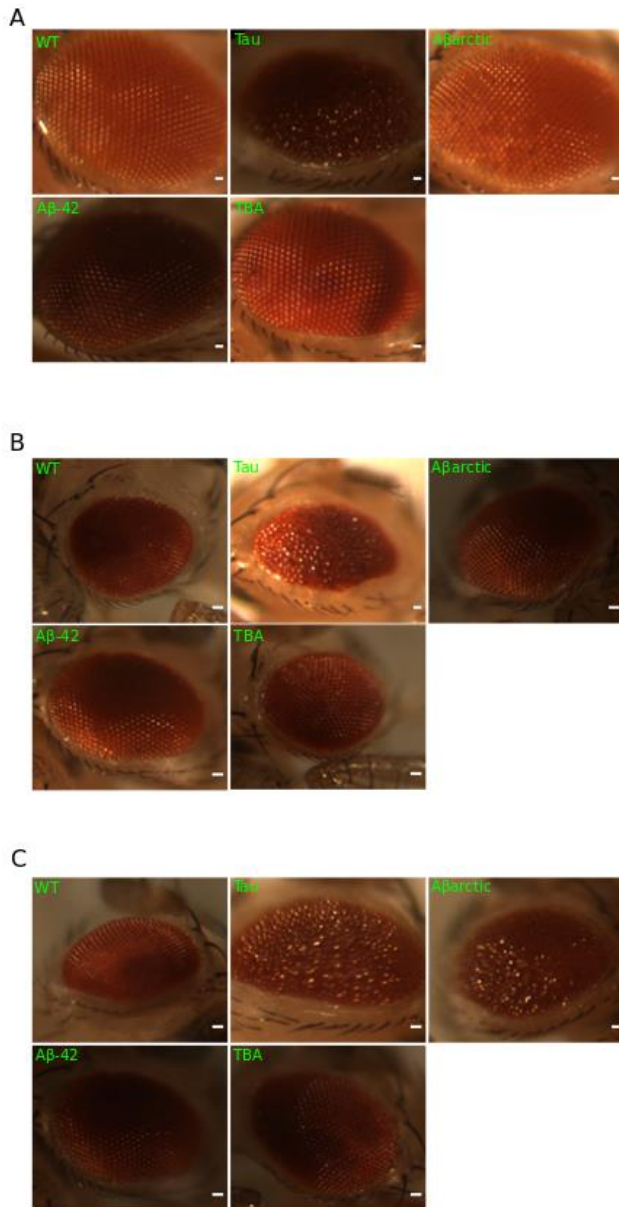


Figure 4. REP development by expressing different AD transgene

A) Eye images of different AD genotypes at day one post eclosion, flies were grown at 25°C.

B) Eye images of different AD genotypes at day 7 post eclosion, flies were grown at 25°C. **C)**

Evaluation of increased temperature, 29°C, on REP development of different AD genotypes.

3.2.3 Characterisation of transgenic A β_{arc} flies and Tau flies brain

AD patients' brains are characterised by the presence of amyloid plaques and neurofibrillary tangles, which are composed of β -peptides aggregates and hyperphosphorylated Tau protein respectively. To study whether these features are present in the fruit fly model we generated, we exploited confocal microscopy to visualize the A β_{arc} and Tau *Drosophila* CNS after 10 and 20 days post-eclosion (Fig.5 A). Quantification of the amyloid aggregates (hereafter referred to as amyloid spots) in A β_{arc} flies showed a significant increase in 10 days old flies (Fig.5 B) when compared to the wild type control. Moreover, the same trend was recorded after the analysis of 20 day old A β_{arc} flies' brains (Fig.5 C), despite no significant difference was recorded between 10 and 20 days A β_{arc} *Drosophila*.

In order to analyse the Tau *Drosophila*' brains, we stained them using a monoclonal antibody against phosphorylated S396 of human Tau protein, a specific residue analysed to estimate Tau protein phosphorylation levels, which is also considered as early stage marker of AD (Mondragón-Rodríguez *et al.* 2014). Signal intensity analysis of the Tau flies' brains showed a significant increase in the Tau group when compared to the wild type control at 10 and 20 days post-eclosion (Fig.5 D, E). These findings suggests that the AD symptoms recorded in both A β_{arc} flies and Tau flies are directly reputable to the accumulation of amyloid spots and NFTs within the AD *Drosophila* brains.

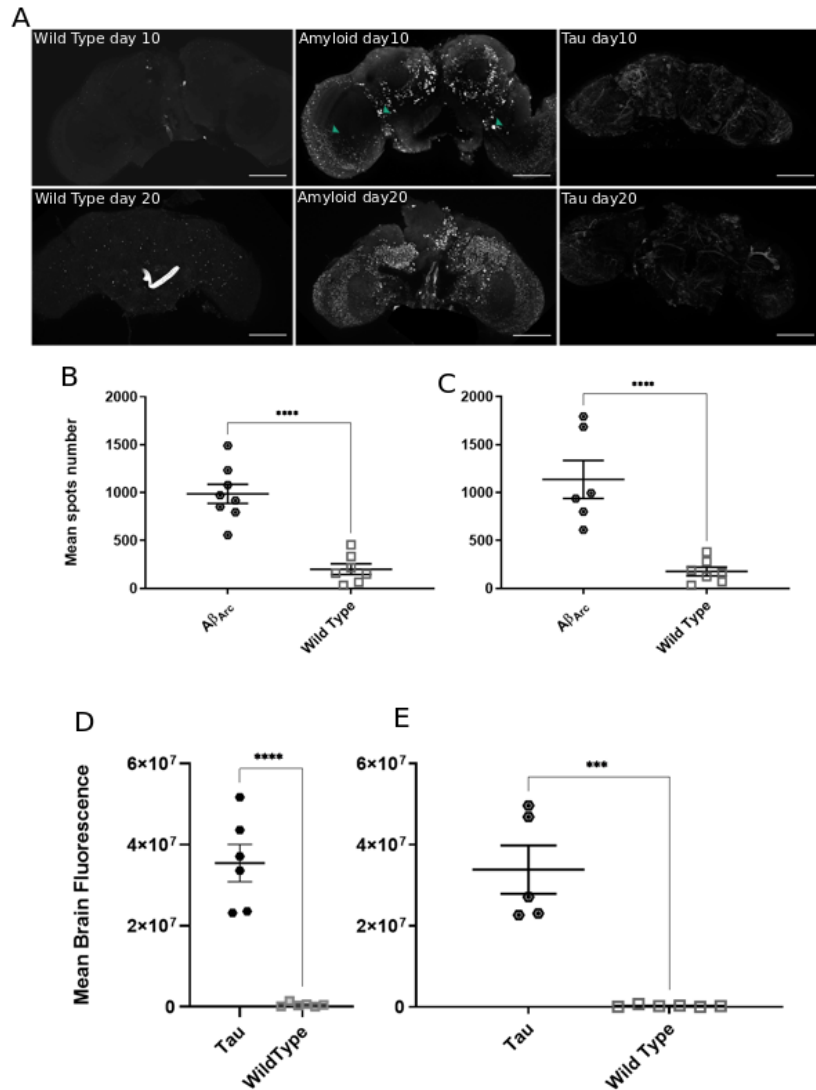


Figure 5. Effects of Tau and Aβ_{arc}-peptides expression on CNS

A) Confocal representative images of *Drosophila melanogaster* expressing either Tau, or Aβ_{arc}-peptides (arrow indicates amyloid spots), at 10 and 20 days post eclosion. Scale bar 100μm **B)** Whole brain quantification of amyloid spots at 10 days post eclosion in Aβ_{arc} flies. Mann-Whitney test was used to compare the differences between two different groups, P<0.05 was considered as significant. **C)** Whole brain quantification of amyloid spots at 20 days post eclosion in Aβ_{arc} flies. Mann-Whitney test was used to compare the differences between two different groups, P<0.05 was considered as significant. **D)** Whole brain quantification of immunostaining intensity at 10 days post eclosion in Tau flies. Mann-Whitney test was used to compare the differences between two different groups, P<0.05 was considered as significant. **E)** Whole brain quantification of immunostaining intensity at 20 days post eclosion in Tau flies. Mann-Whitney test was used to compare the differences between two different groups, P<0.05 was considered as significant. Data is presented as mean ± SEM. n = 3 , with a minimum of 5 animals per experiment analysed. * P<0.05; **P<0.01; *** P<0.001; ****P<0.0001.

3.3 Discussion

Drosophila melanogaster is a powerful and efficient *in vivo* model of a number of human diseases, such as Parkinson's, cancer and AD (Feany *et al.* 2000; Rudrapatna *et al.* 2012; Tue *et al.* 2020). Because of the defined lifespan, behaviour and easily accessible CNS, *Drosophila* models of neurodegenerative diseases can serve as quick *in vivo* tools for initial screening of compound libraries. Previously reported *Drosophila* models have relied on the expression of either A β ₄₂, or Tau, in order to study the pathophysiological effects of these two crucial hallmarks in AD progression (Cornelison *et al.* 2019; Nepovimova *et al.* 2014).

Our results indicate that the expression of the A β peptides harbouring the Arctic mutation, as well as the expression of human Tau isoform 2N4R, lead to the development of *Drosophila* models characterised by a symptomatology similar to that described in human patients. Both Tau and A β _{arc} flies recorded the most severe reduction in survival time when compared to the wild type control. In addition to this, Tau and A β _{arc} flies have shown significant reduction of their locomotive functions, whilst TBA and A β ₄₂ did not. Moreover, expression of Tau (at both 25°C and 29°C) and A β _{arc} (at 29°C only) in the ommatidia resulted in a REP. In contrast, TBA and A β ₄₂ flies did not develop any REP, further suggesting that the expression of these transgenes was not suitable to develop a reliable AD model.

To further characterise the selected genotypes as AD models, we investigated the protein deposition features present in the fly CNS at multiple time points. We successfully detected deposition of amyloid plaques, as early as 10 days post-eclosion in A β _{arc} flies, with the same trend being recorded at 20 days post-eclosion. Tau flies,

showed a significant increase in phosphorylation levels on S396, at both time points when compared to the wild type control.

To summarize, we have screened different human AD transgene expression in *Drosophila melanogaster*, and evaluated multiple parameters related to the human symptomatology. The expression of mutant A β peptides and Tau 2N4R has led to the development of fruit fly AD models, which symptoms and neuroanatomical features have been quantified. In addition to this, we provided a novel time recorded analysis for amyloid deposition and Tau hyperphosphorylation.

The characterised parameters of A β_{arc} and Tau *Drosophila* can be used to evaluate the efficacy of compound library for initial *in vivo* evaluation as potential AD therapy.

4 XJP-1 treatment ameliorates amyloid-induced symptomatology in A β _{arc} flies

4.1 Introduction

The brain of AD patients is characterised by the presence of amyloid plaques, which are recognised as one of the key hallmarks for this disorder. They are formed of amyloid β -peptides, secreted by neurons, which form insoluble toxic aggregates that lead to local neuroinflammatory and neurodegenerative responses (Gouras *et al.* 2005; Meyer-Luehmann *et al.* 2008). ~~The amyloidogenic pathway can generate amyloid β -peptides of various lengths, ranging from 17–42aa. Sequential cleavages of the amyloid precursor protein performed by β - and γ -secretase, is required to generate neurotoxic A β peptide, which is primarily 40 or 42aa in length (Yan *et al.* 1994; Pike *et al.* 1993).~~ To date, the mechanism activating the amyloidogenic pathway is still unknown, with the exception of genetic mutations causing familial AD (Trambauer *et al.* 2020).

In particular mutation in *APP* gene, such as the Swedish (Lys595Asn), London (Val717Ile), and Arctic (Glu693Gly), are known to cause early-onset AD (Shin *et al.* 2010; Talarico *et al.* 2010; Nilsberth *et al.* 2001). The *APP* gene harbouring the Arctic mutation, is known to cause severe cognitive and locomotive defects, along with accumulation of amyloid plaques since early stages of AD (Basun *et al.* 2008; Norlin *et al.* 2012). In addition, A β peptides bearing the Arctic mutation are known to have a faster aggregation rate, compared to the wild type form, resulting in a rapid formation of protofibrils, which are known to be severely synaptotoxic (Johansson *et al.* 2006; O'Nuallain *et al.* 2010).

Despite not a clear link between cholinergic network and amyloid cascade, several reports highlight the involvement of the cholinergic system in AD pathogenesis and progression (Hampel *et al.* 2018).

According to the cholinergic hypothesis, a drop in the level of cholinergic markers, acetylcholine and acetyl-transferase, is the starting point of AD pathogenesis in the brain. Furthermore, depletion of acetylcholine is linked with an aberrant vasomotor control of the BBB, leading to a defective clearance of the amyloid peptides (Hunter *et al.* 2012).

Thus, targeting acetylcholinesterase for AD therapy is still a promising route, due to strong evidence linking AChE enzyme to amyloid aggregation (Nepovimova *et al.* 2014; Inestrosa *et al.* 1996; Jiang *et al.* 2019). It has been suggested that AChE facilitates amyloid aggregation by acting as a nucleation point, in particular the PAS is strongly linked with this function (Lushchekina *et al.* 2017). Thus, the development of new AChE inhibitors, able to both increase the level of acetylcholine, therefore improve cognitive symptomatology, and also reduce the available AChE surface for amyloid interaction, and subsequent aggregation, remain an open challenge.

The FDA has also approved an NMDAR antagonist, named Memantine, as an AD therapy. Several reports have highlighted the involvement of the glutamatergic system in AD disease progression (Tayeb *et al.* 2012). Memantine is as well administrated in combination with Donepezil in patients with severe cases of AD, therapy named Namzaric, despite some disagreeing reports on the further beneficial effects of this combined therapy (Parsons *et al.* 2013).

.

4.1.1 Experimental aim

Following the characterization of the *Drosophila melanogaster* AD model expressing the mutant amyloid peptide harbouring the Arctic mutation, we have evaluated the efficacy on the induced symptomatology of the novel AChE inhibitor XJP-1 after reports of efficacy *in vitro* (Wang *et al.* 2015; Wang *et al.* 2018).

We have exploited the same $A\beta_{arc}$ *Drosophila* model to evaluate the efficacy of all the currently approved FDA therapy on this particular model, in order to further compare the results obtained from our drug candidate to the drugs used at various stages of AD.

4.1.2 Experimental procedures

This chapter describes the data collected using 4 experimental procedures as follows:

- 1- Efficacy evaluation of all therapies studied in improving $A\beta_{arc}$ flies survival time.
- 2- Effects of therapies studied on amyloid-induced locomotive defects.
- 3- Quantification of CNS amyloid spots after treatments at multiple time points.
- 4- Evaluation of amyloid peptides aggregation rate in presence of AChE enzyme alone, and with AChE inhibitors.

4.2 Results

4.2.1 XJP-1 treatment improves life expectancy in $A\beta_{arc}$ flies

In order to find the appropriate dosage to treat flies, we attempted to replicate previous published result in which Donepezil was administrated at 30 μ M dosage to treat AD *Drosophila* model (Zhang, Wang, *et al.* 2016).

$A\beta_{arc}$ flies treated with 30 μ M Donepezil, did not show any significant increase of the survival time, with the same results being replicated at 0.2mM and 0.4mM (Fig.S1 A, B). We then decided to further increase the Donepezil concentration to 0.5mM, which resulted in a significant improvement of $A\beta_{arc}$ flies survival time (Fig.S1 A, B).

To understand whether this would be replicated by XJP-1, $A\beta_{arc}$ flies were treated with 0.5mM and 0.4mM concentration of the novel compound. However, XJP-1 treatment at these concentrations resulted in a toxic effect, with a drop of the survival time

Figure 6. A β_{Arc} flies lifespan under different treatment

A) Kaplan-Meier survival trajectories of A β_{Arc} flies under different drug treatments. **B)** Mean survival time of A β_{Arc} flies on different treatments. Kuskar-Wallis test followed by Dunn's post-hoc was used to compare the differences between different groups. Data are expressed as mean \pm SEM, n = 3 with a minimum of 100 animal per experiment. P<0.05 was considered as significant. * P<0.05; **P<0.01; *** P<0.001; ****P<0.0001.

4.2.2 XJP-1 treatment improves locomotive functions in A β _{arc} flies

The climbing assay is a behavioural test, based on negative geotaxis against gravity, which is used to assess locomotive functions in *Drosophila* (Au - Nichols *et al.* 2012). A β _{arc} flies recorded a time-dependent worsening of climbing ability, thereby faithfully recapitulating symptoms observed in human patients (Fig.7 A).

Inhibition of AChE enzyme by XJP-1 resulted in a significant amelioration of the locomotive symptomatology in A β _{arc} flies (Fig.7 B). In addition to this, among the FDA approved therapies only Donepezil treatment showed results comparable to XJP-1 (Fig.7 C). On the other hand, Rivastigmine, Galantamine and Memantine treatment did not result in a constant beneficial effect on locomotive functions, as seen in flies treated with XJP-1 and Donepezil (Fig.7 D-F). Following the same trend, flies treated with combined therapies did not show any significant improvement when compared to untreated A β _{arc} *Drosophila*, and worst results when compared to XJP-1, Memantine, and Donepezil monotherapies (Fig.7 G-H).

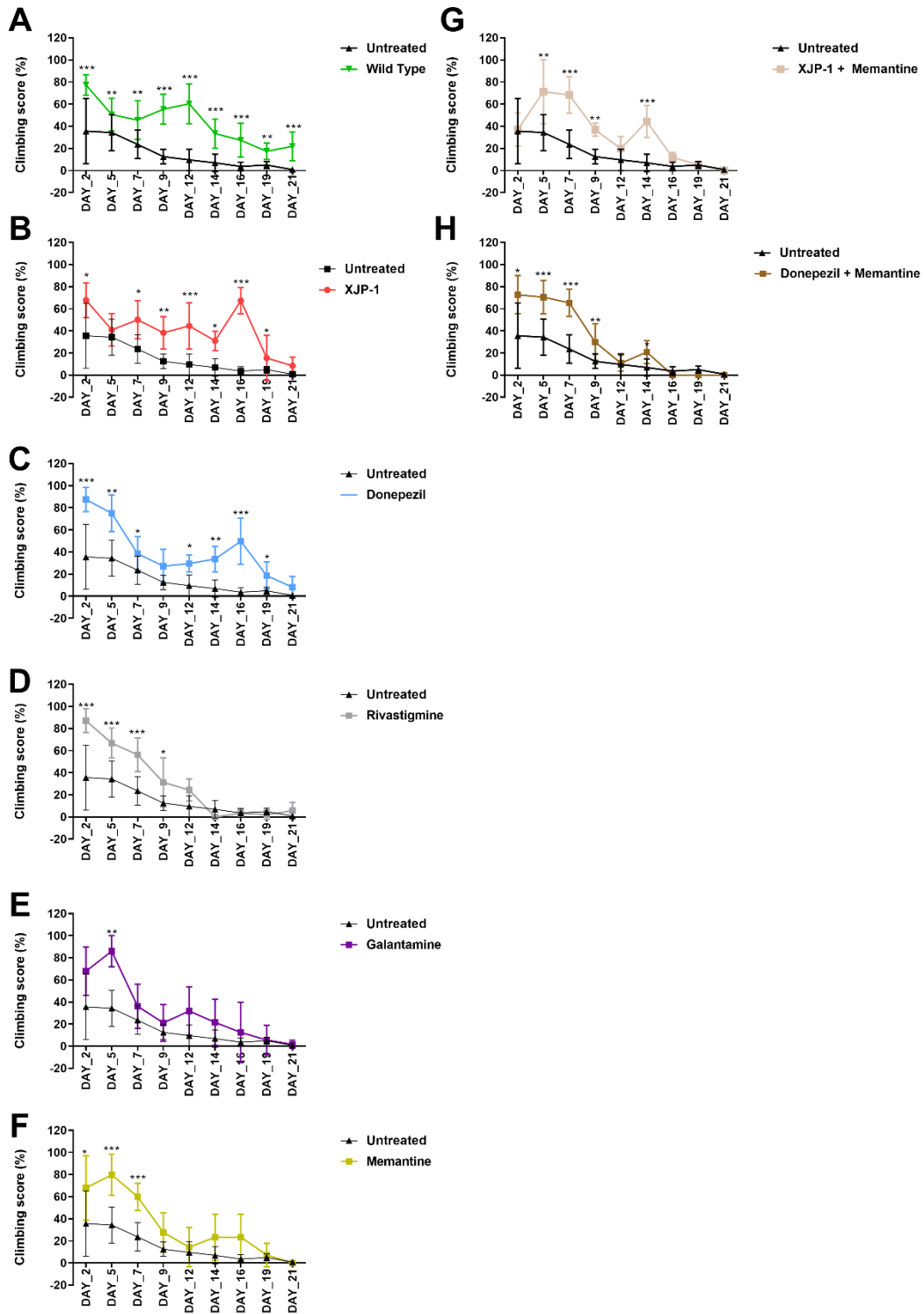


Figure 7. Treated A β _{arc} flies climbing assay

A β _{arc} flies climbing assay under different treatments. Data shows the climbing performance trends over a 21 day period. Data generated from the climbing index was processed as a percentage of the total. In order to compare vials with a different number of flies, repeated measures analysis of variance was used to compare climbing scores between treated and untreated groups. **A)** Climbing assay of A β _{arc} flies untreated. **B)** Climbing assay of A β _{arc} flies

XJP-1 treated. **C)** Climbing assay of A β_{arc} flies Donepezil treated. **D)** Climbing assay of A β_{arc} flies Rivastigmine treated. **E)** Climbing assay of A β_{arc} flies Galantamine treated. **F)** Climbing assay of A β_{arc} flies Memantine treated. **G)** Climbing assay of A β_{arc} flies XJP-1 and Memantine treated. **H)** Climbing assay of A β_{arc} flies Donepezil and Memantine treated. Data presented in the figure as the mean \pm SD. n = 3 (number of independent experiments, each experiment, with a minimum of 10 animals per treatment). P<0.05 was considered as significant. * P<0.05; **P<0.01; *** P<0.001; ****P<0.0001.

4.2.3 XJP-1 reduces the number of amyloid plaques in the brain

The deposition, accumulation, and aggregation of amyloid peptides in the CNS is a crucial point in the development of Alzheimer's symptomatology. Using confocal microscopy, we found that A β_{arc} fly brains to possess large and extensively distributed amyloid spots at 10 days post-eclosion (Fig.8 A). To understand whether treatment with XJP-1, or commercially available therapies, would result in any change in amyloid pathology in the CNS, we imaged A β_{arc} fly brains following 10 days of treatment (Fig.8 A). Subsequent quantification showed a significant reduction in amyloid spots count in flies treated with either XJP-1, or XJP-1 and Memantine combined. None of the commercially approved therapies had comparable results to the new AChE inhibitor (Fig.8 B). To further investigate whether there was a remarkable difference in amyloid spots count in those brain areas rich in cholinergic neurons, we exploited the Fly Brain Observatory software to determine areas of the brain that are rich in cholinergic neurons. We found that mushroom bodies (Fig. 9A), fan-shaped bodies (Fig.9 B), Medulla (Fig. 9 C), and Optic Lobes (Fig. 9 D), were rich in cholinergic neurons compared to other areas such as Antennal Lobes (Fig.9 E) and subesophageal ganglion (Fig.9 F) (Xu *et al.* 2020). Analysis of Mushroom body and Fan-shaped body areas recorded a significant reduction of amyloid spots in flies treated with both XJP-1 monotherapy, and XJP-1 and Memantine combined therapy (Fig.8

C). Conversely, none of the treatments tested had a beneficial impact on the Medulla and Optic lobe amyloid spots count (Fig.8 D).

To assess whether AD progression alters these amyloid spots count results, we also analysed the $A\beta_{arc}$ flies brains at 20 days post-eclosion (Fig.10 A). The whole brain analysis showed a significant reduction of the amyloid spots count, similar to that observed at 10 days, in flies treated with XJP-1, Donepezil, and Memantine, whilst Galantamine and Rivastigmine failed to show any significant effect (Fig.10 B). The same reduction trends were recorded in the Mushroom bodies and Fan-Shaped bodies (Fig.10 C). Although none of the treatments tested reduced the amyloid spot counts in the Medulla and Optical Lobes areas after 10 days (Fig.10 D), analysis of samples treated for 20 days showed a significant decrease in the amyloid spot levels for all treatment tested, with exception of Galantamine and Rivastigmine (Fig.10 D). The combined therapies investigated however, did not show any further beneficial effects than the single therapies (Fig.S2 B-G).

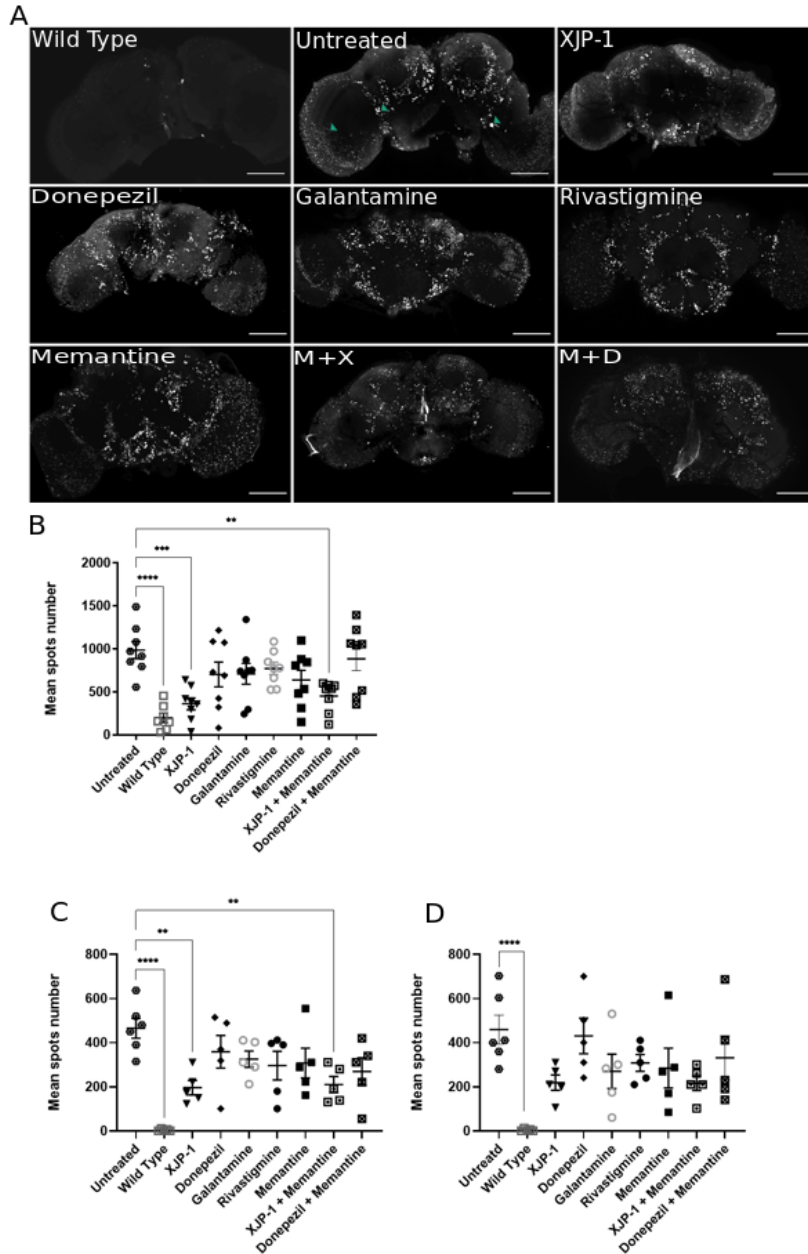


Figure 8. Amelioration of amyloid spots in A β arc flies CNS after 10 days of treatment.

A) Representative confocal images of WT (top left panel) or A β arc brains; arrows show amyloid spots; scale bar: 100 μ m. **B)** Whole brain quantification of amyloid spots. ANOVA test followed by Bonferroni's post hoc was used to compare the differences between three or more groups, $P < 0.05$ was considered as significant. **C)** Mushroom body and fan-shaped body quantification of amyloid spots. ANOVA test followed by Bonferroni's post hoc was used to compare the differences between three or more groups, $P < 0.05$ was considered as significant. **D)** Medulla and Optic lobe quantification of amyloid spots. ANOVA test followed by Bonferroni's post hoc was used to compare the differences between three or more groups, $P < 0.05$ was considered as significant. Data are presented as mean \pm SEM. $n = 3$, with a

minimum of 1 animal per experiment analysed. * $P < 0.05$; ** $P < 0.01$; *** $P < 0.001$;
**** $P < 0.0001$.

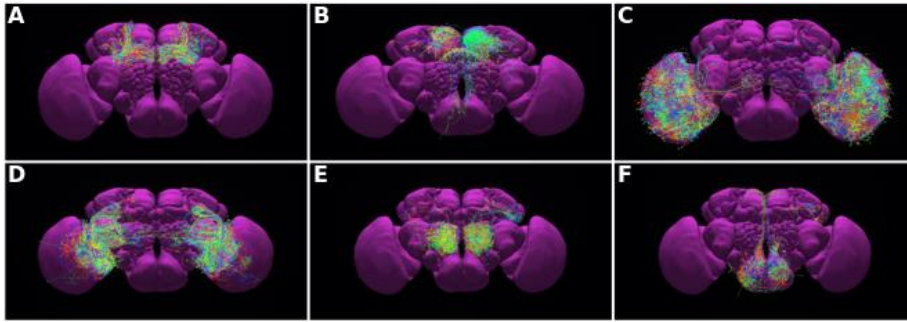


Figure 9. Representative images of cholinergic neurons network in *Drosophila Melanogaster* brain obtained from the Virtual Fly Observatory

A) Cholinergic neurons within the mushrooms bodies. **B)** Cholinergic neurons within the fan-shaped bodies. **C)** Cholinergic neurons within the medulla. **D)** Cholinergic neurons within the optic lobes. **E)** Cholinergic neurons within the antennal lobes. **F)** Cholinergic neurons within the subesophageal ganglion.

The different colours observed in the image do not highlight any difference among neurons. The different colour pattern is used to discriminate between individual neurons.

A

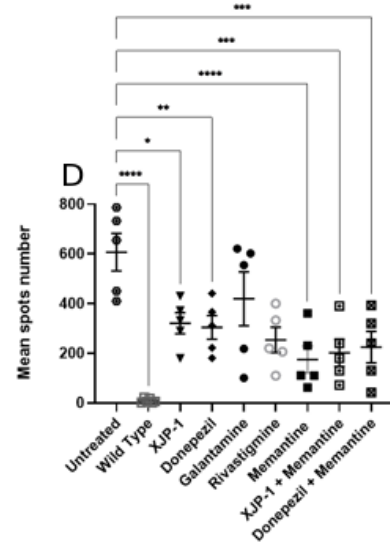
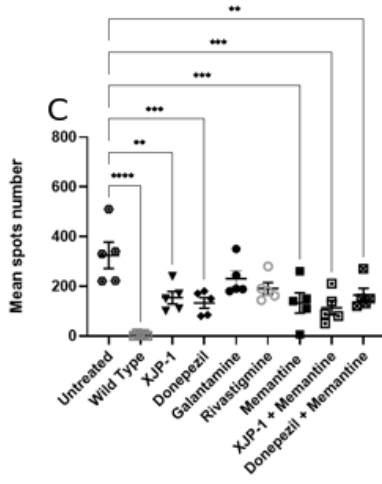
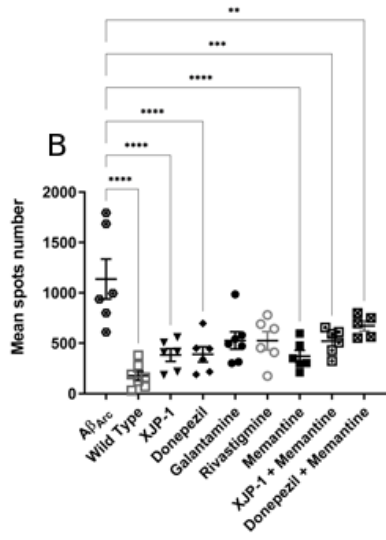
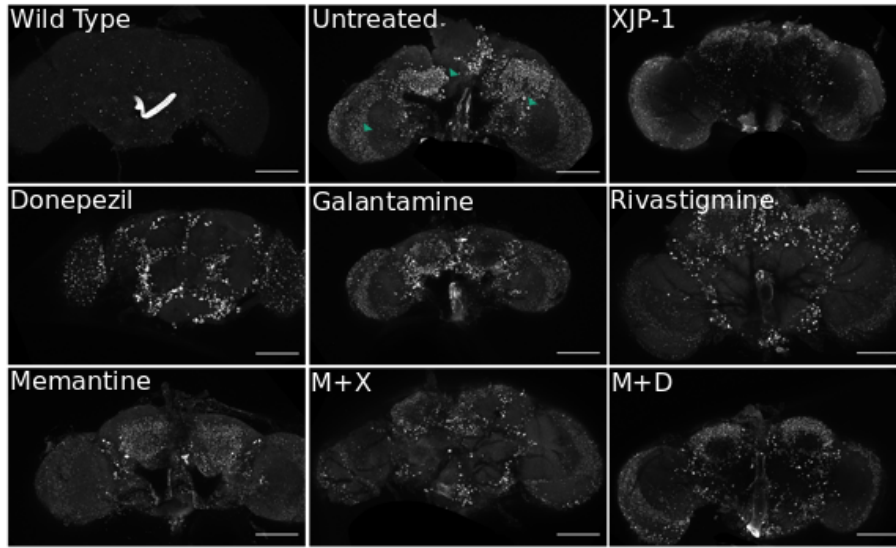


Figure 10. Amelioration of amyloid spots in A β arc flies CNS after 20 days of treatment

A) Representative confocal images of WT (top left panel – bright mark is a gastroesophageal residue carried during dissection) or A β arc brains; arrows show amyloid spots; scale bar: 100 μ M. Bright central spot is a gastroesophageal residue carried during dissection **B)** Whole brain quantification of amyloid spots. ANOVA test followed by Bonferroni's post hoc was used to compare the differences between three or more groups, $P < 0.05$ was considered as significant. **C)** Mushroom body and fan-shaped body quantification of amyloid spots. ANOVA test followed by Bonferroni's post hoc was used to compare the differences between three or more groups, $P < 0.05$ was considered as significant. **D)** Medulla and Optic lobe quantification of amyloid spots. ANOVA test followed by Bonferroni's post hoc was used to compare the differences between three or more groups, $P < 0.05$ was considered as significant. Data are presented as mean \pm SEM. $n = 3$, with a minimum of 1 animal per experiment analysed. * $P < 0.05$; ** $P < 0.01$; *** $P < 0.001$; **** $P < 0.0001$.

4.2.4 XJP-1 reduces amyloid aggregation via AChE inhibition

To confirm that the observed reduction in amyloid spot aggregation was not a result of a reduced quantity of amyloid peptides within the $A\beta_{arc}$ fly brains, we quantified amyloid peptide expression following 10 and 20 days of treatment. At both time points, and for all drug treatments, amyloid peptide expression was statistically similar to untreated brains (Fig.S3 A-D). This result was expected since the expression of the transgene is determined by the UAS/Gal4 system and is not targeted by any of the drugs studied. We hypothesized that the AChE enzyme was functioning as a nucleation point for amyloid peptide aggregation, as previously reported (Inestrosa *et al.* 1996; Rees *et al.* 2003; Lushchekina *et al.* 2017).

We used an *in vitro* assay to evaluate $A\beta_{arc}$ peptides aggregation rate in presence of AChE enzyme and inhibitors.

$A\beta$ peptides carrying the Arctic mutation were co-incubated with AChE enzyme in presence, or not, of all the AChE inhibitors tested as therapy, or as combined therapy. We found a significant drop in all treatments studied, with the greatest reductions observed for XJP-1 and Donepezil, both recording an almost 80% decrease in aggregation rate (Fig.11). Once again, the combined therapies did not result in any further decrease in amyloid aggregation rate (Fig.11).

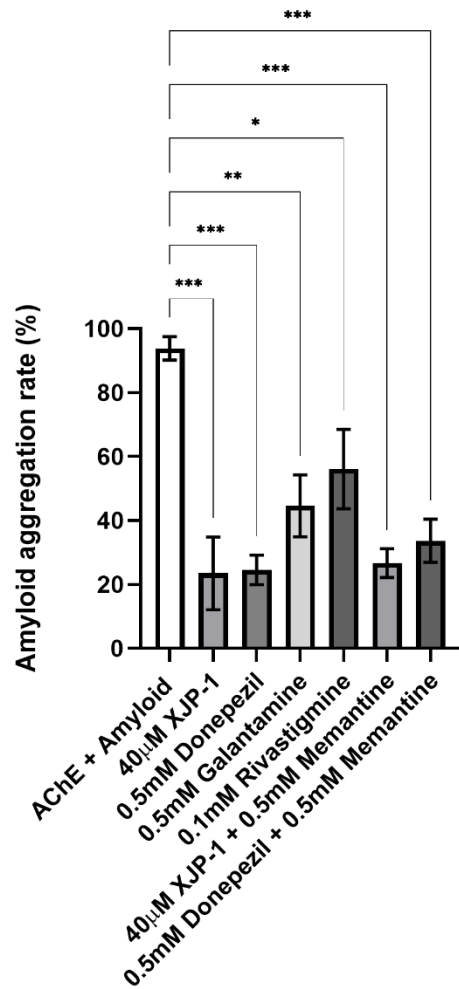


Figure 11. Reduction of AChE-induced A β -peptide aggregation rates in the presence of AChE Inhibitors

ANOVA test followed by Bonferroni's post hoc was used to compare the differences between three or more groups. Data are presented as mean \pm SEM of n = 3. * P<0.05; **P<0.01; *** P<0.001; ****P<0.0001.

4.3 Discussion

Over the past 10 years, the fruit fly has emerged as a powerful *in vivo* model for neurodegenerative diseases, including AD (Tue *et al.* 2020; Ali *et al.* 2019; Hwang *et al.* 2019; Cornelison *et al.* 2019; Miyazaki *et al.* 2019; Higham *et al.* 2019; Sivanantharajah *et al.* 2019; Pham *et al.* 2018; Zhang, Li, *et al.* 2016). Transgenic *Drosophila* AD models have been employed as a model organism for a number of drug

testing studies involving different targets such as AChE, GSK-3 β , lysozyme, Tau protein and dopaminergic receptors. (Miyazaki *et al.* 2019; Sandin *et al.* 2016; Pham *et al.* 2018; Zhong *et al.* 2019; Hwang *et al.* 2019; Zhang, Li, *et al.* 2016; Ali *et al.* 2019). In the work described in this chapter, we demonstrated the capacity of a new compound, XJP-1, to reduce amyloid- β aggregation, and consequent amelioration of the behavioural phenotype in the A β_{arc} transgenic *Drosophila* AD model.

Further to this, we have tested all commercially available therapies, including combined therapy Donepezil and Memantine, showing that XJP-1 treatment results in a better, or comparable, improvement of AD symptomatology at a much lower concentration than the FDA approved therapies.

XJP-1 treatment resulted in an overall improvement of the amyloid induced defects, with an increase of mean survival time of about 13 days, and an amelioration of the locomotive functions throughout the entire assay time. The benefits observed in the amyloid-derived symptomatology are the results of the reduction of amyloid plaques within the *Drosophila* brain, because of the potent drop in amyloid aggregation rate induced by AChE enzyme in presence of XJP-1. Flies treated with Donepezil obtained similar results, except for the 10 days analysis of amyloid spots count where this treatment did not result in any significant difference. Other than that, our results also show a discrepancy from already published work, in which Donepezil was claimed to effectively improve transgenic AD *Drosophila* at a concentration as low as 30 μ M (Zhang, Wang, *et al.* 2016; Zhang, Li, *et al.* 2016; Shin *et al.* 2020)

XJP-1 and Memantine combined treatment did not result in a further significant improvement when compared to XJP-1 treatment alone, as well as Donepezil and Memantine therapy, which did not result in any further improvement when compared to the monotherapy. It has to be clarified that combined therapy is usually only given to patients when they enter an advanced stage of the disease, when Memantine is added to patients already on Donepezil therapy (Tayeb *et al.* 2012; Parsons *et al.* 2013).

In this study, all drugs were administrated continuously from 24 hours upon eclosion, including combined therapies, giving a possible explanation on why Donepezil with Memantine, and XJP-1 with Memantine, did not show any further beneficial effect, when compared to single therapy on this AD model. This highlighted limitation may explain as well, the poor efficacy of Galantamine and Rivastigmine compared to Donepezil, as they are currently prescribed to Alzheimer's patients with mild to moderate stages of AD, whilst Donepezil is given to AD patients at all stages of the disease, from mild to severe (Haake *et al.* 2020).

Our study has shown a clear involvement of AChE inhibition on amyloid aggregation resulting in a symptomatology amelioration. The effect of XJP-1 on A β_{arc} transgenic flies were partially replicated only by Donepezil at a concentration 10 times higher than our drug candidate, with XJP-1 having better results in reducing the amyloid spots count after 10 days of treatment. Other than that, the other FDA approved AChE inhibitors, Galantamine and Rivastigmine, reduced the amyloid aggregation rate of about 50%, whilst XJP-1 and Donepezil reduced it of about 80%, giving a potential explanation for the limited beneficial effects observed in A β_{arc} flies treated with Galantamine and Rivastigmine.

Docking studies carried out on XJP-1 showed a dual-binding property for both the peripheral anionic site (PAS) and catalytic active site (CAS) of AChE enzyme (Wang *et al.* 2015), which may further explain the low dosage needed to slow down the amyloid aggregation, since the PAS of AChE has been linked to increase A β -peptides aggregation rate (Inestrosa *et al.* 1996). Despite not being tested in this study, XJP-1 was predicted to have anti-inflammatory and anti-oxidant properties (Wang *et al.* 2018; Wang *et al.* 2015), which may have as well played a role in ameliorating the AD symptomatology in A β_{arc} flies.

5 AChE inhibition by XJP-1 treatment does not result in reduction of Tau phosphorylation in *Drosophila melanogaster* AD model

5.1 Introduction

AD and related dementias are characterised by the presence of neurofibrillary tangles, as a result of the abnormal phosphorylation of Tau protein (Bloom 2014). The latter is a MAP encoded by the *MAPT* gene, which contains a number of different residues potentially target of post-translational modifications (Götz *et al.* 2019). Tau protein serves as microtubule stabilizer, by promoting tubulin polymerization, which in neurons plays crucial role in axon morphology and axonal transport (Kadavath *et al.* 2015). In a number of different neurodegenerative diseases, Tau protein undergoes a number of post-translational modifications, in particular phosphorylation, leading to a loss of affinity to the microtubules, which results in a loss of microtubule architecture and axon morphology in neurons (Götz *et al.* 2019).

To study this neuroanatomical feature, *Drosophila Melanogaster* was successfully exploited to develop several AD model of Tau hyperphosphorylation, by expressing human Tau isoform 2N4R in a *pan*-neuronal manner (Cornelison *et al.* 2019; Higham *et al.* 2019; Sivanantharajah *et al.* 2019; Sun *et al.* 2015).

Moreover AD *Drosophila* models have been used to investigate drug efficacy and to perform drug screening to target Tau toxicity and hyperphosphorylation, which results can be easily translated to higher species due to the highly conserved pathways involved in these processes (Kizhakke P *et al.* 2019; Pham *et al.* 2018; Zhang, Li, *et al.* 2016).

5.1.1 Experimental aim

As described in the previous chapter, we have successfully proved XJP-1 efficacy in ameliorating AD symptomatology in $A\beta_{arc}$ flies. In addition to this, we have demonstrated that XJP-1 treatment results in a reduction of amyloid spots in the fruit fly brain.

Other than that, we successfully proved that AChE inhibition resulted in a slower $A\beta$ peptides aggregation rate, giving a possible explanation for the reduction of amyloid spots within the $A\beta_{arc}$ flies.

Because of these findings, we decided to further investigating the effects of XJP-1 treatment on another important AD hallmark, Tau hyperphosphorylation.

The latter plays a crucial role in exacerbating AD cognitive symptomatology, and it is responsible of several other dementias known as tauopathies. In addition to this, AChE inhibition was reported to inhibit GSK3- β driven Tau hyperphosphorylation (Noh *et al.* 2009; Yoshiyama *et al.* 2010).

Thus, we decided to investigate the effects of XJP-1 treatment, and FDA approved therapies, by exploiting the Tau *Drosophila* model we have developed as described in Chapter 3.

5.1.2 Experimental procedures

This chapter describes the data collected using 4 experimental procedures as follows:

- 1- Efficacy evaluation of all therapies studies in improving Tau flies survival time.
- 2- Effects of therapies studied on hyperphosphorylated Tau-induced locomotive defects.

- 3- Quantification of phosphorylated S396 immunostaining signal at multiple time points after treatment.
- 4- Investigation on the ability of all therapies studied in preventing REP derived by the expression of human Tau 2N4R.

5.2 Results

5.2.1 XJP-1 treatment improves Tau flies lifespan, but does not result in improved locomotive functions

Expression of human 2N4R isoform of Tau protein resulted in a significant drop in *Drosophila* survival time as previously described (Fig.2 A, B). To investigate the effects of the new AChE inhibitor XJP-1, Tau flies were fed with food containing a final 40 μ M concentration of the new compound. In order to assess the effects of the FDA therapies on this *Drosophila* model, separated groups of Tau flies were fed with the commercially available AD therapies.

Flies fed with food containing a final 40 μ M concentration of XJP-1 recorded a significant increase in survival time when compared to the untreated group (Fig.12 A, B). A similar trend was recorded for Tau flies treated with 0.5mM Donepezil, and 0.5mM Galantamine. On the other hand, Rivastigmine and Memantine treatment, administrated at 0.1mM and 0.5mM respectively, did not results in a significant increase of Tau flies lifespan. Other than that, combined therapies Donepezil plus Memantine, and XJP-1 plus Memantine, recorded a significant increment in Tau flies survival time, despite not recording a significant difference when compared to AChE inhibitors therapy alone (Fig.12 A, B).

To assess whether XJP-1 treatment would results in an improvement of Tau flies climbing performances, a climbing assay on Tau expressing flies under different treatments was performed (Fig.13).

Following an opposite trend from the result obtained on the lifespan assay, XJP-1 treatment did not result in any significant improvement of the locomotive functions at any of the time points analysed (Fig.13 B). Donepezil, the most potent currently FDA

approved therapy for AD treatment, improved Tau flies climbing scores at only one time point analysed, day 12, and failed to produce further significant improvement of the locomotive functions (Fig.13 C). On the same trend, Memantine, Galantamine, and Rivastigmine treatment did not record any significant difference when compared to the untreated Tau flies (Fig.13 D-F).

Among the combined therapy tested, only XJP-1 plus Memantine, had a limited beneficial effect on Tau flies climbing scores, with a significant improvement being recorded at day 9 and 12 of analysis, whilst Donepezil plus Memantine did not score any significant difference from the untreated group (Fig.13 G, H)

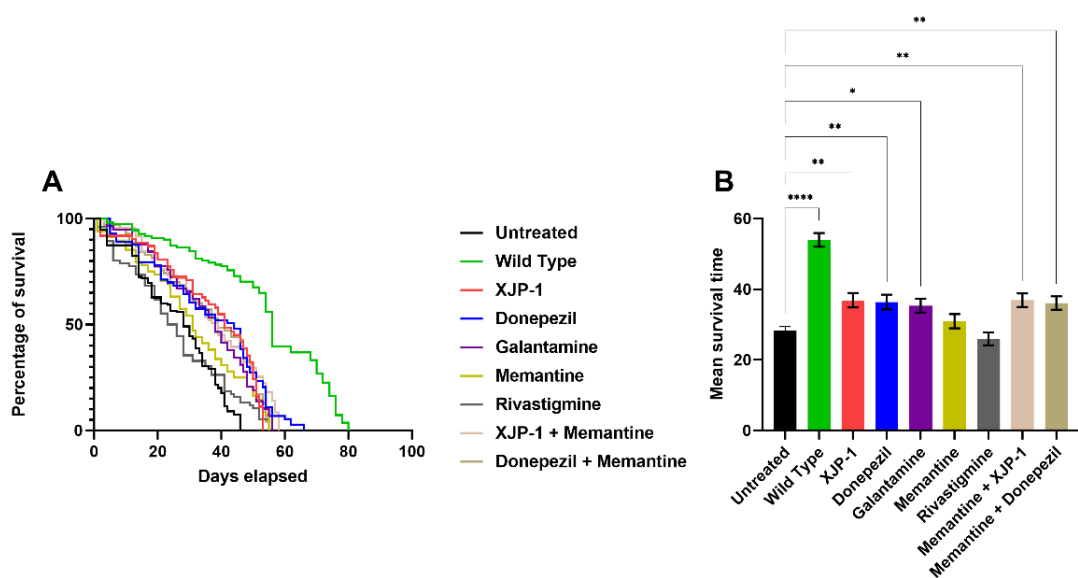


Figure 12. Tau flies lifespan under different treatment

A) Kaplan-Meier survival trajectories of Tau flies under different drug treatments. **B)** Mean survival time of Tau flies on different treatments. Kuskar-Wallis test followed by Dunn's post-hoc was used to compare the differences between different groups. Data are expressed as mean \pm SEM, n = 3 with a minimum of 100 animals per experiment. P<0.05 was considered as significant. * P<0.05; **P<0.01; *** P<0.001; ****P<0.0001.

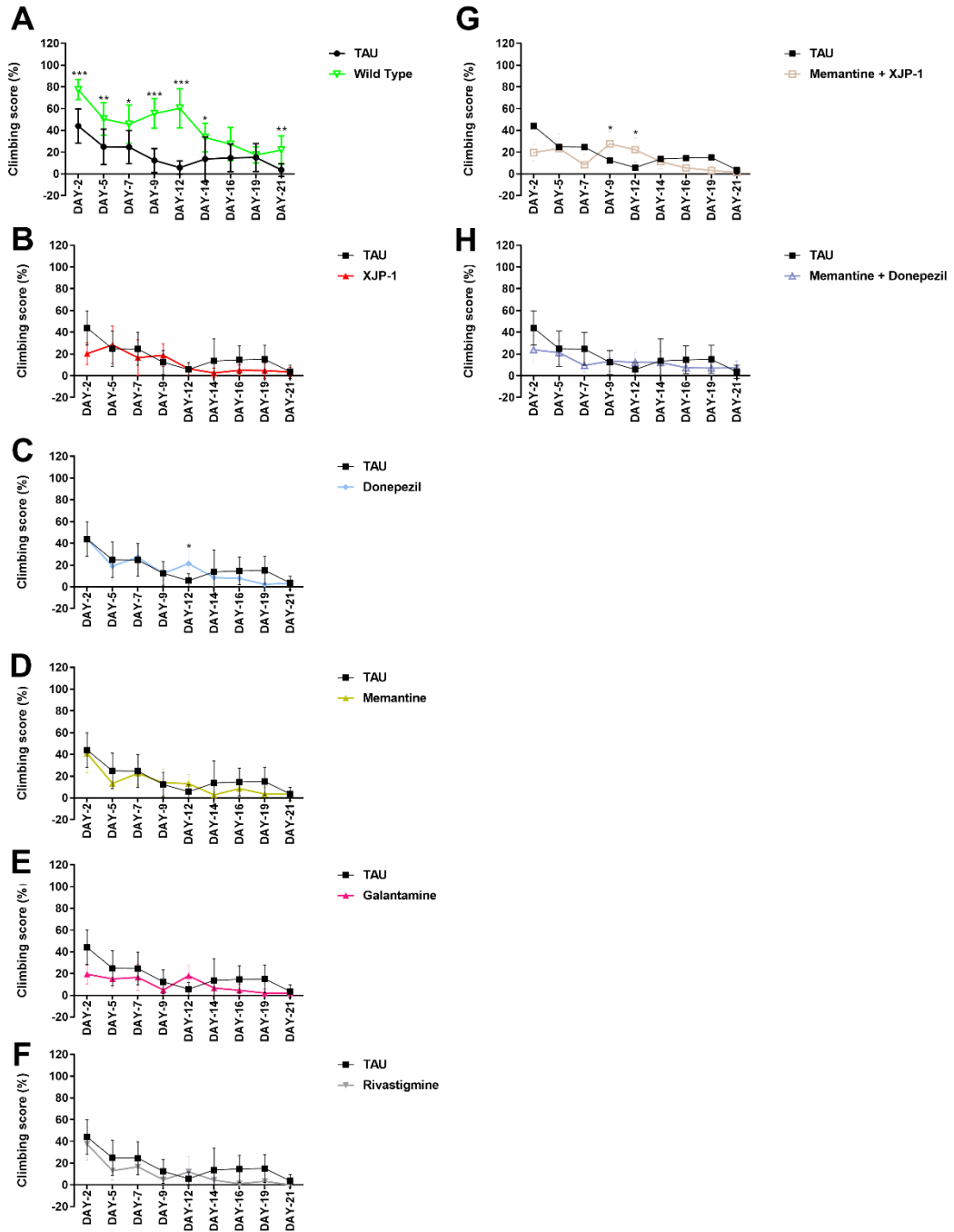


Figure 13. Treated Tau flies climbing assay

Tau flies climbing assay under different treatments. Data shows the climbing performance trends over a 21 day period. Data generated from the climbing index was processed as a percentage of the total. In order to compare vials with a different number of flies, repeated measures analysis of variance was used to compare climbing scores between treated and untreated groups. **A)** Climbing assay of Tau flies untreated. **B)** Climbing assay of Tau flies XJP-1 treated. **C)** Climbing assay of Tau flies Donepezil treated. **D)** Climbing assay of Tau flies Memantine treated. **E)** Climbing assay of Tau flies Galantamine treated. **F)** Climbing

assay of Tau flies Rivastigmine treated. **G)** Climbing assay of Tau flies XJP-1 and Memantine treated. **H)** Climbing assay of Tau flies Donepezil and Memantine treated. Data are presented in the figure as the mean \pm SD. n = 3 (number of independent experiments, each experiment, with a minimum of 10 animals per treatment). P<0.05 was considered as significant. * P<0.05; **P<0.01; *** P<0.001; ****P<0.0001.

5.2.2 Tau hyperphosphorylation in Tau *Drosophila* cannot be prevented, or reduced, by XJP-1 treatment

NTFs are a major consequence of Tau hyperphosphorylation, resulting in neurotoxicity and neuronal cells death. In order to estimate the phosphorylation levels of Tau protein within the *Drosophila* CNS, confocal microscopy was exploited to visualize phosphorylated Tau residue S396, which is considered to be a marker of the early stage of Tau hyperphosphorylation events (Foidl *et al.* 2018; Mondragón-Rodríguez *et al.* 2014).

We analysed Tau flies brain after 10 days of treatment (Fig.14 A) and recorded a significant increase in Tau phosphorylation at S396 when compared to the wild type control (Fig.14 B). Moreover, none of the treatment studied resulted in a significant reduction of the Tau phosphorylation when compared to the untreated group (Fig.14 B).

To investigate whether a continuous treatment for a longer period would result in any change in Tau phosphorylation levels, Tau flies were allowed to grow for 20 days on food containing the drugs under assessment. Confocal analysis, after 20 days, of Tau flies CNS (Fig.15 A) confirmed the same trend observed previously, with none of the therapies being able to reduce Tau hyperphosphorylation levels significantly (Fig.15 B).

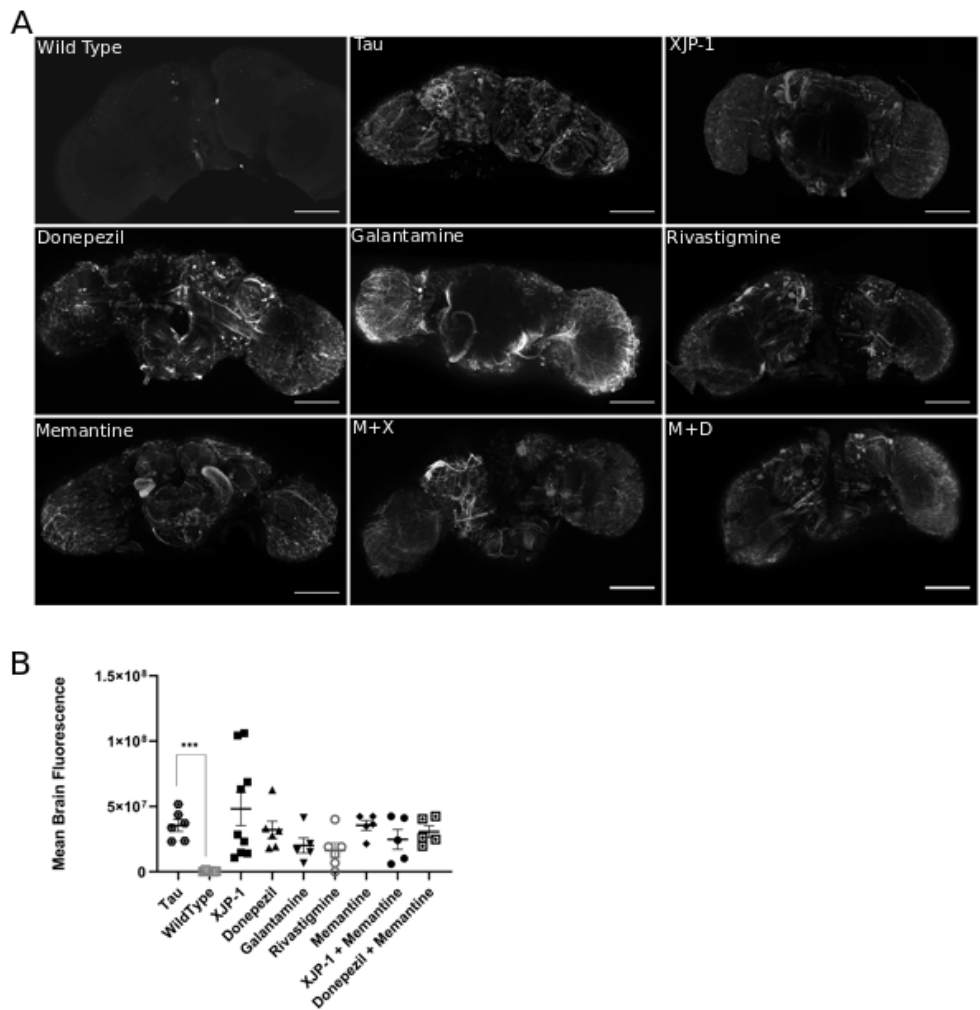


Figure 14. CNS analysis of Tau hyperphosphorylation after 10 days of treatment

A) Representative confocal images of WT (top left panel) or Tau brains; scale bar: 100µM. **B)** Whole brain quantification of Tau (phosphor S396) immunostaining signal. ANOVA test followed by Bonferroni's post hoc was used to compare the differences between three or more groups, $P < 0.05$ was considered as significant. Data are presented as mean \pm SEM. $n = 3$, with a minimum of 1 animal per experiment analysed. * $P < 0.05$; ** $P < 0.01$; *** $P < 0.001$; **** $P < 0.0001$.

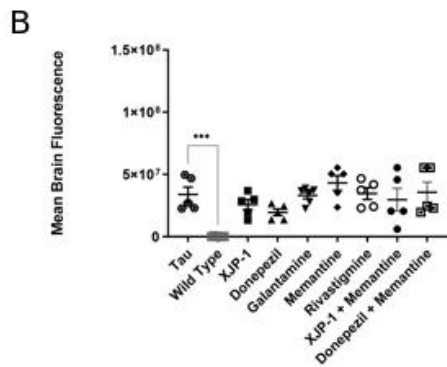
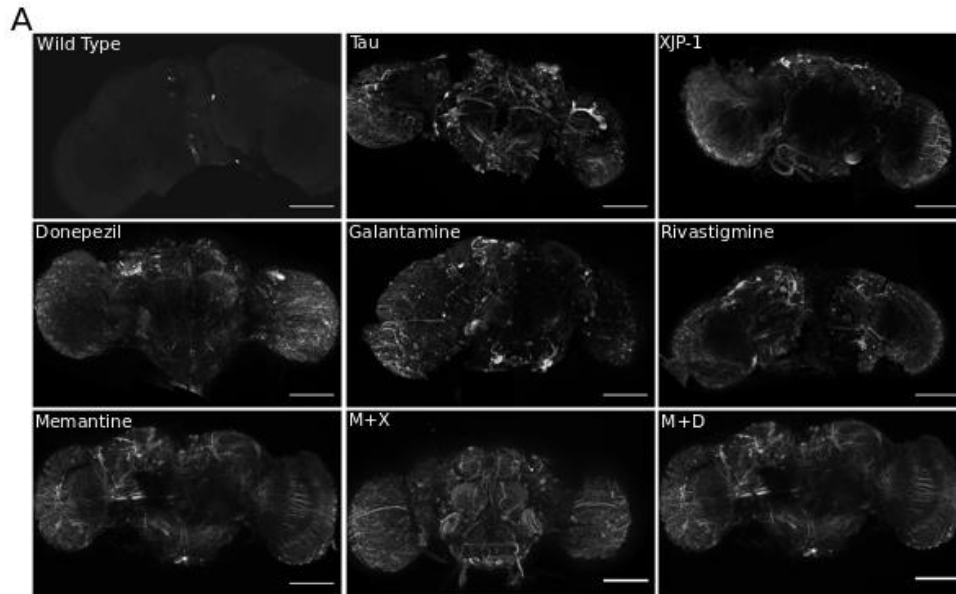


Figure 15. CNS analysis of Tau hyperphosphorylation after 20 days of treatment

A) Representative confocal images of WT (top left panel) or Tau brains; scale bar: 100 μ M. **B)** Whole brain quantification of Tau (phosphor S396) immunostaining signal. ANOVA test followed by Bonferroni's post hoc was used to compare the differences between three or more groups, $P < 0.05$ was considered as significant. Data are presented as mean \pm SEM. $n = 3$, with a minimum of 1 animals per experiment analysed. * $P < 0.05$; ** $P < 0.01$; *** $P < 0.001$; **** $P < 0.0001$.

5.2.3 XJP-1 treatment does not rescue REP induced by human Tau expression and hyperphosphorylation

After all therapies under investigation recorded negative results on CNS analysis for Tau hyperphosphorylation, we decided to assess whether a partial neuroprotection from neurodegeneration resulting after Tau aberrant phosphorylation could be achieved. To do so, we have exploited the REP induced by human Tau expression in the *Drosophila* eye. As each ommatidia is connected to 8 photoreceptor neurons, small defects in the complex architecture can be easily visualised.

Tau expression in the *Drosophila* eye results in a jeopardized structure when compared to the wild type (Fig.16). Among the drug we have assessed, only Donepezil at 0.5mM concentration completely rescued the Tau-induced phenotype. XJP-1 treatment, as well as the other FDA therapies, failed to produce any visible improvement in the ommatidia architecture (Fig.16).

Surprisingly, none of the combined therapies tested rescued the REP, a results in contrast to what we recorded with Donepezil (Fig.16).

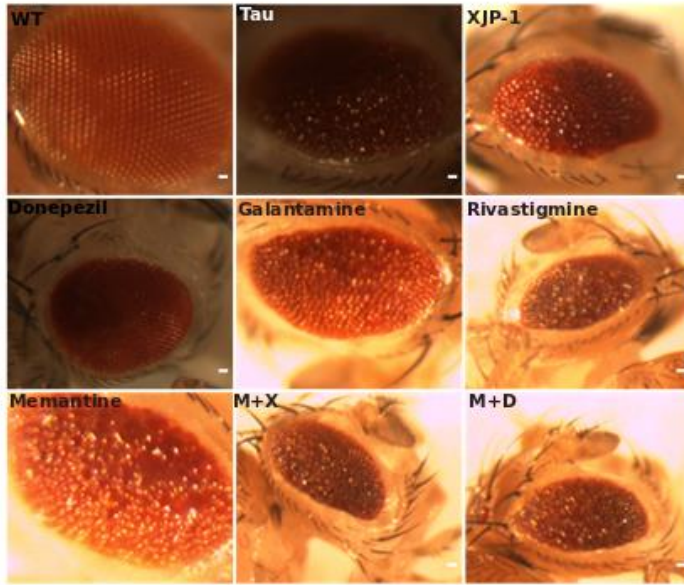


Figure 16. Treated REP images

REP images of flies under different treatment, scale bar 1mm. Visible ommatidia architecture changes were estimated by the operator. $n = 3$, with a minimum of 10 animals per experiment visualised.

5.3 Discussion

Tau abnormal phosphorylation levels, and subsequent formation of NFTs, are one of the major challenges to be tackled in order to develop an AD therapy with disease-modifying properties.

The *Drosophila* model we have generated, well recapitulated the human symptomatology, with a shortened lifespan, locomotive defects and neurodegeneration (Xia *et al.* 2017; Shinosaki *et al.* 2000). In addition to this, Tau derived pathology has been recently highlighted as potential key-player in AD symptoms exacerbation (Busche *et al.* 2019).

Treatment with novel AChE inhibitor resulted in limited beneficial effects, with significant improvements in the symptomatology recorded only in the lifespan assay. In contrast, XJP-1 failed to ameliorate the locomotive symptomatology, and to reduce Tau hyperphosphorylation in AD flies. Further assessment on neuroprotection, through REP imaging, did not show any visible improvement in the ommatidia architecture. This is in contrast with the available literature, which claims that AChE inhibition results in an amelioration of climbing function, along with reduction of Tau phosphorylation on similar Tau *Drosophila* model (Zhang, Wang, *et al.* 2016; Zhang, Li, *et al.* 2016). We hypothesize that activation of relevant ACh receptor can eventually play a role in preventing Tau aberrant phosphorylation, but this cannot be controlled using by XJP-1 administration. The inhibition of AChE enzyme results in an increased level of ACh only, without specific activation of a post-synaptic receptor, suggesting a possible explanation for the poor results obtained.

The investigation of efficacy of the FDA approved therapies on this particular model showed negative results as well, with the exception of Galantamine, Donepezil, and combined therapies studied, which therapy resulted in an increased survival time.

Despite reports of Donepezil treatment being able to inhibit GSK3- β enzyme, and reduction of Tau phosphorylation levels, we were not able to replicate these results on this particular model (Noh *et al.* 2009). In fact, Donepezil treatment rescued the REP, and increased the survival time of Tau flies only, whilst no significant reduction of Tau phosphorylation levels was recorded after both 10 and 20 days of treatment. Moreover, 30 μ M Donepezil treatment was reported to improved locomotive functions of human Tau expressing *Drosophila*, in a time period up to 40 days (Zhang, Li, *et al.* 2016). In this study, we have showed that 0.5mM Donepezil does not result in any improvement of the climbing scores.

None of the AChE inhibitors tested resulted in a drop in Tau phosphorylation, suggesting that a more specific target within Tau phosphorylation pathway is needed to ameliorate the dysfunction observed on this particular model.

6 Development and characterization of neuron-like model of AD and screening of novel AChE and dual AChE/GSK3- β inhibitors

6.1 Introduction

The identification of novel therapeutic targets able to modify the natural course, and progression, of AD is a crucial step to revert the outcome of the disease.

In this context, NFTs resulting from Tau hyperphosphorylation have been highlighted as potential target with disease-modifying properties (Tapia-Rojas *et al.* 2019; Mi *et al.* 2006). Multiple factors are involved in the triggering of Tau hyperphosphorylation, such as amyloid plaques, glucose metabolism impairment, and RAGE-pathway activation (Gasparotto *et al.* 2018; Lauretti *et al.* 2017; Bloom 2014). Despite through different pathways, all factors involved in altering Tau phosphorylation levels lead to the activation of specific kinases enzyme, or inhibition of phosphatases enzymes (Götz *et al.* 2019).

In particular, GSK3- β enzyme has been defined to be responsible of Tau phosphorylation on several residues, disrupting the protein binding affinity to microtubules (Wagner *et al.* 1996). GSK3- β is responsible of phosphorylating Tau on residue S396, which abnormal phosphorylation is considered to be an early marker of subsequent hyperphosphorylation (Foidl *et al.* 2018). GSK3- β is the downstream kinase activated by multiple pathways linked to Tau hyperphosphorylation (Zhang *et al.* 2020; Foidl *et al.* 2018; Chu *et al.* 2017; Li, Liu, *et al.* 2012; Batkulwar *et al.* 2018). Thus, targeting GSK3- β could result in the inhibition of Tau phosphorylation induced by multiple pathways in AD and, therefore, blocking the disease progression.

Further to innovative drug candidates, novel AD models are necessary. In fact, many AD models have intrinsic biases which makes it difficult to perform drug screenings. *Drosophila melanogaster* models, have been developed by overexpressing human

genes, involved in AD pathogenesis, especially mutant genes reported in familial cases of AD, despite genetic AD accounts for only 1% of the total patients (Sivanantharajah *et al.* 2019; Tue *et al.* 2020; Nikolac Perkovic *et al.* 2019). Moreover, the fruit fly model does not allow to have an homogenous dosage among different flies, since the drug is administrated within the food. Mice AD models mainly rely as well on the expression of mutant proteins present in familial forms of the disease, in addition to having a complicated route for ethical approval of any experiment (Davis *et al.* 2004). Novel approaches exploiting AD patient derived iPSC have some limitations as well, mainly due to the heterogeneity of epigenetic modification, which differ from each donor, that can be maintained after reprogramming protocols (Drummond *et al.* 2017). Cell-line SH-SY5Y has been used as cell-culture model of AD, despite bearing the crucial limitation of being constantly dividing, a feature not present in human neurons (Himeno *et al.* 2011; Yan *et al.* 1994; Shang *et al.* 2019; Da Pozzo *et al.* 2014). However, several approaches have been proposed to further improve the SH-SY5Y cell model. Different neuronal differentiation protocols have been defined using mainly retinoic acid as differentiation factor, and deprivation of FBS to enter cells in G0 phase and, therefore, preventing cells division (Shiple 2016; Agholme *et al.* 2010; Constantinescu *et al.* 2007; Korecka *et al.* 2013; Presgraves *et al.* 2003). Moreover, a number of methods exploiting undifferentiated SH-SY5Y have achieved Tau hyperphosphorylation through different mechanisms, such as hypothermia, okadaic acid administration, and glyceraldehyde exposure (Zhang and Simpkins 2010; Bretteville *et al.* 2012; Koriyama *et al.* 2015). In particular, the usage of GA to induce Tau hyperphosphorylation is of peculiar interest, since GA treatment leads to increased levels of AGEs, which receptor, RAGE, activates an important and well-studied

pathway in GSK3- β activation (Koriyama *et al.* 2015; Li, Liu, *et al.* 2012; Batkulwar *et al.* 2018).

6.1.1 Experimental aim

Our approach to target AChE enzyme with XJP-1 to treat AD has resulted in contradictory results, in which the novel inhibitor produced significant amelioration of the AD symptomatology induced by amyloid peptides overexpression, but failed on improving the AD symptomatology in Tau *Drosophila* model. To overcome this problem, Prof. Xu research group (CPU – Nanjing) has synthesized a novel dual AChE/GSK3- β inhibitor in order to reduce AChE-induced amyloid aggregation, and to prevent GSK3- β catalysed Tau phosphorylation. In addition to this, Prof. Xu provided several novel AChE inhibitors to be tested, which structure was derived from XJP-1, and have lower IC₅₀.

To better study this new molecules, we decided to develop a novel cell culture AD model by combining RA-induced differentiation of SH-SY5Y cell lines, along with GA treatment to induce Tau hyperphosphorylation (Koriyama *et al.* 2015; Shipley 2016).

6.1.2 Experimental procedures

This chapter describes the data collected from 6 different experimental procedures:

1. Differentiation of SH-SY5Y into neurons.
2. Characterization of GA treatment, at different concentration, on SH-SY5Y derived neurons morphology.
3. Characterization of GA treatment, at different concentration, on SH-SY5Y derived neurons Tau phosphorylation on residue S199 and S396.

4. Characterization of GA treatment, at different concentration, on SH-SY5Y derived neurons cells viability.
5. Characterization of novel AChE inhibitors, novel dual AChE/GSK3- β inhibitor, and control drugs Donepezil (AChE inhibitor) and Tideglusib (GSK3- β inhibitor) on novel AD model.
6. Evaluation of AChE-induced amyloid aggregation rate in presence of novel AChE inhibitors, and novel dual GSK3- β inhibitor.

6.2 Results

6.2.1 GA treatment induces abnormal Tau phosphorylation and axon degeneration in SH-SY5Y-differentiated neurons

In order to develop a neuron-like model of AD bearing Tau hyperphosphorylation, differentiation of SH-SY5Y in neurons was firstly performed as described by Shipley (Shipley 2016). SH-SY5Y derived neurons were subsequently imaged by confocal microscopy (Fig.17 A) to compare morphological differences. Differentiated neurons exhibited a significant increment in neurite density and neurite length when compared to undifferentiated SH-SY5Y cells (Fig.17 B, C).

After validating neuronal differentiation of SH-SY5Y cells, we investigated whether GA treatment for 24 hours would result in any AD defects in differentiated neurons, as described by Koriyama in undifferentiated SH-SY5Y cells (Koriyama *et al.* 2015). Confocal imaging, and subsequent axon length analysis, showed a significant reduction of neurite length in neurons treated with 0.7mM GA and 1mM GA when compared to untreated neurons (Fig.17 A, C). In addition to this, an assessment of Tau phosphorylation levels was performed on neurons treated with GA. Tau residue S199 was found to be abnormally phosphorylated following administration of both 0.7mM GA and 1mM GA (Fig.17 D). The same trend was recorded on S396 residue, recording a significant increment of phosphorylation levels following 0.7mM GA and 1mM GA administration (Fig.17 E).

Furthermore, we evaluated whether GA treatment, and resulting Tau hyperphosphorylation, would result in any change in neuronal cells viability. To assess neuronal viability, an MTT assay was performed 24 hours after GA administration, with both 0.7mM GA and 1mM GA treatment resulting in a significant drop in cells viability (Fig.17 F).

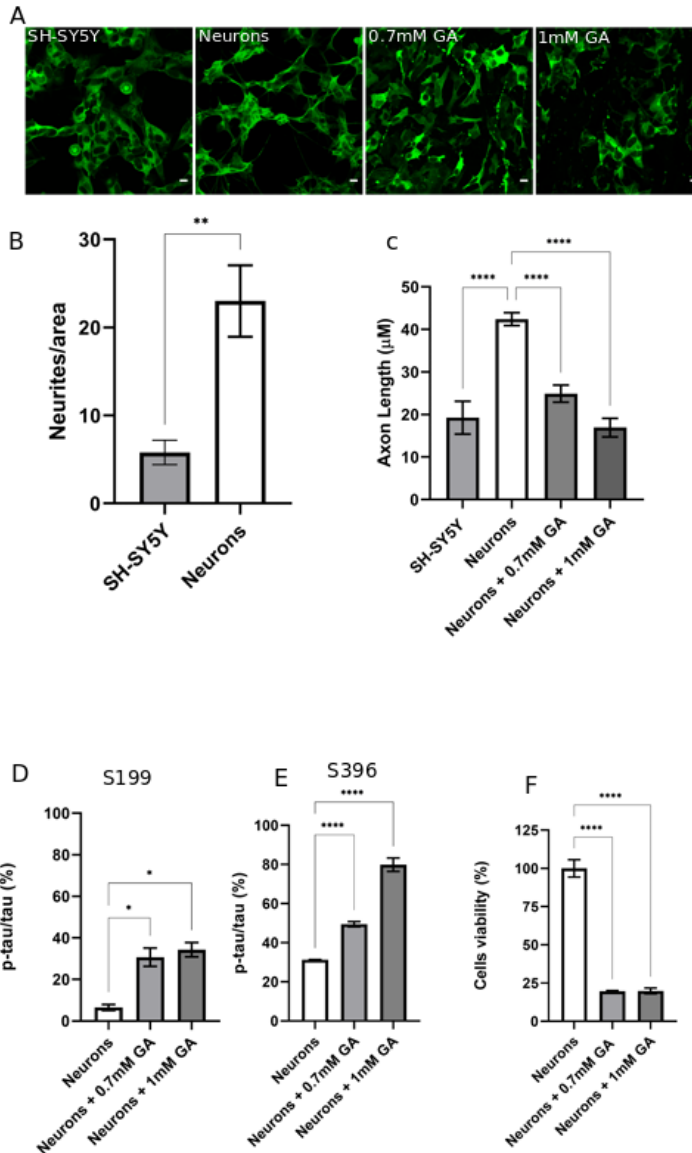


Figure 17. Initial characterization of novel AD model

A) Confocal images of SH-SY5Y cells, SH-SY5Y-derived neurons, and SH-SY5Y neuron treated with 0.7mM GA or 1mM GA. B) Neurite density quantification of SH-SY5Y cells and SH-SY5Y derived neurons. Mann-Whitney test was used to compare differences between different groups. C) Neurite length quantification of SH-SY5Y cells, SH-SY5Y derived neurons, and SH-SY5Y derived neurons following GA treatment at different concentration. Ordinary one-way ANOVA followed by Tukey's post-hoc test was used to compare differences between different groups. D) Quantification of phosphorylation ratio pTau/tTau on S199 of SH-SY5Y differentiated neurons following 0.7mM GA or 1mM treatment. ANOVA followed by Tukey's post-hoc test was used to compare differences between different groups. E) Quantification of phosphorylation ratio pTau/tTau on S396 of SH-SY5Y differentiated neurons following 0.7mM GA or 1mM GA treatment. ANOVA followed by Tukey's post-hoc test was used to compare differences between different groups. F) Cell

viability assay of SH-SY5Y differentiated neurons following GA treatment at different concentration. Ordinary one-way ANOVA followed by Tukey's post-hoc test was used to compare differences between different groups.

Data are presented as mean \pm SEM. n = 3, with a minimum of 5 repetition per experiment analysed. * P<0.05; **P<0.01; *** P<0.001; ****P<0.0001.

6.2.2 Novel compounds inhibit AChE enzyme activity in SH-SY5Y differentiated neurons

Upon validation that GA treatment results in Tau abnormal phosphorylation in SH-SY5Y derived neurons, we decided to investigate the inhibitory activity of the novel AChE inhibitors provided.

In 0.7mM GA exposed neurons we recorded a significant inhibition of AChE activity by XJP-1 at a concentration up to 0.5 μ M, with the same trend being scored by all other AChE inhibitors investigated (Fig.18 A-E). However, Donepezil and FAD showed a significant inhibition at 50nM concentration as well in 0.7mM GA treated neurons (Fig.18 B, E).

Investigation on dual AChE/GSK3- β inhibitor 16g showed a significant inhibition at 5 μ M concentration only (Fig.18 F).

Study on 1mM GA exposed neurons showed a drop in AChE activity following treatment with all inhibitors tested at a concentration up to 50nM with the exception of SAD-2 (Fig.19 A-E).

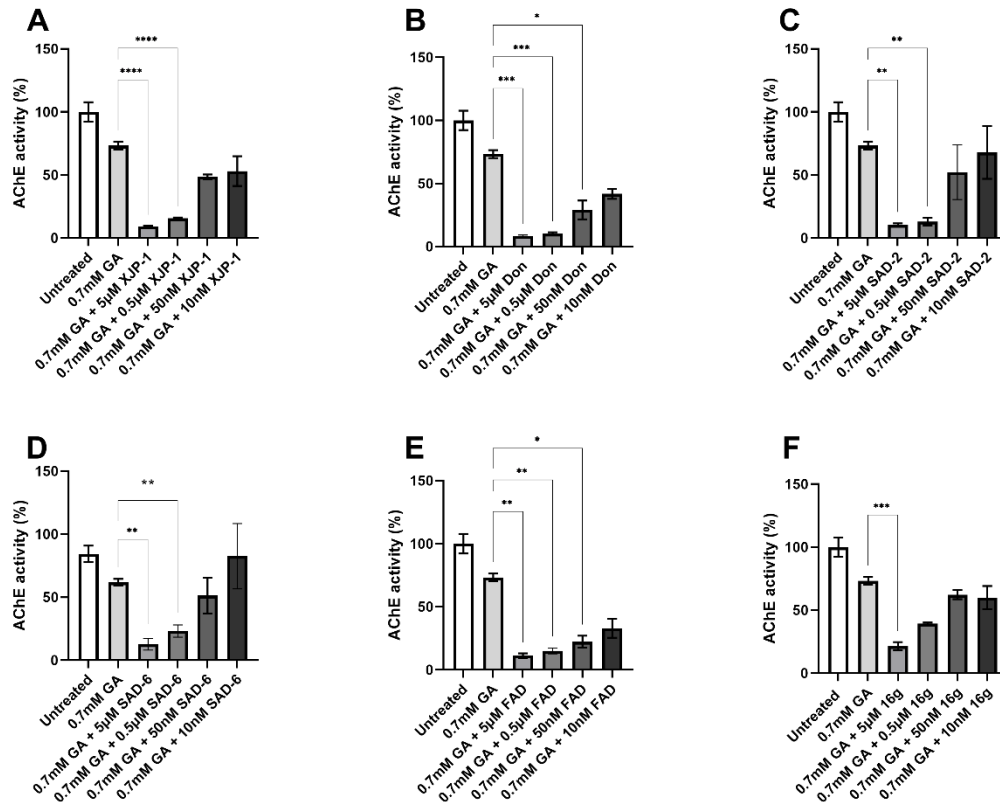


Figure 18. AChE inhibition by novel compounds at different concentration in 0.7mM GA exposed SH-SY5Y-derived neurons

A) Inhibitory activity of compound XJP-1 in 0.7mM GA exposed neurons. **B)** Inhibitory activity of compound Donepezil in 0.7mM GA exposed neurons. **C)** Inhibitory activity of compound SAD-2 in 0.7mM GA exposed neurons. **D)** Inhibitory activity of compound SAD-6 in 0.7mM GA exposed neurons. **E)** Inhibitory activity of compound FAD in 0.7mM GA exposed neurons. **F)** Inhibitory activity of compound 16g in 0.7mM GA exposed neurons. Ordinary one-way ANOVA followed by Tukey’s post-hoc test was used to compare differences between different groups. Data are presented as mean \pm SEM. $n = 3$, with a minimum of 5 repetition per experiment analysed. * $P < 0.05$; ** $P < 0.01$; *** $P < 0.001$; **** $P < 0.0001$.

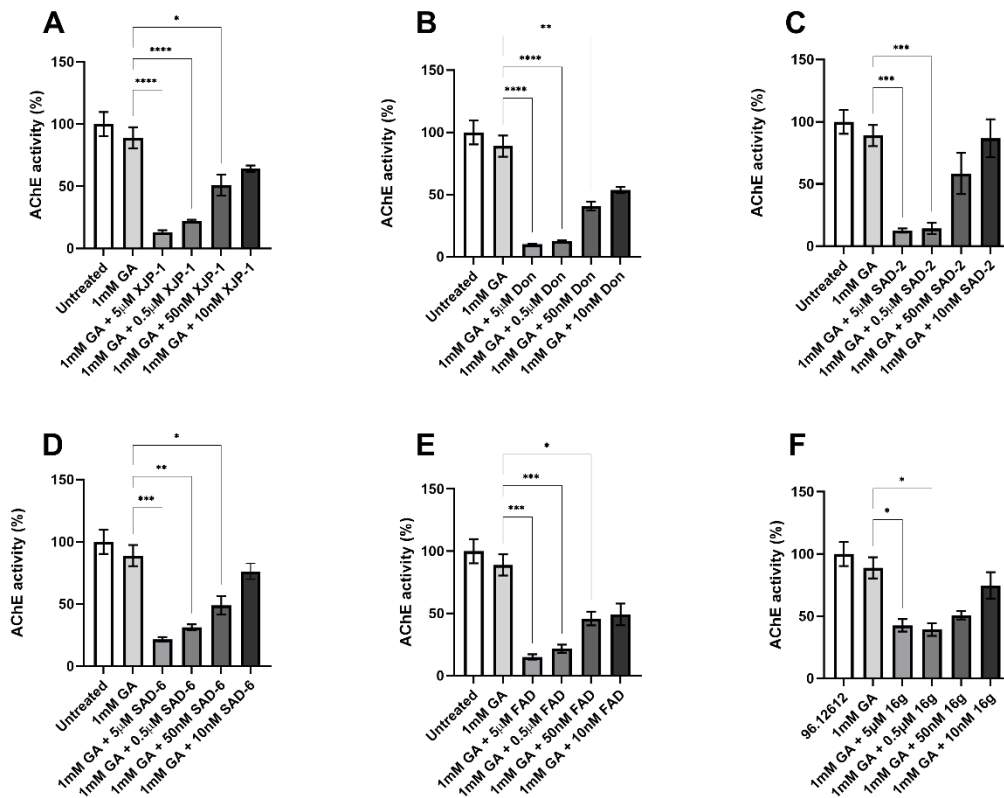


Figure 19. AChE inhibition by novel compounds at different concentration in 1mM GA exposed SH-SY5Y-derived neurons

A) Inhibitory activity of compound XJP-1 in 1mM GA exposed neurons. **B)** Inhibitory activity of compound Donepezil in 1mM GA exposed neurons. **C)** Inhibitory activity of compound SAD-2 in 1mM GA exposed neurons. **D)** Inhibitory activity of compound SAD-6 in 0.7mM GA exposed neurons. **E)** Inhibitory activity of compound FAD in 1mM GA exposed neurons. **F)** Inhibitory activity of compound 16g in 1mM GA exposed neurons. Ordinary one-way ANOVA followed by Tukey's post-hoc test was used to compare differences between different groups. Data are presented as mean \pm SEM. $n = 3$, with a minimum of 5 repetition per experiment analysed. * $P < 0.05$; ** $P < 0.01$; *** $P < 0.001$; **** $P < 0.0001$.

6.2.3 AChE inhibition prevents GA-induced Tau phosphorylation on S396, but not on S199.

After validating the inhibitory activity of the novel compounds on AChE enzyme (Fig.18, 19), we investigated whether GA-induced Tau hyperphosphorylation could be prevented by AChE inhibition exerted by novel compounds. Exposure of neuronal cells to 0.7mM GA dramatically increased Tau phosphorylation levels on S199 (Fig.17 D), whilst AChE inhibitor XJP-1, at 5 μ M and 0.5 μ M concentration, significantly reduced Tau hyperphosphorylation on S199 in neurons treated with 0.7mM GA (Fig.20 A), with the same trend being scored by the control AChE inhibitor Donepezil (Fig.20 B). On the other hand, treatment with novel AChE inhibitors SAD-2 did not reduce S199 phosphorylation in 0.7mM GA exposed SH-SY5Y differentiated neurons (Fig.20 C), whilst compounds SAD-6 and FAD recorded a significant reduction of S199 abnormal phosphorylation when administrated at 5 μ M concentration only (Fig.20 D, E). Moreover, in SH-SY5Y differentiated neurons treated with 1mM GA, none of the AChE inhibitors tested, including Donepezil, showed a significant reduction of Tau phosphorylation on S199 (Fig.21 A-E).

To further assess the efficacy of the novel compounds in preventing Tau abnormal phosphorylation, another residue S396 was examined. In neurons treated with 0.7mM GA, all therapies under study showed a potent effect in reducing S396 phosphorylation, at all concentration tested (Fig.22 A-E).

Moreover, an overlapping trend was found in neurons treated with 1mM GA, with all the novel compounds inducing a significant reduction of phosphorylation levels on Tau S396, at a concentration as low as 10nM (except SAD-6) (Fig.23 A-E). Moreover, dual inhibitor 16g showed a significant inhibition at 5 μ M and 0.5 μ M concentrations.

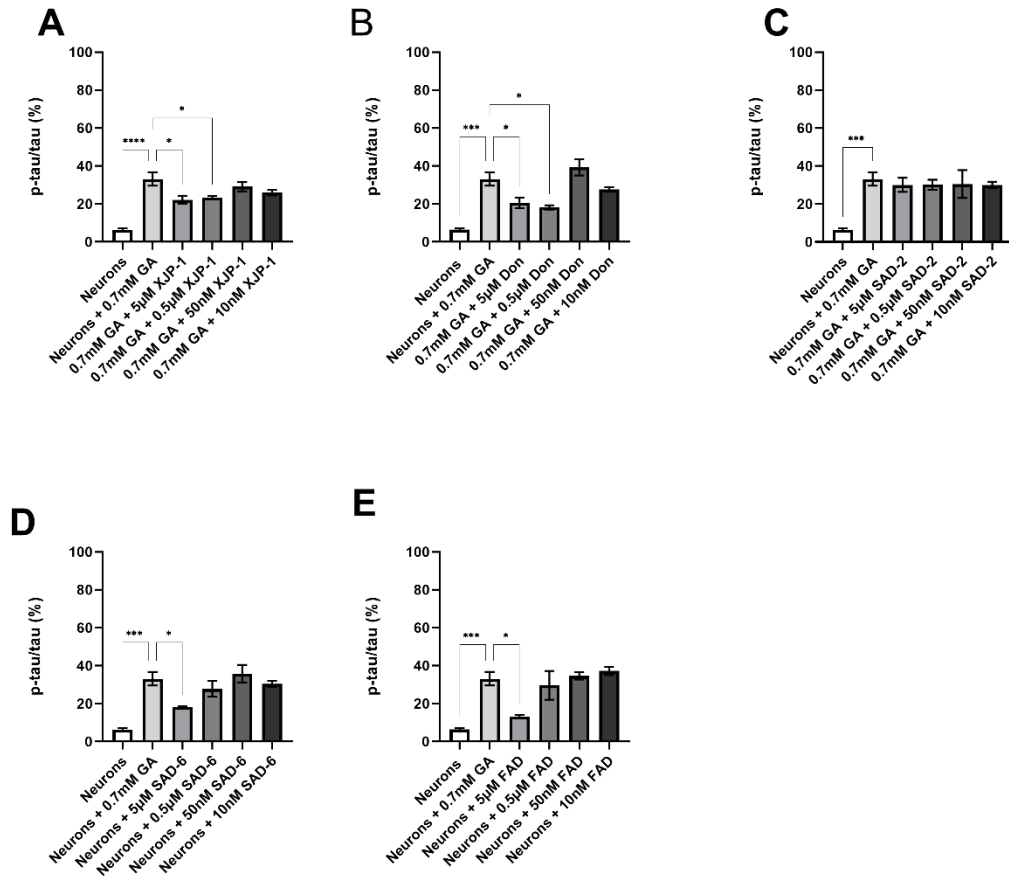


Figure 20. Tau S199 phosphorylation levels in 0.7mM GA exposed neurons after treatment with novel AChE inhibitors

A) Quantification of phosphorylation ratio pTau/tTau on S199 of 0.7mM GA treated SH-SY5Y differentiated neurons after XJP-1 treatment. **B)** Quantification of phosphorylation ratio pTau/tTau on S199 of 0.7mM GA treated SH-SY5Y differentiated neurons after Donepezil treatment. **C)** Quantification of phosphorylation ratio pTau/tTau on S199 of 0.7mM GA treated SH-SY5Y differentiated neurons after SAD-2 treatment. **D)** Quantification of phosphorylation ratio pTau/tTau on S199 of 0.7mM GA treated SH-SY5Y differentiated neurons after SAD-6 treatment. **E)** Quantification of phosphorylation ratio pTau/tTau on S199 of 0.7mM GA treated SH-SY5Y differentiated neurons after FAD treatment. Kuskar-Wallis test followed by Dunn's post-hoc was used to compare the differences between different groups. Data are expressed as mean \pm SEM, $n=3$ with at least 5 repetition per experiment, * $P<0.05$; ** $P<0.01$, *** $P<0.001$, **** $P<0.0001$.

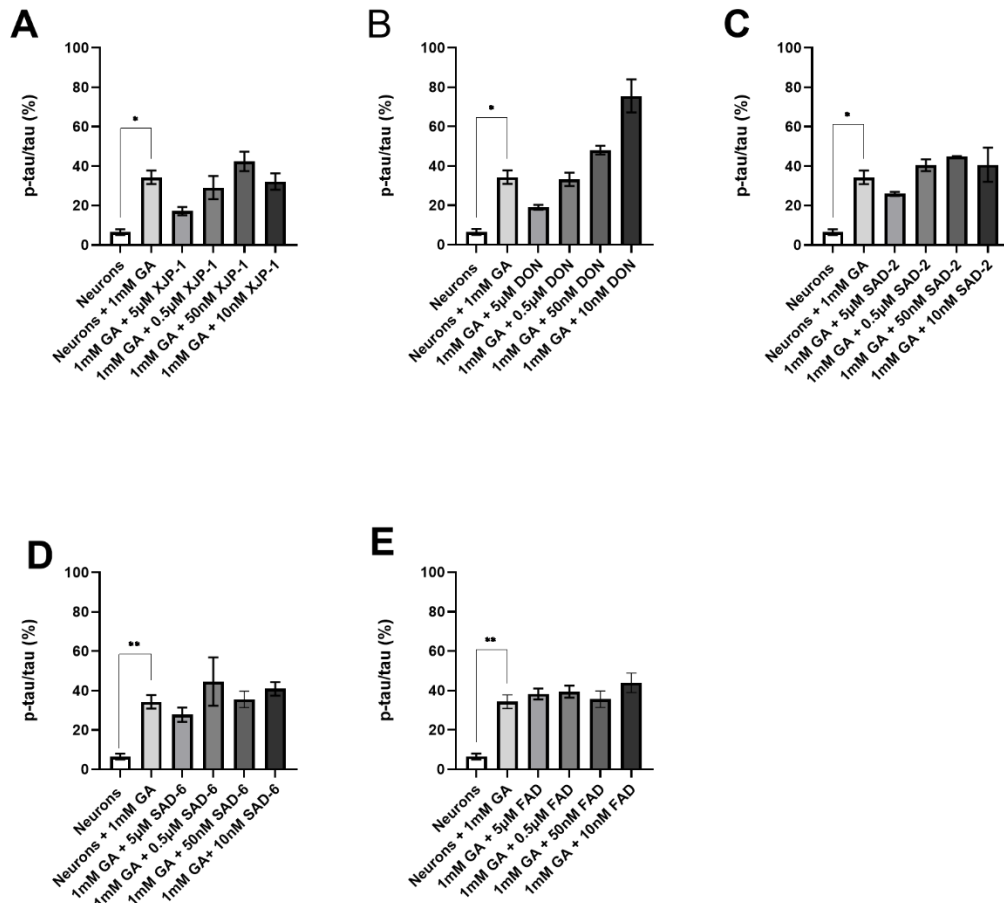


Figure 21. Tau S199 phosphorylation levels in 1mM GA exposed neurons after treatment with novel AChE inhibitors

A) Quantification of phosphorylation ratio pTau/tTau on S199 of 1mM GA treated SH-SY5Y differentiated neurons after XJP-1 treatment. **B)** Quantification of phosphorylation ratio pTau/tTau on S199 of 1mM GA treated SH-SY5Y differentiated neurons after Donepezil treatment. **C)** Quantification of phosphorylation ratio pTau/tTau on S199 of 1mM GA treated SH-SY5Y differentiated neurons after SAD-2 treatment. **D)** Quantification of phosphorylation ratio pTau/tTau on S199 of 1mM GA treated SH-SY5Y differentiated neurons after SAD-6 treatment. **E)** Quantification of phosphorylation ratio pTau/tTau on S199 of 1mM GA treated SH-SY5Y differentiated neurons after FAD treatment. Kuskar-Wallis test followed by Dunn’s post-hoc was used to compare the differences between different groups. Data are expressed as mean \pm SEM, $n=3$ with at least 5 repetition per experiment, * $P<0.05$; ** $P<0.01$, *** $P<0.001$, **** $P<0.0001$.

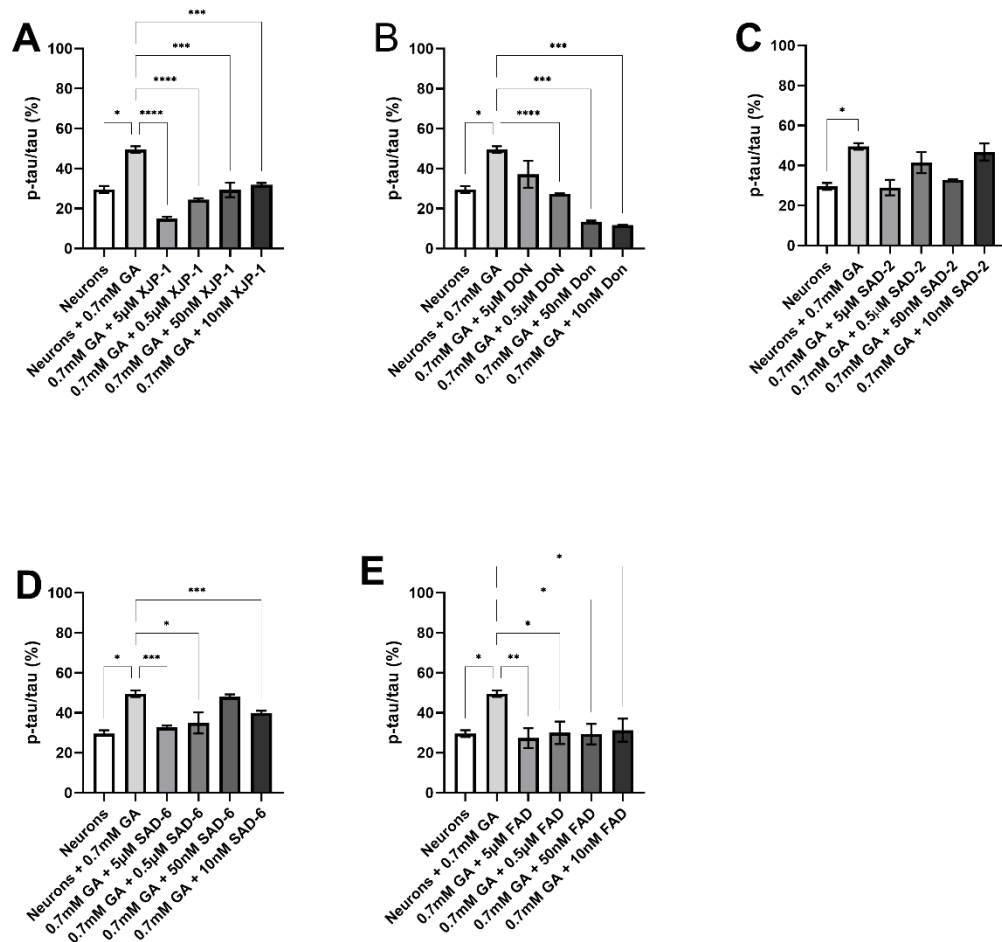


Figure 22. Tau S396 phosphorylation levels in 0.7mM GA exposed neurons after treatment with novel AChE inhibitors

A) Quantification of phosphorylation ratio pTau/tTau on S396 of 0.7mM GA treated SH-SY5Y differentiated neurons after XJP-1 treatment. **B)** Quantification of phosphorylation ratio pTau/tTau on S396 of 0.7mM GA treated SH-SY5Y differentiated neurons after Donepezil treatment. **C)** Quantification of phosphorylation ratio pTau/tTau on S396 of 0.7mM GA treated SH-SY5Y differentiated neurons after SAD-2 treatment. **D)** Quantification of phosphorylation ratio pTau/tTau on S396 of 0.7mM GA treated SH-SY5Y differentiated neurons after SAD-6 treatment. **E)** Quantification of phosphorylation ratio pTau/tTau on S396 of 0.7mM GA treated SH-SY5Y differentiated neurons after FAD treatment. Kuskar-Wallis test followed by Dunn's post-hoc was used to compare the differences between different groups. Data are expressed as mean \pm SEM, $n=3$ with at least 5 repetition per experiment, * $P<0.05$; ** $P<0.01$, *** $P<0.001$, **** $P<0.0001$.

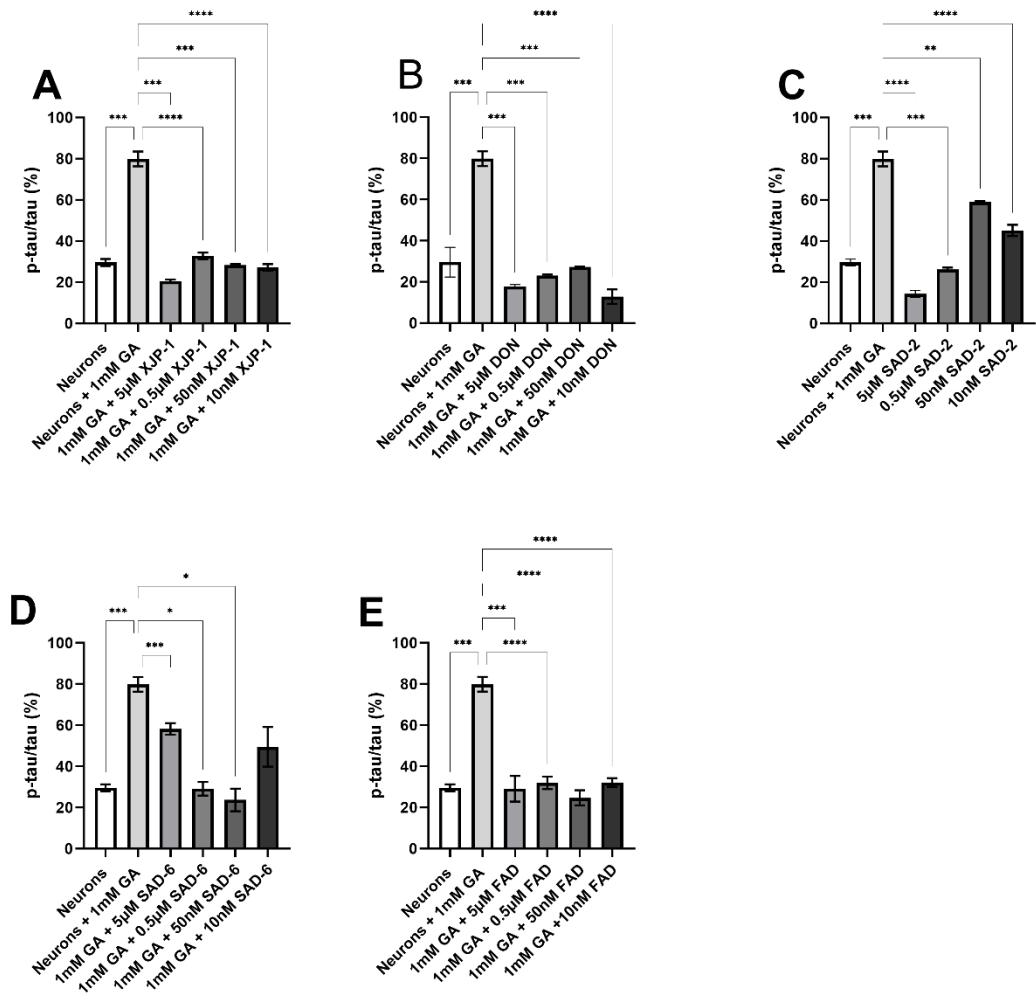


Figure 23. Tau S396 phosphorylation levels in 1mM GA exposed neurons after treatment with novel AChE inhibitors

A) Quantification of phosphorylation ratio pTau/tTau on S396 of 1mM GA treated SH-SY5Y differentiated neurons after XJP-1 treatment. **B)** Quantification of phosphorylation ratio pTau/tTau on S396 of 1mM GA treated SH-SY5Y differentiated neurons after Donepezil treatment. **C)** Quantification of phosphorylation ratio pTau/tTau on S396 of 1mM GA treated SH-SY5Y differentiated neurons after SAD-2 treatment. **D)** Quantification of phosphorylation ratio pTau/tTau on S396 of 1mM GA treated SH-SY5Y differentiated neurons after SAD-6 treatment. **E)** Quantification of phosphorylation ratio pTau/tTau on S396 of 1mM GA treated SH-SY5Y differentiated neurons after FAD treatment. **F)** Quantification of phosphorylation ratio pTau/tTau on S396 of 1mM GA treated SH-SY5Y differentiated neurons after 16g treatment. **G)** Quantification of phosphorylation ratio pTau/tTau on S396 of 1mM GA treated SH-SY5Y differentiated neurons after Tideglusib treatment. Kuskar-Wallis test followed by Dunn’s post-hoc was used to compare the differences between different groups. Data are

expressed as mean \pm SEM, $n=3$ with at least 5 repetition per experiment, * $P<0.05$; ** $P<0.01$, *** $P<0.001$, **** $P<0.0001$.

6.2.4 Dual AChE/GSK3- β inhibitor 16g modulates Tau phosphorylation on S199 and S396

To investigate the effects of treatment with dual GSK3- β /AChE inhibitor 16g, Tau phosphorylation on S199, in 0.7mM GA treated neurons was investigated. The novel compound showed a significant reduction of S199 phosphorylation levels, when compared to the untreated 0.7mM GA neurons, in a dose dependant manner up 50nM concentration (Fig.24 A), whilst commercial GSK3- β inhibitor Tideglusib reduced S199 phosphorylation at 5 μ M concentration only (Fig.24 B). However, the novel dual inhibitor, was not able to significantly reduce S199 phosphorylation in neurons exposed to 1mM GA (Fig.25 A, B), despite GSK3- β inhibitor Tideglusib successfully reduced S199 phosphorylation at 5 μ M and 0.5 μ M concentration (Fig.25 B).

To further characterise the efficacy of compound 16g in reducing Tau hyperphosphorylation, residue S396 was examined. A significant drop in S396 phosphorylation levels was recorded, up to 50nM concentration, in 0.7mM GA exposed neurons treated with compound 16g, with Tideglusib scoring similar results (Fig.26 A, B). Moreover, inhibition of both AChE and GSK3- β enzymes resulted in a significant reduction for all concentration tested of compound 16g in 1mM GA exposed neurons, with the same results being scored by the control drug Tideglusib (Fig.26 A, B).

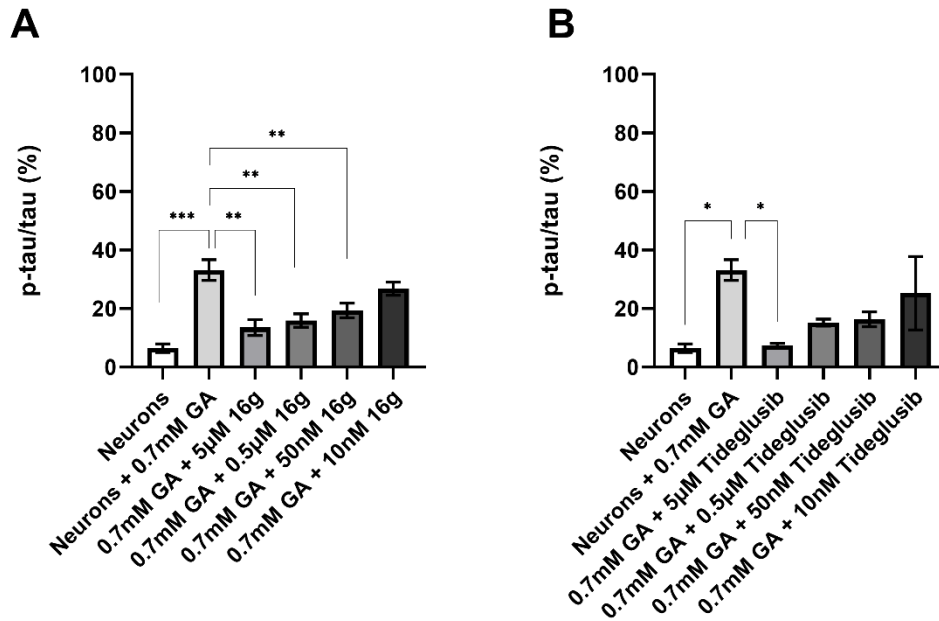


Figure 24. Reduction of Tau S199 phosphorylation after 16g treatment in 0.7mM GA exposed neurons

A) Quantification of phosphorylation ratio pTau/tTau on S199 of 0.7mM GA treated SH-SY5Y differentiated neurons after 16g treatment. **B)** Quantification of phosphorylation ratio pTau/tTau on S199 of 0.7mM GA treated SH-SY5Y differentiated neurons after Tideglusib treatment. Kuskar-Wallis test followed by Dunn's post-hoc was used to compare the differences between different groups. Data are expressed as mean \pm SEM, $n=3$ with at least 5 repetition per experiment, * $P<0.05$; ** $P<0.01$, *** $P<0.001$, **** $P<0.0001$.

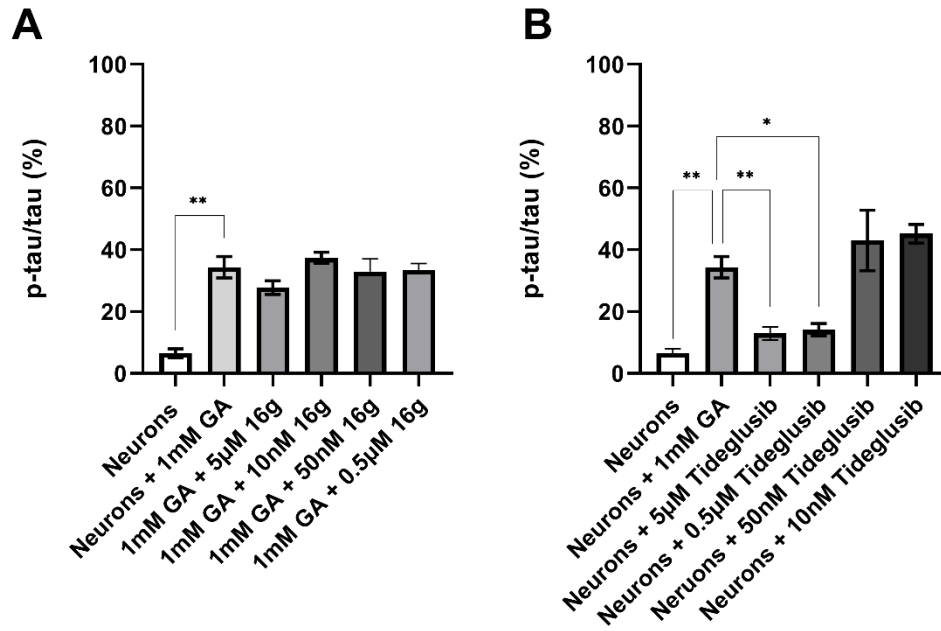


Figure 25. Reduction of Tau S199 phosphorylation after 16g treatment in 1mM GA exposed neurons

A) Quantification of phosphorylation ratio pTau/tTau on S199 of 1mM GA treated SH-SY5Y differentiated neurons after 16g treatment. **B)** Quantification of phosphorylation ratio pTau/tTau on S199 of 1mM GA treated SH-SY5Y differentiated neurons after Tideglusib treatment. Kuskar-Wallis test followed by Dunn's post-hoc was used to compare the differences between different groups. Data are expressed as mean \pm SEM, $n=3$ with at least 5 repetition per experiment, * $P<0.05$; ** $P<0.01$, *** $P<0.001$, **** $P<0.0001$.

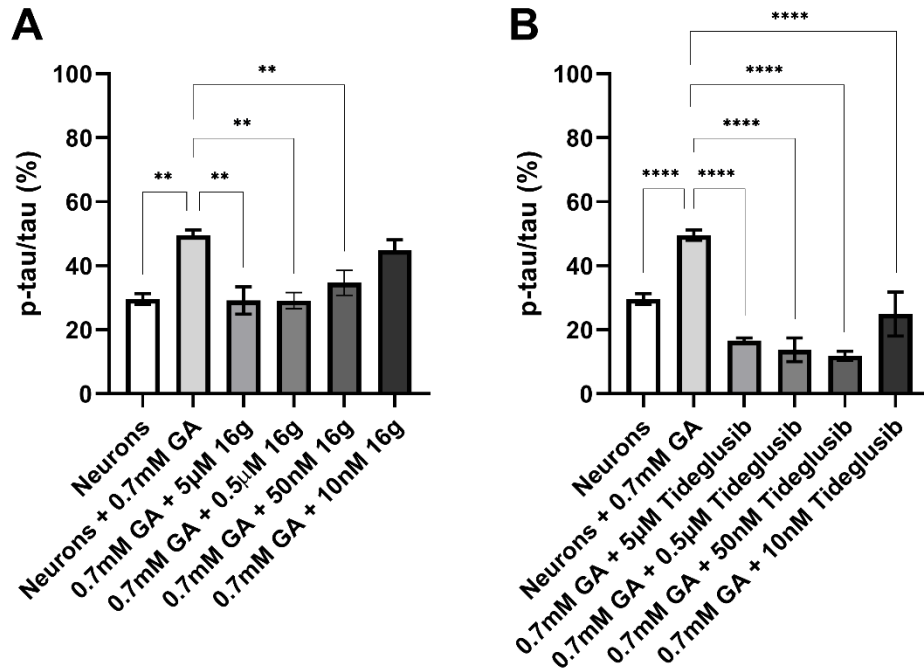


Figure 26. Reduction of Tau S396 phosphorylation after 16g treatment in 0.7mM GA exposed neurons

A) Quantification of phosphorylation ratio pTau/tTau on S396 of 0.7mM GA treated SH-SY5Y differentiated neurons after 16g treatment. **B)** Quantification of phosphorylation ratio pTau/tTau on S396 of 0.7mM GA treated SH-SY5Y differentiated neurons after Tideglusib treatment. Kuskar-Wallis test followed by Dunn's post-hoc was used to compare the differences between different groups. Data are expressed as mean \pm SEM, $n=3$ with at least 5 repetition per experiment, * $P<0.05$; ** $P<0.01$, *** $P<0.001$, **** $P<0.0001$.

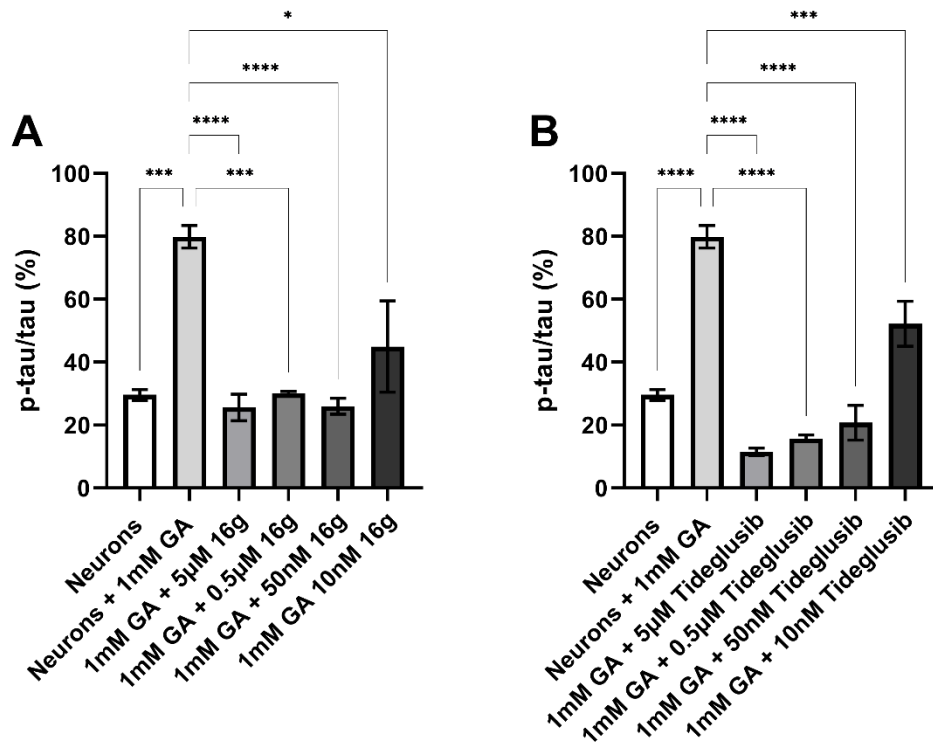


Figure 27. Reduction of Tau S396 phosphorylation after 16g treatment in 1mM GA exposed neurons

A) Quantification of phosphorylation ratio pTau/tTau on S396 of 1mM GA treated SH-SY5Y differentiated neurons after 16g treatment. **B)** Quantification of phosphorylation ratio pTau/tTau on S396 of 1mM GA treated SH-SY5Y differentiated neurons after Tideglusib treatment. Kuskar-Wallis test followed by Dunn's post-hoc was used to compare the differences between different groups. Data are expressed as mean \pm SEM, $n=3$ with at least 5 repetition per experiment, * $P<0.05$; ** $P<0.01$, *** $P<0.001$, **** $P<0.0001$.

6.2.5 Efficacy of AChE inhibitors in preventing hyperphosphorylated Tau-induced neurodegeneration

Microtubule architecture plays a fundamental role in cytoskeletal structure in neuronal cells, assuring a correct morphology and axonal transport. The presence of hyperphosphorylated forms of Tau protein lead to a jeopardized microtubule architecture, resulting in a disrupted axon morphology and neurodegeneration. Treatment with GA at 0.7mM and 1mM concentrations resulted in a dramatic increment of Tau phosphorylation levels, which led to morphology defects and neurite shortening (Fig.16 A, C).

To assess whether any of the novel AChE inhibitors compounds was able to prevent the formation of morphological defects in GA treated neurons, we exploited confocal microscopy to image neurons treated with either 5 μ M or 0.5 μ M of the novel therapies. Treatment with AChE inhibitor XJP-1 resulted in increased axon length, with results being better than the positive control AChE inhibitor Donepezil, which failed to score any significant amelioration (Fig.28 A-C). On the other hand, AChE inhibitor SAD-2, SAD-6, and FAD were not able to prevent axon shortening at any of the concertation studied on 0.7mM GA treated neurons (Fig.28 D-F). Study on axon length in 1mM GA treated neurons (Fig.29 A), confirmed that XJP-1 treatment significantly prevent neurite shortening, with better results than Donepezil, which was able to replicate XJP-1 results only when administrated at 0.5 μ M concentration (Fig.29 B-C). Despite not scoring any significant improvement in neuronal morphology in 0.7mM GA treated neurons, AChE inhibitors SAD-2, SAD-6, and FAD, significantly prevented neurite shortening in 1mM GA treated neurons (Fig.29 D-F)

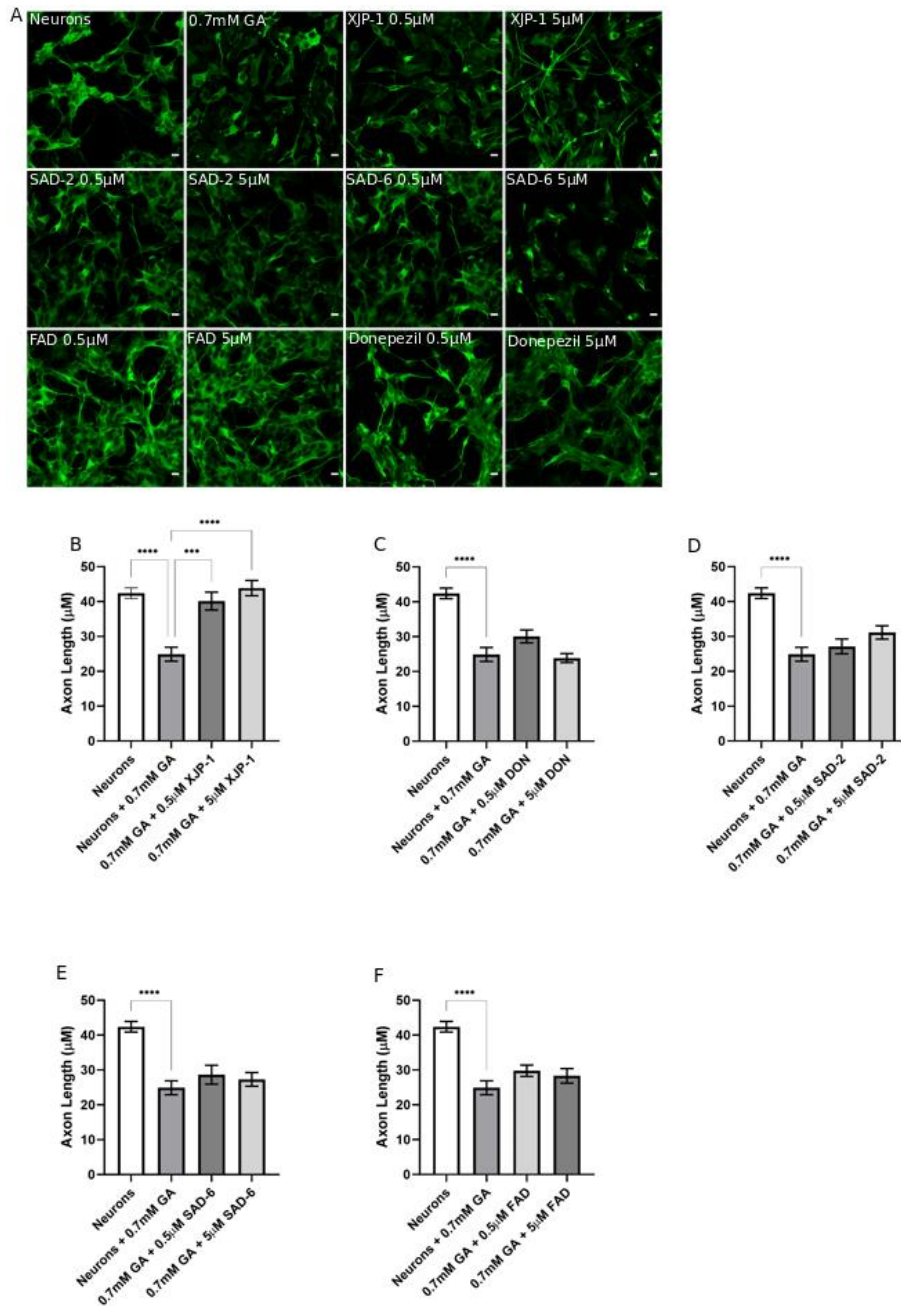


Figure 28. Morphological analysis of 0.7mM GA exposed neurons after different AChE inhibitors treatment

A) Confocal images of SH-SY5Y-derived neurons under different treatment. **B)** Neurite length quantification of 0.7mM GA treated SH-SY5Y differentiated neurons after XJP-1 treatment. **C)** Neurite length quantification of 0.7mM GA treated SH-SY5Y differentiated neurons after Donepezil treatment. **D)** Neurite length quantification of 0.7mM GA treated SH-SY5Y differentiated neurons after SAD-2 treatment. **E)** Neurite length quantification of 0.7mM GA treated SH-SY5Y differentiated neurons after SAD-6 treatment. **F)** Neurite length quantification of 0.7mM GA treated SH-SY5Y differentiated neurons after FAD treatment. Ordinary one-way ANOVA followed by Tukey's post-hoc test was used to compare

differences between different groups. Data is presented as mean \pm SEM, $n=3$ with at least 5 repetition per experiment, * $P<0.05$; ** $P<0.01$; *** $P<0.001$; **** $P<0.0001$.

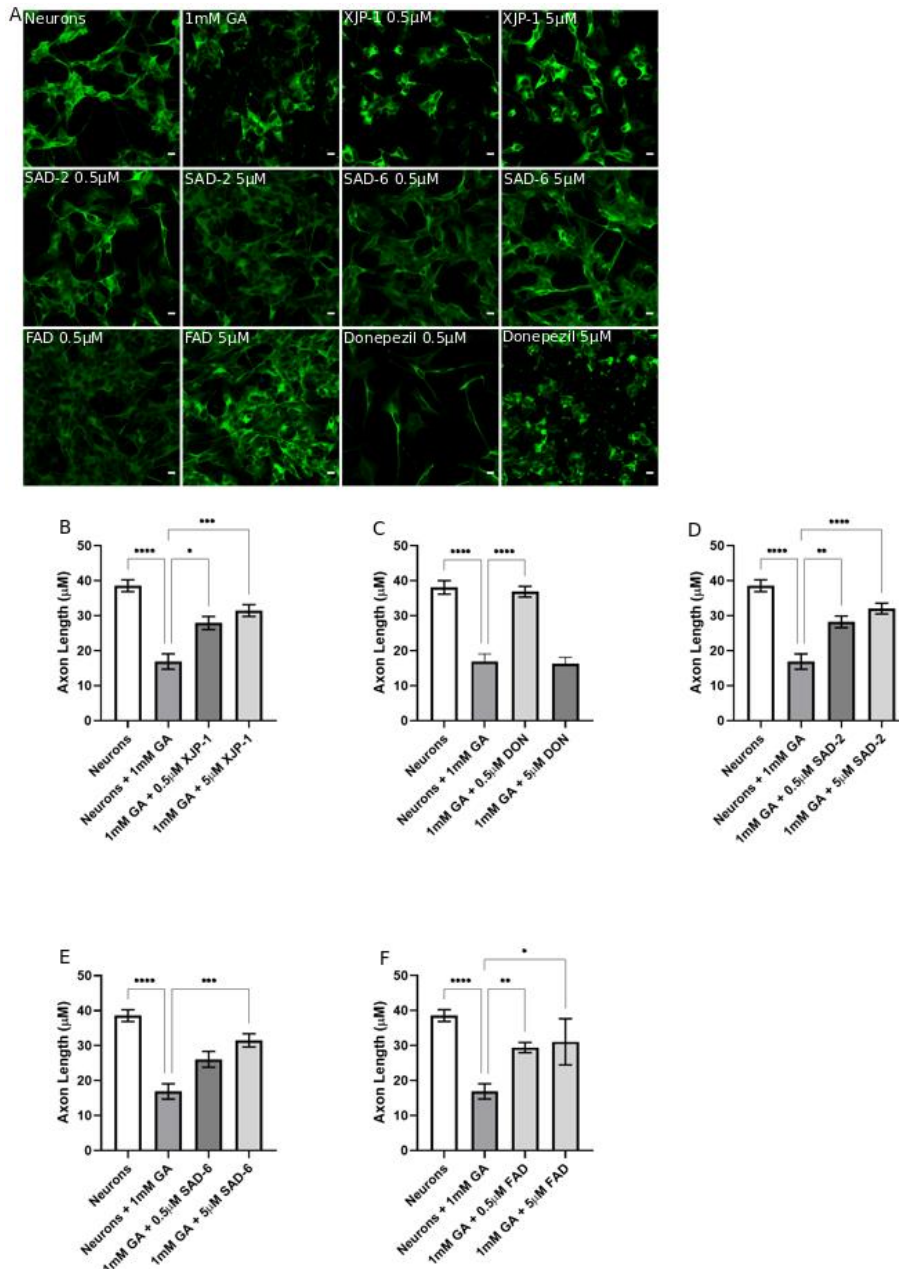


Figure 29. Morphological analysis of 1mM GA exposed neurons after different AChE inhibitors treatment

A) Confocal images of SH-SY5Y-derived neurons under different treatment. **B)** Neurite length quantification of 1mM GA treated SH-SY5Y differentiated neurons after XJP-1 treatment. **C)** Neurite length quantification of 1 mM GA treated SH-SY5Y differentiated neurons after Donepezil treatment. **D)** Neurite length quantification of 1mM GA treated SH-SY5Y differentiated neurons after SAD-2 treatment. **E)** Neurite length quantification of 1mM GA

treated SH-SY5Y differentiated neurons after SAD-6 treatment. **F)** Neurite length quantification of 1mM GA treated SH-SY5Y differentiated neurons after FAD treatment. Ordinary one-way ANOVA followed by Tukey's post-hoc test was used to compare differences between different groups. Data is presented as mean \pm SEM, $n=3$ with at least 5 repetition per experiment, * $P<0.05$; ** $P<0.01$; *** $P<0.001$; **** $P<0.0001$.

6.2.6 Treatment with compound 16g prevents Tau-induced neurodegeneration

During AD progression, the formation of aggregated forms of hyperphosphorylated Tau leads to the disruption of neuronal morphology. As a consequence, neural architecture and connectivity is lost, therefore resulting in a loss of brain circuits and functions. Thus, prevention the neurite degeneration is a fundamental test for a potential AD therapy. 24 hours after incubation with 0.7mM GA and compound 16g at various concentrations, we have exploited confocal microscopy to investigate the neuronal morphology for the presence of any ameliorations. We found that compound 16g treatment significantly prevented neurite shortening in a dose-dependent manner, and exhibited more potent improvement effects than Tideglusib at the same concentrations (Fig.30 A-C).

Also, inhibition of both AChE and GSK3- β by compound 16g confirmed the positive trend by preventing neurite shortening in 1mM GA treated neurons as well, overlapping Tideglusib results (Fig.31 A-C).

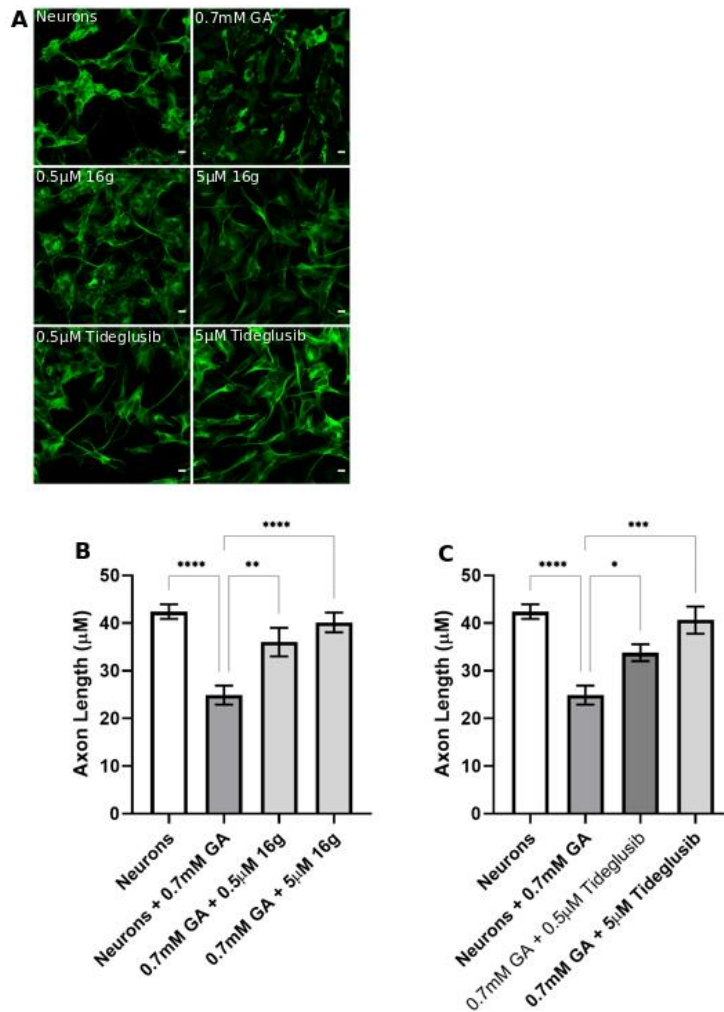


Figure 30. Dose-dependent amelioration of neurite morphology by compound 16g in 0.7mM GA exposed neurons

A) Confocal images of SH-SY5Y-derived neurons under different treatment. B) Neurite length quantification of 0.7mM GA treated SH-SY5Y differentiated neurons after 16g treatment. C) Neurite length quantification of 0.7mM GA treated SH-SY5Y differentiated neurons after Tideglusib treatment. Ordinary one-way ANOVA followed by Tukey's post-hoc test was used to compare differences between different groups. Data is presented as mean \pm SEM, $n=3$ with at least 5 repetition per experiment, * $P<0.05$; ** $P<0.01$; *** $P<0.001$; **** $P<0.0001$.

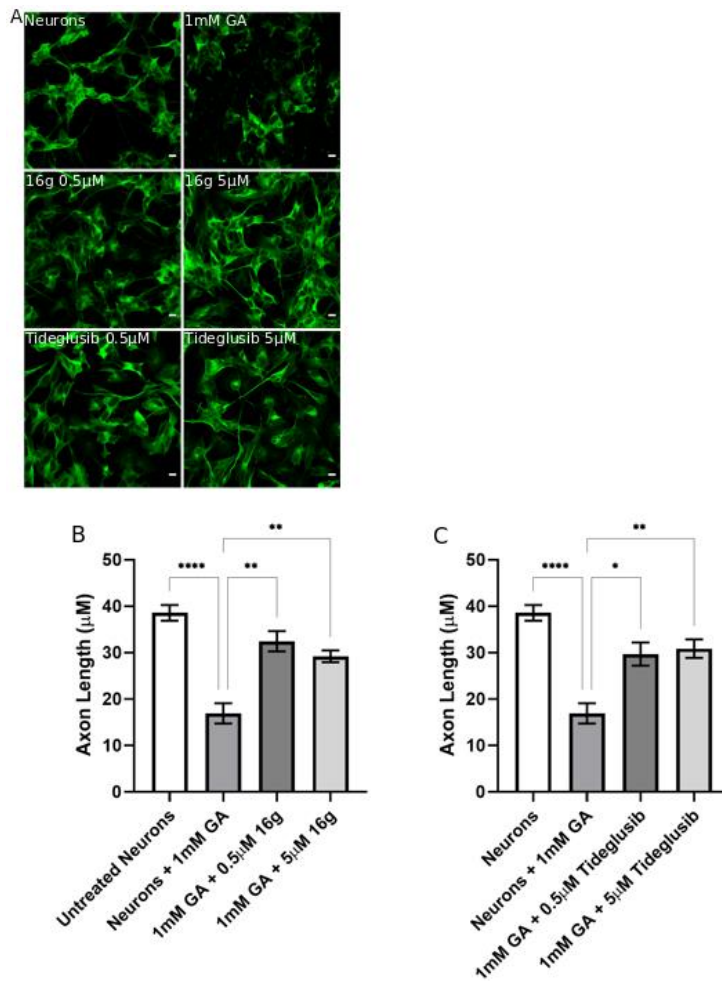


Figure 31. Amelioration of neurite morphology by compound 16g in 1mM GA exposed neurons

A) Confocal images of SH-SY5Y-derived neurons under different treatment. B) Neurite length quantification of 1mM GA treated SH-SY5Y differentiated neurons after 16g treatment. C) Neurite length quantification of 1mM GA treated SH-SY5Y differentiated neurons after Tideglusib treatment. Ordinary one-way ANOVA followed by Tukey's post-hoc test was used to compare differences between different groups. Data is presented as mean \pm SEM, $n=3$ with at least 5 repetition per experiment, * $P<0.05$; ** $P<0.01$; *** $P<0.001$; **** $P<0.0001$.

6.2.7 Increased cell viability following novel AChE inhibitor treatment

Depletion of cholinergic neurons is a well-known characteristic of AD pathogenesis, with the major circuits involved in memory and learning functions, being represented by this type of neurons. In order to study whether inhibition of AChE enzyme would result in an increased cells viability after 0.7 or 1mM GA treatment an MTT assay was performed.

In neurons treated with 0.7mM GA, all AChE inhibitors tested significantly prevented the dramatic cell death observed in untreated neurons, with the exception of compound FAD (Fig.32 A-E). On the other hand, XJP-1 showed no efficacy in preventing cell deaths in 1mM GA treated neurons, whilst SAD-2 and Donepezil successfully did with overlapping results (Fig.33 A-C). Moreover, AChE inhibitors SAD-6, and FAD, prevented neuronal cell death, but only at 5 μ M and 0.5 μ M respectively (Fig.33 D, E).

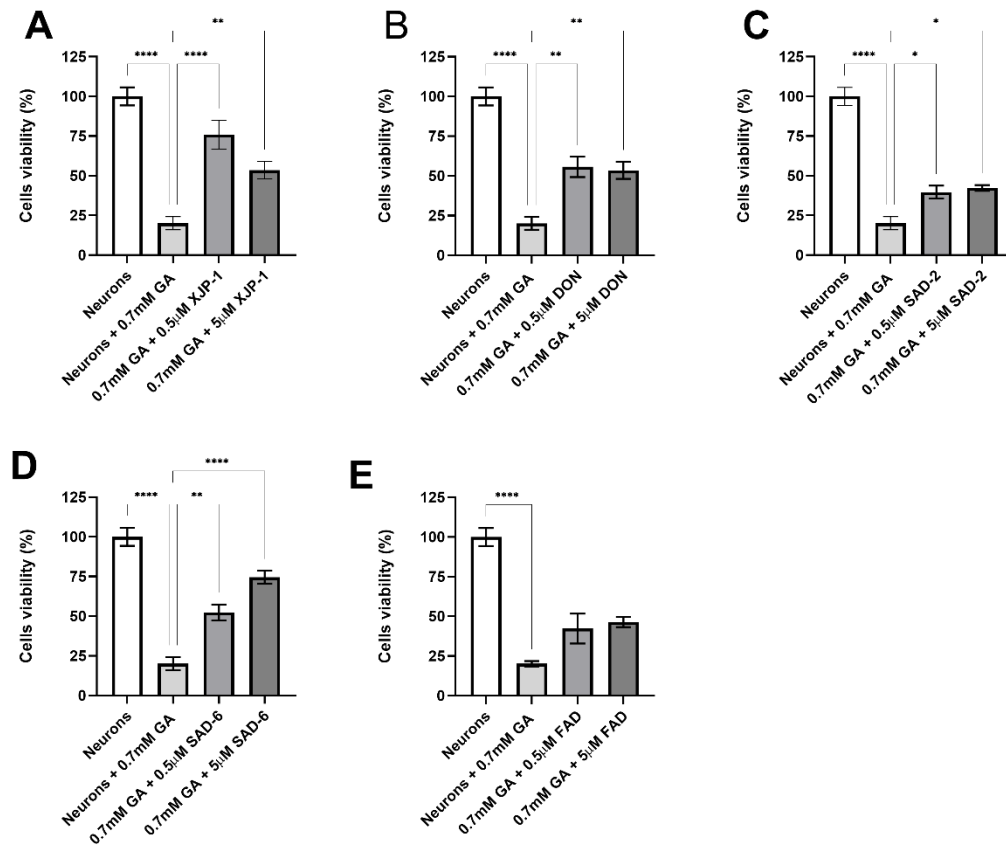


Figure 32. Cell viability quantification of 0.7mM GA exposed SH-SY5Y differentiated neurons after treatment with different AChE inhibitor

A) MTT assay of SH-SY5Y differentiated neurons following 0.7mM GA treatment and compound XJP-1. B) MTT assay of SH-SY5Y differentiated neurons following 0.7mM GA treatment and compound Donepezil. C) MTT assay of SH-SY5Y differentiated neurons following 0.7mM GA treatment and compound SAD-2. D) MTT assay of SH-SY5Y differentiated neurons following 0.7mM GA treatment and compound SAD-6. E) MTT assay of SH-SY5Y differentiated neurons following 0.7mM GA treatment and compound FAD. Ordinary one-way ANOVA followed by Tukey's post-hoc test was used to compare differences between different groups. Data is presented as mean \pm SEM, $n=3$ with at least 5 repetition per experiment, * $P<0.05$; ** $P<0.01$; *** $P<0.001$; **** $P<0.0001$.

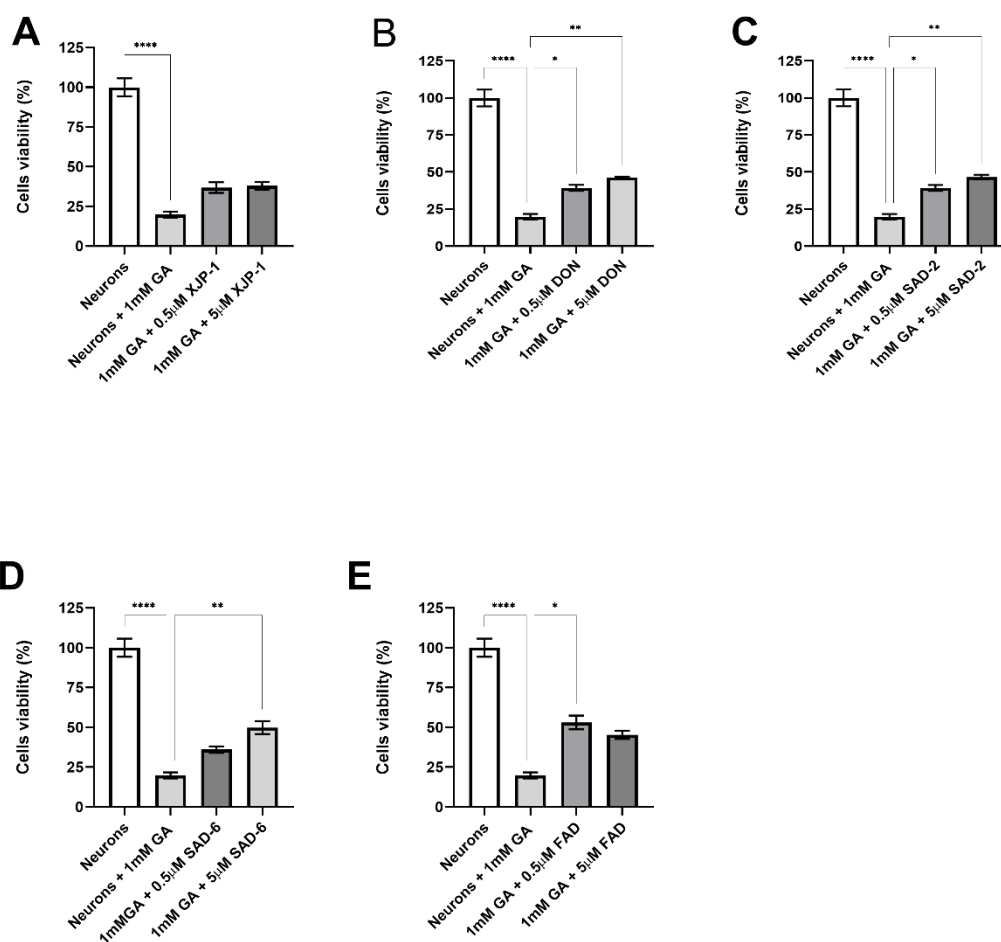


Figure 33. Cell viability quantification of 1mM GA exposed SH-SY5Y differentiated neurons after treatment with different AChE inhibitors

A) MTT assay of SH-SY5Y differentiated neurons following 1mM GA treatment and compound XJP-1. **B)** MTT assay of SH-SY5Y differentiated neurons following 1mM GA treatment and compound Donepezil. **C)** MTT assay of SH-SY5Y differentiated neurons following 1mM GA treatment and compound SAD-2. **D)** MTT assay of SH-SY5Y differentiated neurons following 1mM GA treatment and compound SAD-6. **E)** MTT assay of SH-SY5Y differentiated neurons following 1mM GA treatment and compound FAD. Ordinary one-way ANOVA followed by Tukey's post-hoc test was used to compare differences between different groups. Data is presented as mean \pm SEM, $n=3$ with at least 5 repetition per experiment, * $P<0.05$; ** $P<0.01$; *** $P<0.001$; **** $P<0.0001$.

6.2.8 Compound 16g prevents neuronal cell death

Neuronal cell death is the major issue of neurodegenerative diseases. Since they do not actively replicate, once a neuron undergoes a programmed cell death it will not be replaced. Thus, prevention of neuronal cell death is a crucial point for a successful AD therapy, since NFTs are a potential cause of neuronal apoptosis.

To investigate whether dual inhibition of both AChE and GSK3- β enzyme would result in preventing neuronal cell death, as a consequence of GA treatment, and subsequent Tau hyperphosphorylation, we assessed cells viability 24 hours after treatment administration. The presence of compounds 16g, as well as Tideglusib, showed neuroprotective effects by significantly increasing neurons viability, despite treatment with 0.7mM GA (Fig.32 A, B). Moreover, cell death was prevented in neurons treated with 1mM GA, suggesting that compound 16g as crucial neuroprotective functions in this particular AD model (Fig.33 A, B).

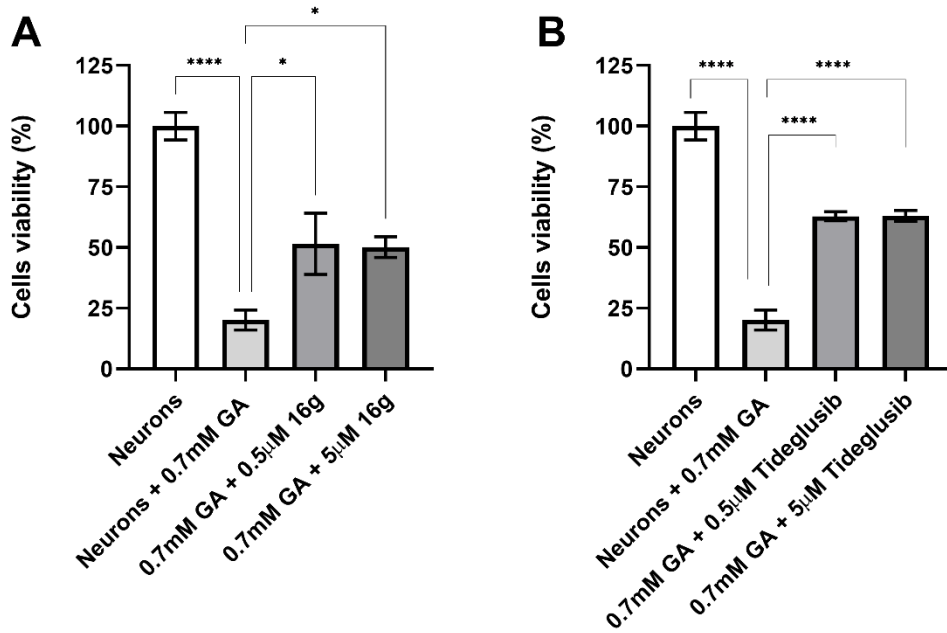


Figure 34. Prevention of 0.7mM GA-induced cell death by compound 16g treatment

A) MTT assay of SH-SY5Y differentiated neurons following 0.7mM GA treatment and compound 16g. **B)** MTT assay of SH-SY5Y differentiated neurons following 0.7mM GA treatment and compound Tideglusib. Ordinary one-way ANOVA followed by Tukey's post-hoc test was used to compare differences between different groups. Data is presented as mean \pm SEM, $n=3$ with at least 5 repetition per experiment, * $P<0.05$; ** $P<0.01$; *** $P<0.001$; **** $P<0.0001$.

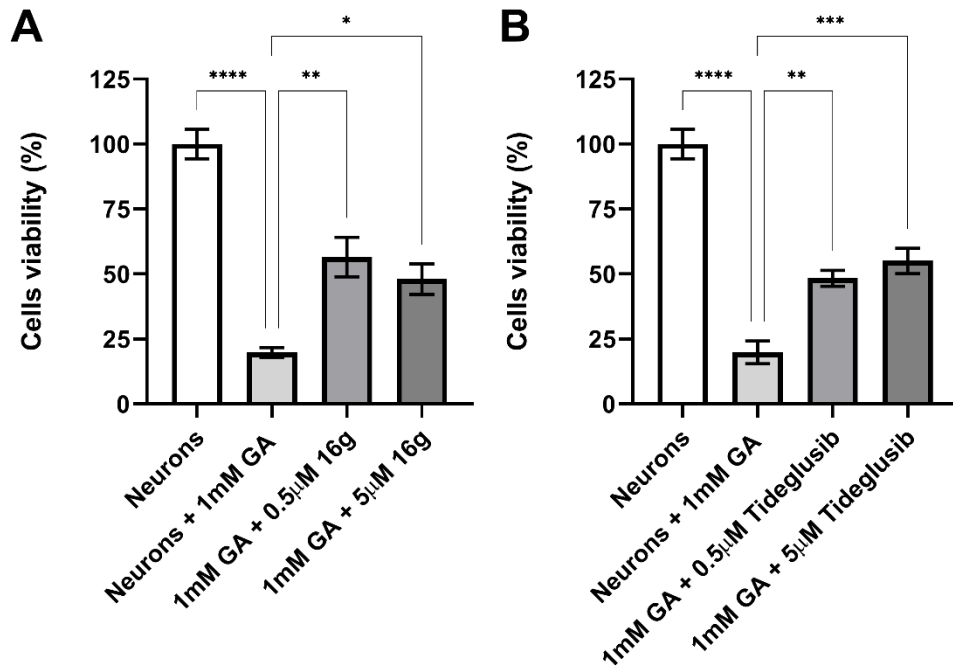


Figure 35. Prevention of 1mM GA-induced cell death by compound 16g treatment

A) MTT assay of SH-SY5Y differentiated neurons following 1mM GA treatment and compound 16g. B) MTT assay of SH-SY5Y differentiated neurons following 1mM GA treatment and compound Tideglusib. Ordinary one-way ANOVA followed by Tukey's post-hoc test was used to compare differences between different groups. Data is presented as mean \pm SEM, $n=3$ with at least 5 repetition per experiment, * $P<0.05$; ** $P<0.01$; *** $P<0.001$; **** $P<0.0001$.

6.2.9 Novel AChE inhibitors and dual AChE/GSK3- β inhibitor reduce AChE-induced amyloid aggregation rate

Tau hyperphosphorylation and deposition of amyloid plaques are considered to be the two major players in AD pathogenesis.

Since AChE enzyme function in promoting β -peptides aggregation, we investigated whether any of the novel compounds could decrease the aggregation rate by binding to AChE enzyme. All of the inhibitors tested showed a significant reduction of amyloid aggregation rate (Fig.36 A-F). In particular, dual AChE/GSK3- β inhibitor showed a significant reduction at a concentration as low as 50nM, with the same results being obtained by Donepezil, the most potent AD therapy approved by the FDA, at the same concentration (Fig.36 B, F).

XJP-1, SAD-2, SAD-6, and FAD, confirmed the theory that inhibition of AChE enzyme is implicated in amyloid aggregation rate reduction, with almost all concentration studied recording a significant drop (Fig.36 C-E).

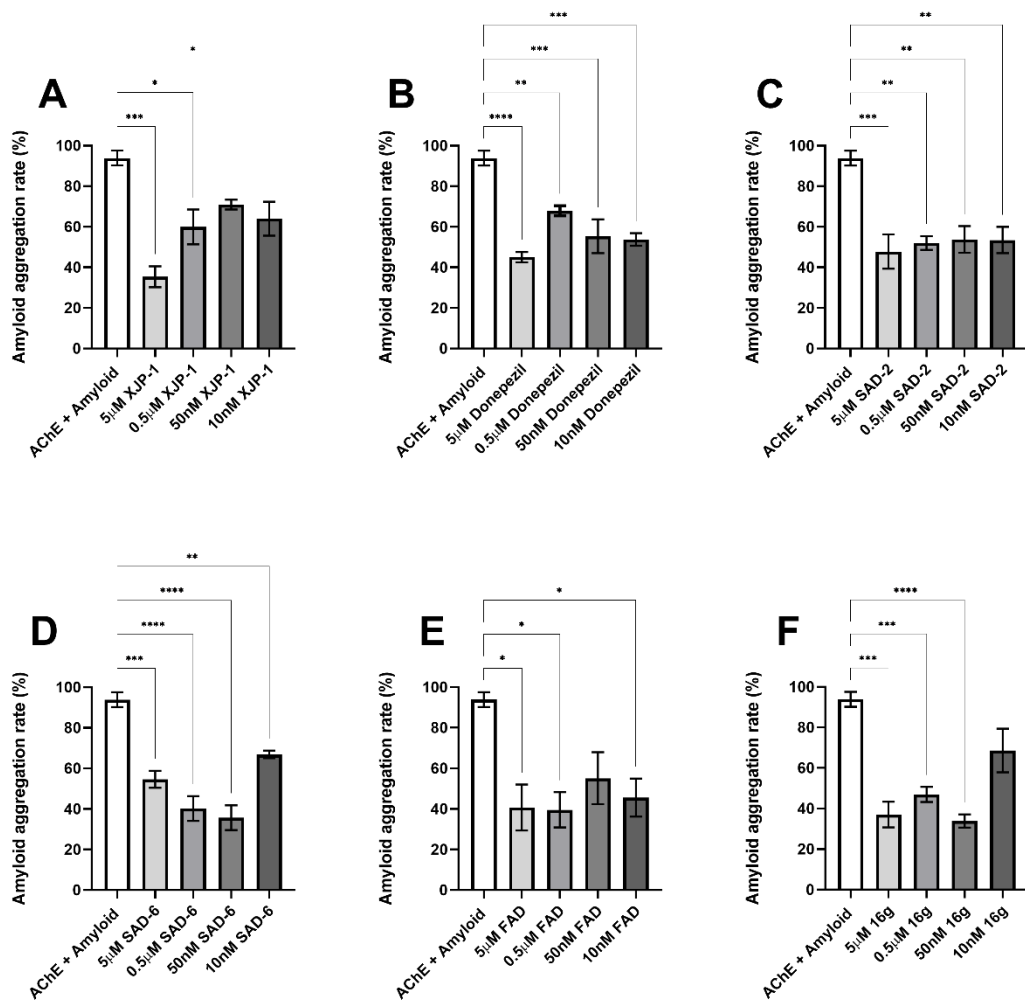


Figure 36. Reduction of amyloid peptides aggregation rate by inhibition of AChE enzyme
 AChE-induced amyloid aggregation A β -peptides aggregation rates in presence of AChE inhibitors: **A)** XJP-1. **B)** Donepezil **C)** SAD-2. **D)** SAD-6. **E)** FAD **F)** FAD.

Ordinary one-way ANOVA followed by Tukey's post-hoc test was used to compare differences between different groups. Data is presented as mean \pm SEM, $n=3$ with at least 5 repetition per experiment, * $P<0.05$; ** $P<0.01$; *** $P<0.001$; **** $P<0.0001$.

6.3 Discussion

In AD the regulation of multiple pathways involved in the pathogenesis and progression of the disease is the main target for a potential disease-modifying therapy. The novel compound 16g aims to do so by inhibiting both AChE enzyme and GSK3- β , with its structure designed using Tacrine and Pyrimidone as models (Eagger *et al.* 1991; Panza *et al.* 2016). In addition to this, the exploitation of a model that well

recapitulates AD neuronal features is an important step to better characterize newly synthesized compound for AD treatment. We have successfully combined two different protocols, in order to develop a neuronal model of AD Tau hyperphosphorylation (Shiple 2016; Koriyama *et al.* 2015). In particular, using GA to inhibit glycolysis, and increase AGEs level, well recapitulates the AD human features, in which accumulation of AGEs, and subsequent activation of RAGE receptor is often described, leading to activation of amyloidogenic pathway and Tau hyperphosphorylation (Deane *et al.* 2012; Donahue *et al.* 2006; Srikanth *et al.* 2011; Yan *et al.* 1996). Accumulation of AGEs as a consequence of GA treatment, results in Tau disease as seen in diabetes patients, which pathology is often linked to the development of AD (Kong *et al.* 2020; Batkulwar *et al.* 2018; Cai *et al.* 2016; Bitel *et al.* 2012). The model developed well recapitulates the neuronal features of AD, with GA treatment leading to abnormal phosphorylation of Tau protein on different residues, neurite degeneration, along with reduced cell viability.

This model is of peculiar relevance as it offers, a novel platform to further study on RAGE signalling, which has often been linked to AD development (Li, Lv, *et al.* 2012b). RAGE is an immunoglobulin superfamily receptor capable of binding, AGEs, Amyloid beta, and other ligands.

In a work involving both SH-SY5Y and hippocampal primary neurons, application of AGEs induced a dose-dependent increase on Tau hyperphosphorylation on multiple residues including S199, S396, S404 (Cai *et al.* 2016). These results overlap our findings obtained after GA treatment, showing an increase aberrant phosphorylation in Tau S199 and S396.

Assessment of dual AChE/GSK3- β inhibitor 16g showed as well promising results, overlapping results obtained by the commercially available GSK3- β inhibitor Tideglusib. In addition to this, 16g showed a significant reduction of amyloid aggregation, suggesting a potential amelioration of amyloid-derived symptomatology as previously observed by other AChE inhibitor. This is of peculiar importance as Tideglusib has already been tested as AD therapy, but failed during phase II clinical trial (Lovestone *et al.* 2015). Therefore, the simultaneous inhibition of AChE and GSK3- β may improve the efficacy on AD treatment, despite further test on amyloid-related pathology are necessary to confirm this.

On the other hand, among the different AChE inhibitors tested did not resulted in a homogenous comparable outcome, despite significant inhibition of the enzyme recorded, suggesting that inhibition of AChE enzyme may modulate different AD pathways involved in the Tau hyperphosphorylation triggered by GA, but in a non-specific manner derived by the distribution and concentration of different acetylcholine receptors. Other than that, for several compounds a non-significant inhibition of AChE enzyme still resulted in a significant amelioration of the parameters analysed, further suggesting that inhibition of AChE enzyme result in a response controlled by the pathways activated by specific acetylcholine receptors.

Despite this, inhibition of AChE enzyme was confirmed to reduce amyloid aggregation rate for all the compounds tested, further confirming the importance of AChE enzyme in amyloid aggregation.

7 Final Discussion

Amyloid plaques aggregation, presence of neurofibrillary tangles, and depletion of cholinergic neurons characterise the pathogenesis and progression of AD (Tiwari *et al.* 2019; Hampel *et al.* 2018). However, a clear causative agent is still missing resulting in a constant failure of AD clinical trial (Cummings *et al.* 2019).

Several reports have highlighted as a triggering mechanism the depletion of cholinergic neurons in crucial memory and learning circuits, others reported the amyloid cascade as AD starting point, while different research groups focused on NFTs as potential causative agent (Zhang *et al.* 2020; Mi *et al.* 2006; Ramos-Rodriguez *et al.* 2013).

What is clear is that all these potential AD triggering mechanisms, and related pathways, are connected to each other, and which balance is disproportionate with aging, the main risk factor of AD, leading to symptoms exacerbation in the elderly population (Sala Frigerio *et al.* 2019). Thus, a therapy able to modulate multiple aspects of AD could potentially stop the disease progression.

In this research project, we have initially investigated the efficacy of a novel AChE inhibitor as AD therapy, as well as the currently FDA approved AChE inhibitors. AChE inhibitors are the first class of molecules approved by the FDA for AD treatment, aiming to increase the acetylcholine levels in those cholinergic network implicated in memory and learning functions (Nordberg *et al.* 1998). However, none of the current AChE inhibitors used for AD treatment has shown disease-modifying effects, with their benefit being limited to a stabilization of the psychiatric symptomatology (Haake *et al.* 2020; Wilkinson *et al.* 2004). Despite these limitations, AChE enzyme is still being used as AD target for its implications in the cognitive

symptomatology, in amyloid plaques aggregation, and for the fact that many of the AChE inhibitors have a beneficial effects for a limited time. (dos Santos Picanco *et al.* 2018; Inestrosa *et al.* 1996; Jiang *et al.* 2019; Rees *et al.* 2003; Shrivastava *et al.* 2019; Silman *et al.* 2008; Tayeb *et al.* 2012; Wang *et al.* 2015; Wang *et al.* 2018).

As a result of our collaboration with Prof. Xu research team, we were able to test novel AChE inhibitors, along with a multi-target drug molecule named 16g. The latter is a dual AChE/GSK3- β enzymes inhibitor, aiming to both modulate the psychiatric symptomatology, along with reducing Tau phosphorylation levels and, therefore, prevent the formation of NFTs.

GSK3- β is a an important kinase in Tau phosphorylation, as it is responsible of phosphorylating a number of different residues, and it is activated by various pathways involved in AD pathogenesis (Chong *et al.* 2012; Hernandez *et al.* 2013; Hooper *et al.* 2008; Li, Lv, *et al.* 2012a).

Several milestones were defined to better test the efficacy of these novel molecules.

We firstly assessed the suitability of different *Drosophila melanogaster* AD models to study the efficacy of novel AChE inhibitors provided by Prof. Xu (CPU – Nanjing). These included defining measurable parameters, which could be used to assess the effect on the induced symptomatology, along with an evaluation of the AD features present in the CNS.

Secondly, we have assessed the efficacy of the novel molecule XJP-1, along with the FDA approved AD therapy, on a transgenic *Drosophila* overexpressing A β_{arc} peptides and, then, on Tau model of *Drosophila*.

Thirdly, we have developed a neuron-like model of AD harbouring Tau hyperphosphorylation features as drug testing platform.

Fourthly, we have assessed the efficacy of the new compound 16g on the novel neuron-like model of AD.

Our work further confirms the extensively reported limited efficacy of AChE inhibitors as AD therapy, with only beneficial effects on amyloid-defects. However, despite such limitation, AChE inhibitor have been an optimal starting point to improve our strategy to treat AD, with clear needs of targeting Tau hyperphosphorylation. This not only paved the way for a dual inhibiting strategy for both AChE and GSK3- β enzyme, but also highlighted the importance of a more detailed model to study this aspect of AD.

7.1 Inhibition of AChE enzyme by XJP-1 results in amelioration of amyloid-induced symptomatology

Activation of amyloidogenic pathway leads to secretion of A β peptides in the extracellular environment, where they aggregates to form senile plaques (Takahashi *et al.* 2017). Despite a triggering mechanism of the amyloid cascade is yet to be discovered, according to the cholinergic hypothesis, a depletion in cholinergic markers such as acetylcholine, and acetyltransferase, anticipates the activation of the amyloidogenic pathway. In addition to this, the NBM, source of main cortical cholinergic innervation undergoes a neurodegenerative process during AD progression, therefore resulting in memory and learning impairments (Mesulam 2013; Bowen *et al.* 1976). Moreover, test on cholinergic antagonist have resulted in AD-like cognitive symptoms, whilst agonist improved the psychiatric symptomatology (Drachman *et al.* 1974).

Recent studies linked the cholinergic system to the exacerbation of amyloid pathology as well, showing that depletion of cholinergic neurons resulted in accumulation of amyloid plaques (Ramos-Rodriguez *et al.* 2013; Potter *et al.* 2011). Other than that, a clear involvement of AChE enzyme in promoting, and accelerating, amyloid aggregation was demonstrated, along with evidences of increased neurotoxicity of A β fibrils (Inestrosa *et al.* 1996; Bartolini *et al.* 2003; Inestrosa *et al.* 2008; Alvarez *et al.* 1998). Furthermore, inhibition of AChE enzyme results in a lower amyloid aggregation rate, therefore limiting amyloid plaques formation (Jiang *et al.* 2019; Carvajal *et al.* 2011).

Thus, inhibiting AChE enzyme has been the main target over the past three decades, with a number of inhibitors approved as AD treatment, despite limited beneficial effects reported (Wilkinson *et al.* 2004; Tayeb *et al.* 2012).

As a result of our collaboration with Prof. Xu research group at CPU, we were provided with a newly synthesized AChE inhibitor, XJP-1, with a reported dual binding activity to both PAS and CAS sites of AChE enzyme, resulting in an increased specificity for AChE over BuChE, which inhibition is commonly known for resulting in potential side effects (Wang *et al.* 2015; Jiang *et al.* 2019). In order to study the efficacy of novel compounds, we exploited *Drosophila melanogaster* overexpressing mutant APP as AD model. The A β_{arc} flies exhibited a severe symptomatology, recapitulating the human features, along with deposition of amyloid plaques within the brain.

Administrated at 40 μ M concentration, XJP-1 increased the life expectancies and locomotive functions of A β_{arc} flies, with results being overlapped only by Donepezil despite this being administrated at 0.5mM.

CNS analysis for amyloid plaques deposition revealed that XJP-1 reduced the amyloid spots count as early as 10 days after commencing the treatment, in crucial regions for cognitive functions of *Drosophila Melanogaster*. Conversely, none of FDA therapies was able to have comparable results, despite administered at a much higher concentrations.

We further assessed the efficacy of XJP-1 on amyloid deposition after 20 days of treatment, which resulted in a significant drop, with the same results being scored by Donepezil only, the most potent AD therapy approved by the FDA.

To understand whether the reduction of amyloid plaques observed in the CNS was a result of a reduced peptide quantity, we quantified the A β peptides in the fly heads, and found no differences between treated and untreated group at any of the time points examined.

Thus, we speculated that AChE inhibition would result in a slower aggregation rate of amyloid peptides, as previously reported (Inestrosa *et al.* 1996; Rees *et al.* 2003). Investigation of amyloid aggregation rate showed a significant reduction in amyloid aggregation rate in presence of AChE and XJP-1, with a drop of about 80% being replicated only by Donepezil at 0.5mM concentration. In addition to this, we evaluated whether combination of NMDAR antagonist Memantine along with AChE inhibitor, XJP-1 or Donepezil, would result in any further beneficial effect on the amyloid-induced defects. However, none of the combined therapies evaluated resulted in a significant improvement when compared to the monotherapy.

Taken together, this data suggests that XJP-1 significantly ameliorates the amyloid-induced symptomatology by reducing the amyloid aggregation, and plaques formation, by inhibiting AChE enzyme.

7.2 Inhibition of AChE enzyme does not result in a clear anti-Tau effect

AD is a complex neurodegenerative disease composed of multiple features acting together in driving its progression. Despite amyloid plaques play a fundamental role in inducing neuronal toxicity and subsequent symptomatology, Tau hyperphosphorylation and NFTs are known to be a crucial player in AD progression and pathogenesis (Bloom 2014; Tapia-Rojas *et al.* 2019). Tau hyperphosphorylation is a consequence of an aberrant activation of different kinases, and/or phosphatases, as a downstream effect of multiple pathways (Grundke-Iqbal *et al.* 1986; Hu *et al.* 2008; Cai *et al.* 2016; Mi *et al.* 2006; Busche *et al.* 2019; Iqbal *et al.* 2005; Zhang *et al.* 2020).

It was reported an involvement of the cholinergic network in Tau hyperphosphorylation pathways and, additionally, that inhibition of AChE enzyme could prevent activation of GSK3- β , a fundamental kinase involved in this process (Yoshiyama *et al.* 2010; Noh *et al.* 2009; Hampel *et al.* 2018).

To investigate whether XJP-1 treatment would results in any beneficial effect against Tau pathology, we used a different *Drosophila* model, expressing human Tau 2N4R isoform to assess the compound efficacy, along with the FDA approved therapies.

Tau fruit flies showed a significant reduction in the lifespan along with locomotive defects. The Tau flies treated with XJP-1 showed increment of the life expectancy, without any improvement of the locomotive functions, with none of the other therapies under investigation having better results than XJP-1. Particularly, Donepezil was reported to improve climbing activity on Tau *Drosophila* at 30 μ M dosage, but despite administrating it at 0.5mM, we were not able to confirm these results (Zhang, Li, *et al.* 2016).

Analysis of CNS for Tau hyperphosphorylation on S396 residue revealed that none of compounds tested showed a significant reduction of the abnormal phosphorylation after both 10 and 20 days of therapy.

Moreover, study on neurodegeneration exploiting the REP model induced by Tau expression, revealed that Donepezil was the only drug able to rescue the eye defects, whilst none of the other therapies did.

Since contradictory results were generated by using Tau *Drosophila* as AD model, we decided to design and develop a neuron-like model to test the novel drug candidate by exploiting SH-SY5Y differentiation, and GA-induced Tau hyperphosphorylation on SH-SY5Y as previously reported (Shiple 2016; Koriyama *et al.* 2015).

Analysis of neurite density resulted in a significant increment of SH-SY5Y cells treated with RA along with an increased neurite length. Subsequently, since GA was reported to induce Tau hyperphosphorylation in SH-SY5Y cells, we assessed whether this result could be replicated in differentiated neurons as well. Analysis of Tau residues S199 and S396 showed a significant increment of phosphorylation levels in neurons treated with either 0.7mM or 1mM GA. Confocal imaging showed a significant reduction of neurite length in GA treated neurons, along with neuronal death. These parameters were then exploited to test XJP-1 along with novel AChE inhibitors, provided by Prof. Xu, named SAD-2, SAD-6, and FAD.

Assessment of the AChE inhibitors on Tau phosphorylation resulted in contradictory results on S199 with beneficial effects being recorded in 0.7mM GA exposed neurons, whilst no reduction was recorded in 1mM GA exposed neurons, despite AChE inhibition of the compounds tested showed overlapping results in both 0.7mM GA and 1mM GA exposed neurons. On the other hand, all AChE inhibitors tested were able to

reduce the phosphorylation levels on S396 in both 0.7mM GA and 1mM GA treated neurons.

Morphology analysis to assess whether AChE inhibition would result in any prevention of neurite degeneration resulting from 0.7mM GA treatment and Tau hyperphosphorylation, showed positive results only in XJP-1 treated neurons, whilst none of the other AChE inhibitors showed a significant difference from the untreated group.

Conversely, 1mM GA exposed neurons treated with AChE inhibitors recorded a significant increment of neurite length compared to the untreated group, with just Donepezil (at 5 μ M concentration) and SAD-6 (at 0.5 μ M) not recording a significant effect.

Further to this, in order to investigate whether AChE inhibition effects on neuronal cell death induced by GA treatment and subsequent abnormal phosphorylation, we performed an MTT assay in 24hours treated cells. All AChE inhibitors tested showed a significant increase in cell viability in 0.7mM GA exposed neurons, with the exception of compound FAD. In 1mM GA exposed neurons XJP-1 administration did not result in a significant increase in cell viability, whilst FAD, which failed on the previous assay, significantly reduced cell death at 5 μ M concentration.

In order to evaluate the ability of novel compounds in reducing the amyloid aggregation rate by inhibiting AChE enzyme, we assessed the peptides aggregation in presence of the new inhibitors. All AChE inhibitors showed a significant reduction of the amyloid aggregation rate at various concentration, up to 10nM, confirming the ability of AChE inhibitors in reducing A β peptides aggregation.

To summarize, these data suggests that AChE inhibition can modulate Tau phosphorylation in an indirect manner. The variety, and often contradictory, results we obtained showed the limitation of the AChE inhibitor therapy, which outcome is not controlled by the drug mechanism itself, but rather from the composition of acetylcholine receptors in the post-synaptic neurons, which then trigger a number of different pathways not controlled by the AChE enzyme itself.

7.3 Dual inhibition of GSK3- β and AChE enzymes modulates Tau phosphorylation in neuron-like model of AD and improves cognitive functions in mice

GSK3- β is a long known kinase involved in a number of different functions. In AD it has been highlighted as fundamental kinase in Tau phosphorylation on multiple residues, as well as in the amyloidogenic pathway (Chu *et al.* 2017; Hernandez *et al.* 2013; Hooper *et al.* 2008). GSK3- β is the downstream kinase activated by multiple different pathways, such as RAGE signalling pathway (Cai *et al.* 2016; Li, Lv, *et al.* 2012b; Ramasamy *et al.* 2005; Takuma *et al.* 2009). The latter is activated as a result of AGEs accumulation, which is often described in diabetes patients and more frequently linked to AD development (Kong *et al.* 2020).

Since GSK3- β is the downstream actor of multiple processes, targeting it with a pharmacological inhibitor could result in the prevention of Tau phosphorylation, and formation of NFTs.

In order to target GSK3- β , Prof. Xu research group, kindly provided us with a novel dual AChE/GSK3- β inhibitor, named 16g, which we tested on the novel Tau model along with the commercial GSK3- β inhibitor Tideglusib as control drug.

Compound 16g, showed a significant dose-dependent reduction of S199 phosphorylation levels in neurons exposed to 0.7mM GA, at a concentration as low as 50nM, whilst Tideglusib recorded a significant reduction only when administrated 5 μ M. On the other hand, no significant reduction was recorded on 1mM GA exposed neurons treated with 16g, while Tideglusib showed a drop in phosphorylation levels in S199.

Analysis of S396 residue revealed a significant reduction of phosphorylation levels on both 0.7mM and 1mM GA exposed neurons after treatment with either 16g or Tideglusib.

In addition to this, 16g treatment prevented neurite degeneration in a dose-dependent manner in 0.7mM GA exposed neurons, with results being replicated by Tideglusib.

Morphology analysis of 1mM exposed neurons incubated with compound 16g showed a significant increase in neurite length; again these results were confirmed by Tideglusib.

Cell viability assessment after treatment with either 16g or control drug Tideglusib recorded a significant increment, at all concentration studied, in both 0.7mM and 1mM GA exposed neuron.

Further to this, we decided to investigate 16g efficacy in inhibiting amyloid aggregation induced by AChE, since its reported dual inhibitory activity against both AChE and GSK3- β enzymes.

Compound 16g significantly reduced amyloid aggregation in presence of AChE enzyme, at a concentration as low as 50nM, suggesting its potential in modulating amyloid aggregation as well.

Animal studies, performed by Prof. Xu and Dr. Pengfe Zhang at CPU, showed a significant improvement of the cognitive functions in an AD animal model as well (Fig.S4 A-C).

To conclude, compound 16g multi-target strategy showed a homogenous effect in preventing GA-induced Tau hyperphosphorylation, with results being overlapped by a commercial GSK3- β inhibitor.

The demonstrated efficacy in modulating Tau phosphorylation on multiple residues, along with the potential of reducing the amyloid aggregation rate, of compound 16g could pave the way for novel multi-target strategy of treating AD.

8 Final Conclusions

The results presented in my PhD thesis suggest that inhibition of AChE enzyme can modulate multiple different pathways involved in AD pathogenesis, despite not being directly controlled by the therapy itself, giving a possible explanation for the often contradictory results observed when assessing different AChE inhibitors.

However, a clear beneficial effect was found in modulating amyloid aggregation, and prevention of amyloid-induced symptoms.

The development of a novel neuron-like model of AD harbours multiple benefits including: reduced costs, Tau phosphorylation on multiple residues, possible platform to study diabetes and AD link. This model has allowed me to overcome the issue faced in the *Drosophila* model, in particular the uncontrolled dosage.

In addition to this, the results obtained on the novel compound 16g suggests that it can modulate different aspects of the disease, which is of crucial importance for treating AD which has an unknown triggering mechanism. Thus, targeting a downstream enzyme such as GSK3- β , implicated in both Tau and amyloid pathways, along with modulation of psychiatric symptomatology, by AChE inhibition, can be a successful way of treating AD.

9 Limitations and future perspectives

There are several parts of the work described in this thesis that highlight the limitations of the model/results obtained, and potential area of further research to overcome them. One of the first limitation is the usage of *Drosophila melanogaster* as AD model. The fruit fly genotype we exploited recapitulates the human symptomatology and CNS features. However, it is a form of EOAD, which account for only the 1% of the total AD cases. Tests on a fruit fly genotype expressing human Tau 2N4R, BACE1 enzyme, and APP protein resulted in a shortened lifespan only, whilst no signs of locomotive defects, nor neurodegeneration were recorded. In addition to this, in order to administrate the drug to the AD flies, each compound was mixed within the food. Thus, there is no control over the actual amount of food/drug eaten by each fly. Moreover, the transgene expression was achieved using the Gal4/UAS system. The *Gal4* gene expression was placed under the control of the genomic enhancer *elav*, resulting a *pan*-neuronal expression of the A β peptides. It is unlikely that, simultaneously, all neurons of an AD patient present an active amyloidogenic pathway.

Future research on *Drosophila* AD models, should be focused on a genotype able to include the human features described in LOAD, along with the definition of different

stages of AD to overcome the unrealistic method of treating AD *Drosophila* from day 1 post eclosion.

Unfortunately, there is no way to control how much each fly eat, leading to different flies being treated with diverse dosage.

Another important limitation of *Drosophila melanogaster* as AD model is the lack of a BBB, which limits the reality of the data obtained on this particular *in vivo* model. The BBB is often identified as a crucial limitation in drug delivery strategies, as it limits the permeability to the majority of drug molecules. To overcome the limitations encountered using the *Drosophila* AD models, we decided to design and develop a neuronal model by combining two existing protocols currently used in SH-SY5Y cell line. However, the model we set up can be further improved.

First, a comprehensive investigation of which pathways are activated following GA treatment should be performed. Despite reports of increase AGEs concentration, and potential activation of RAGE signalling, this should be elucidated in differentiated neurons as well. Moreover, the cell culture set up did not include microglia cells, which are a fundamental player in AD pathogenesis. Further to this, the 2D cell culture set up can be biased by the fact that neurons do not form a proper 3D network.

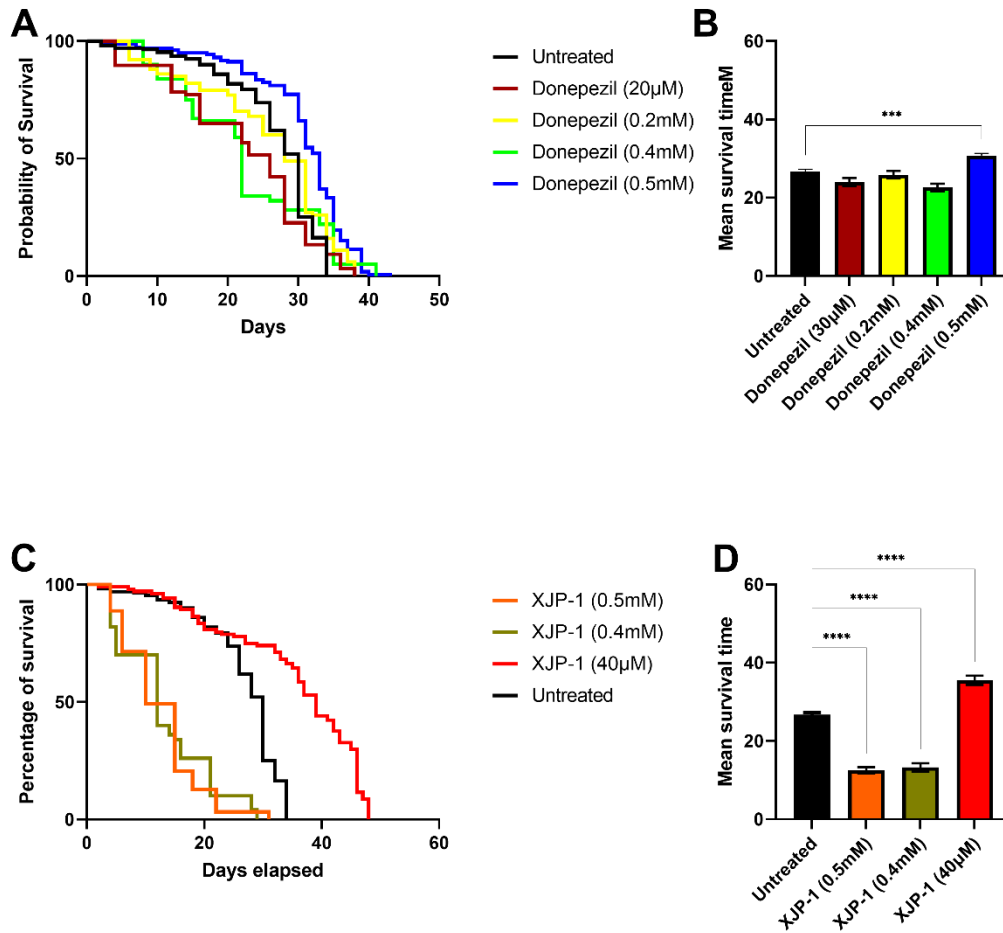
An investigation on the pathways activated by GA, along with a 3D set up of the cell culture would benefit this type of model. Other than that, electrophysiology studies on neuron treated with GA, and compounds, can be useful to enhance the understanding of AD and better characterise the therapy effects.

A further limitation of this work is the fact that all data about drug efficacy was obtained on models recapitulating one feature of AD, such as amyloid plaques and hyperphosphorylated Tau. This is a major concern, since AD pathogenesis is composed of an array of different pathways, involving not only amyloid plaques and

NFTs. Thus, drug screenings should be performed on the most realistic model of AD which recapitulates all features observed in human patients. This would benefit not only the outcome data, which would be more realistic, but also the chances of success of a potential clinical trial.

Despite a number of limitations can be highlighted, this novel cell culture AD model offers the possibility of further optimization and research. First, Crispr/Cas9 technology can be used to knockout selective genes in order to model multiple aspects of AD. For instance, by inserting a point mutation on APP gene the A β peptides deposition can be triggered offering the possibility to study both amyloid and Tau pathology in the same dish. Secondly, the model itself can be used to evaluate whether GA application causes an amyloidogenic cleavage of APP, as a result of GSK3- β activation (Llorens-Martín *et al.* 2014). Thus, we believe that the novelty of this model, offers the possibility of further dissecting several aspects of AD pathogenesis, and a testing platform for novel drug candidates.

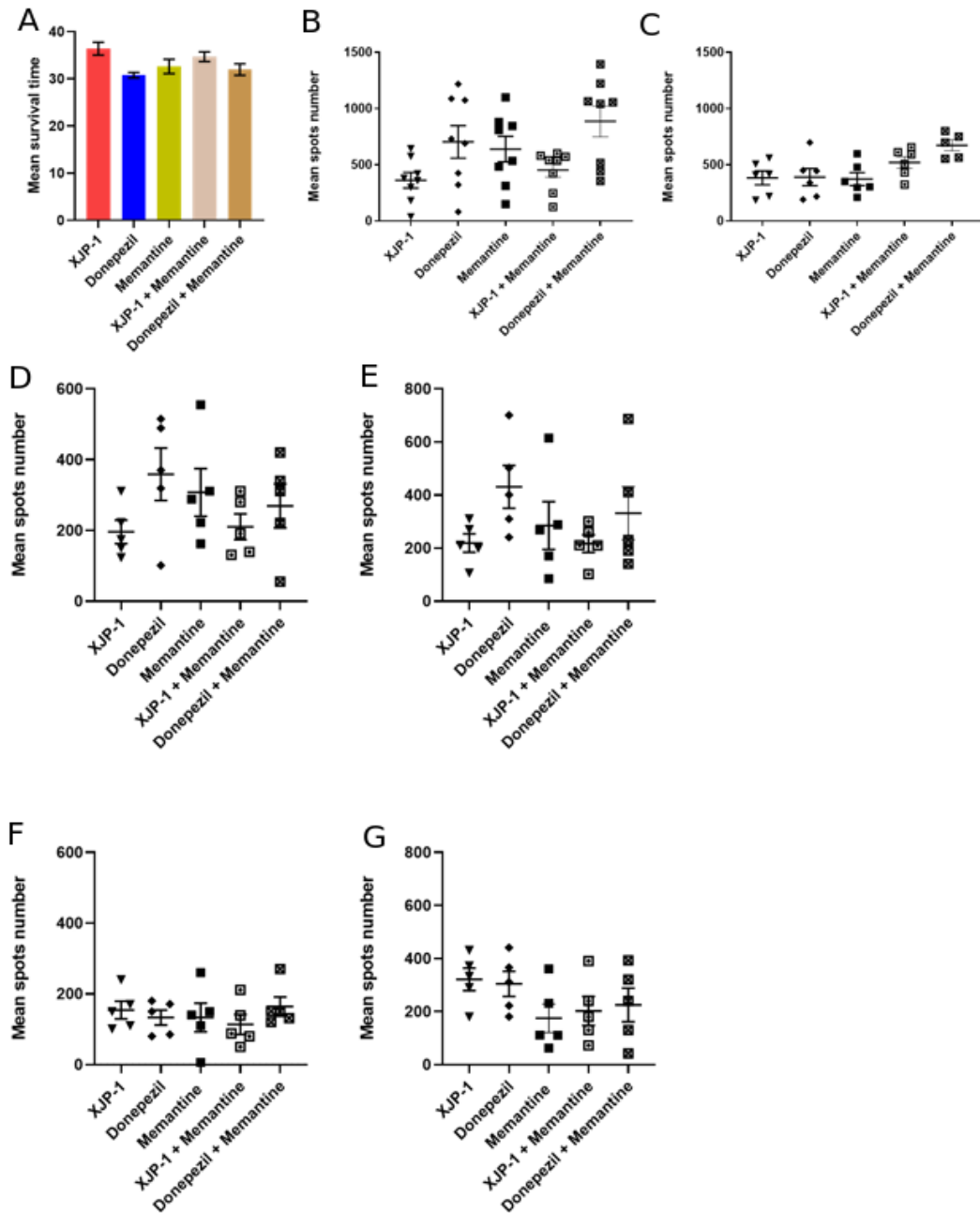
10 Supplementary figures



Supplementary figure 1. Dosage screening

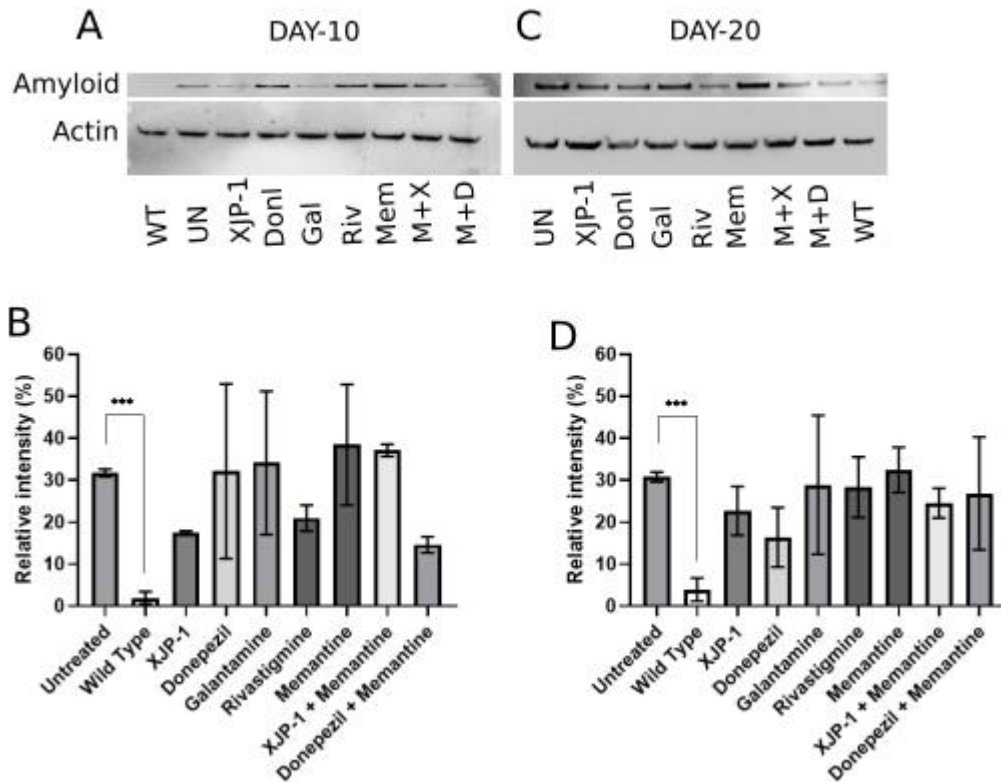
A) Kaplan-Meier survival trajectories of $A\beta_{Arc}$ flies under Donepezil treatment at different dosage. **B)** Mean survival time of $A\beta_{Arc}$ flies under Donepezil treatment at different dosage. **C)** Kaplan-Meier survival trajectories of $A\beta_{Arc}$ flies under XJP-1 treatment at different dosage. **D)** Mean survival time of $A\beta_{Arc}$ flies under XJP-1 treatment at different dosage.

Kuskar-Wallis test followed by Dunn's post-hoc was used to compare the differences between different groups. Data are expressed as mean \pm SEM, $n = 3$. $P < 0.05$ was considered as significant. * $P < 0.05$; ** $P < 0.01$; *** $P < 0.001$; **** $P < 0.0001$.



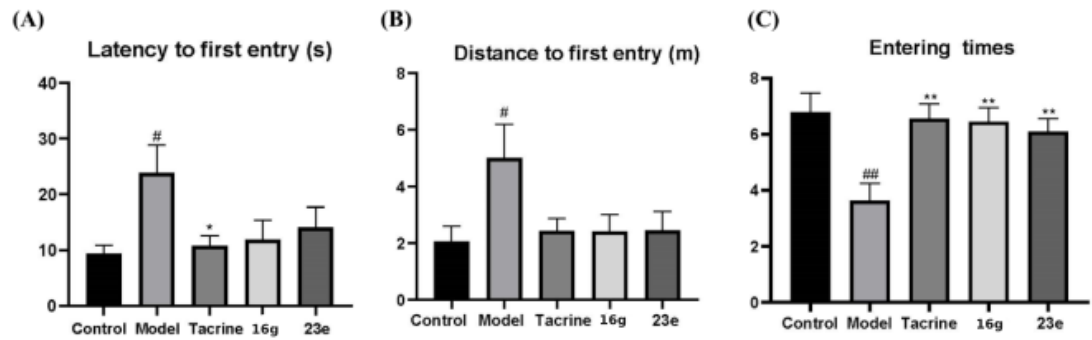
Supplementary figure 2. Comparisons between combined therapies and monotherapies on A β_{arc} flies

A) Survival time comparison **B)** Comparison of CNS amyloid spots count after 10 days. **C)** Comparison of CNS amyloid spots count after 20 days. **D)** Comparison of Mushrooms bodies and fan-shaped bodies amyloid spots count after 10 days. **E)** Comparison of Medulla and Optic Lobes amyloid spots count after 10 days. **F)** Comparison of Mushrooms bodies and fan-shaped bodies amyloid spots count after 20 days. **G)** Comparison of Medulla and Optic Lobes amyloid spots count after 20 days. Data are presented as mean \pm SEM, of n = 3 $P < 0.05$ was considered as significant. * $P < 0.05$; ** $P < 0.01$; *** $P < 0.001$; **** $P < 0.0001$.



Supplementary figure 3. Amyloid peptides quantity in A β _{Arc} flies' heads

A) Representative images of WB membranes showing amyloid peptides quantity after 10 days of treatment. B) Day-10 A β _{Arc} peptide quantification by membrane image analysis. C) Representative images of WB membranes showing amyloid peptides quantity after 20 days of treatment. D) Day-20 A β _{Arc} peptide quantification by membrane image analysis. ANOVA test followed by Bonferroni's post-hoc was used to compare the differences between different groups. Data are presented as mean \pm SEM, n = 3. $P < 0.05$ was considered as significant. * $P < 0.05$; ** $P < 0.001$; *** $P < 0.0001$.



Supplementary figure 4. Effects of compound 16g on scopolamine treated mice

Effects of intraperitoneal administration of 16g (15 mg/kg), 23e (15 mg/kg), and Tacrine (4, 15 mg/kg) on scopolamine-induced cognitive impairment in ICR mice evaluated by the Morris water maze test. **A)** Latency to first entry. **B)** Distance to first entry. **C)** Entering time. . Data are presented as the mean \pm SEM (n = 8; #p \leq 0.05, ##p \leq 0.01 vs blank control group; *p \leq 0.05, **p \leq 0.01 vs scopolamine group). This image and caption are courtesy of Prof. Jinyi Xu and Dr. Pengfei Zhang of CPU. The data presented in this image is the result of work carried out by Prof. Jinyi Xu and Dr. Pengfei Zhang

Bibliography

- Adler, G., B. Mueller, and K. Articus. 2014. 'The transdermal formulation of rivastigmine improves caregiver burden and treatment adherence of patients with Alzheimer's disease under daily practice conditions', *Int J Clin Pract*, 68: 465-70.
- Agholme, Lotta, Tobias Lindström, Katarina Kågedal, Jan Marcusson, and Martin Hallbeck. 2010. 'An In Vitro Model for Neuroscience: Differentiation of SH-SY5Y Cells into Cells with Morphological and Biochemical Characteristics of Mature Neurons', *Journal of Alzheimer's Disease*, 20: 1069-82.
- Albuquerque, Edson X., Edna F. R. Pereira, Manickavasagam Alkondon, and Scott W. Rogers. 2009. 'Mammalian nicotinic acetylcholine receptors: from structure to function', *Physiol Rev*, 89: 73-120.
- Ali, F., Rahul, S. Jyoti, F. Naz, M. Ashafaq, M. Shahid, and Y. H. Siddique. 2019. 'Therapeutic potential of luteolin in transgenic Drosophila model of Alzheimer's disease', *Neurosci Lett*, 692: 90-99.
- Alvarez, Alejandra, Rodrigo Alarcón, Carlos Opazo, Eliseo O. Campos, Francisco José Muñoz, Frances H. Calderón, Federico Dajas, Mary K. Gentry, Bhupendra P. Doctor, Fernando G. De Mello, and Nivaldo C. Inestrosa. 1998. 'Stable Complexes Involving Acetylcholinesterase and Amyloid- β Peptide Change the Biochemical Properties of the Enzyme and Increase the Neurotoxicity of Alzheimer's Fibrils', *The Journal of Neuroscience*, 18: 3213-23.
- Alzheimer, Alois. 1907. 'Über eine eigenartige Erkrankung der Hirnrinde', *Zentralbl. Nervenhe. Psych.*, 18: 177-79.
- Association, Alzheimer's. 2019. '2019 Alzheimer's disease facts and figures', *Alzheimer's & Dementia*, 15: 321-87.
- Au - Ernst, Orna, and Tsaffir Au - Zor. 2010. 'Linearization of the Bradford Protein Assay', *JoVE*: e1918.
- Au - Nichols, Charles D., Jaime Au - Becnel, and Udai B. Au - Pandey. 2012. 'Methods to Assay Drosophila Behavior', *JoVE*: e3795.
- Avila, J., J. J. Lucas, M. Perez, and F. Hernandez. 2004. 'Role of tau protein in both physiological and pathological conditions', *Physiol Rev*, 84: 361-84.
- Bartolini, Manuela, Carlo Bertucci, Vanni Cavrini, and Vincenza Andrisano. 2003. ' β -Amyloid aggregation induced by human acetylcholinesterase: inhibition studies', *Biochemical Pharmacology*, 65: 407-16.
- Basun, Hans, Nenad Bogdanovic, Martin Ingelsson, Ove Almkvist, Jan Näslund, Karin Axelman, Thomas D. Bird, David Nochlin, Gerard D. Schellenberg, Lars-Olof Wahlund, and Lars Lannfelt. 2008. 'Clinical and Neuropathological Features of the Arctic APP Gene Mutation Causing Early-Onset Alzheimer Disease', *Archives of Neurology*, 65: 499-505.
- Batkulwar, Kedar, Rashmi Godbole, Reema Banarjee, Omar Kassar, Robert J. Williams, and Mahesh J. Kulkarni. 2018. 'Advanced Glycation End Products Modulate Amyloidogenic APP Processing and Tau Phosphorylation: A Mechanistic Link between Glycation and the Development of Alzheimer's Disease', *ACS Chemical Neuroscience*, 9: 988-1000.
- Baumkötter, Frederik, Katja Wagner, Simone Eggert, Klemens Wild, and Stefan Kins. 2012. 'Structural aspects and physiological consequences of APP/APLP trans-dimerization', *Experimental brain research*, 217: 389-95.

- Beaulieu, J. M. 2012. 'A role for Akt and glycogen synthase kinase-3 as integrators of dopamine and serotonin neurotransmission in mental health', *J Psychiatry Neurosci*, 37: 7-16.
- Bhuvanendran, Saatheeyavaane, Yatinesh Kumari, Iekhsan Othman, and Mohd Farooq Shaikh. 2018. 'Amelioration of Cognitive Deficit by Embelin in a Scopolamine-Induced Alzheimer's Disease-Like Condition in a Rat Model', *Frontiers in pharmacology*, 9: 665-65.
- Bilen, J., and N. M. Bonini. 2005. 'Drosophila as a model for human neurodegenerative disease', *Annu Rev Genet*, 39: 153-71.
- Birks, J., J. Grimley Evans, V. Iakovidou, M. Tsolaki, and F. E. Holt. 2009. 'Rivastigmine for Alzheimer's disease', *Cochrane Database Syst Rev*: Cd001191.
- Bitel, Claudine L., Chinnaswamy Kasinathan, Rajesh H. Kaswala, William L. Klein, and Peter H. Frederikse. 2012. 'Amyloid- β and Tau Pathology of Alzheimer's Disease Induced by Diabetes in a Rabbit Animal Model', *Journal of Alzheimer's Disease*, 32: 291-305.
- Bloom, George S. 2014. 'Amyloid- β and Tau: The Trigger and Bullet in Alzheimer Disease Pathogenesis', *JAMA Neurology*, 71: 505-08.
- Bowen, D. M., C. B. Smith, P. White, and A. N. Davison. 1976. 'Neurotransmitter-related enzymes and indices of hypoxia in senile dementia and other abiotrophies', *Brain*, 99: 459-96.
- Brand, A.H., and N. Perrimon. 1993. 'Targeted gene expression as a means of altering cell fates and generating dominant phenotypes', *Development*, 118: 401-15.
- Bretteville, Alexis, François Marcouiller, Carl Julien, Noura B. El Khoury, Franck R. Petry, Isabelle Poitras, Didier Mougnot, Georges Lévesque, Sébastien S. Hébert, and Emmanuel Planel. 2012. 'Hypothermia-induced hyperphosphorylation: a new model to study tau kinase inhibitors', *Sci Rep*, 2: 480.
- Brookmeyer, R., E. Johnson, K. Ziegler-Graham, and H. M. Arrighi. 2007. 'Forecasting the global burden of Alzheimer's disease', *Alzheimers Dement*, 3: 186-91.
- Busche, Marc Aurel, Susanne Wegmann, Simon Dujardin, Caitlin Commins, Julia Schiantarelli, Naomi Klickstein, Tarun V. Kamath, George A. Carlson, Israel Nelken, and Bradley T. Hyman. 2019. 'Tau impairs neural circuits, dominating amyloid- β effects, in Alzheimer models in vivo', *Nat Neurosci*, 22: 57-64.
- Buschert, Verena, Arun L. W. Bokde, and Harald Hampel. 2010. 'Cognitive intervention in Alzheimer disease', *Nature Reviews Neurology*, 6: 508-17.
- Cai, Zhiyou, Nannuan Liu, Chuanling Wang, Biyong Qin, Yingjun Zhou, Ming Xiao, Liying Chang, Liang-Jun Yan, and Bin Zhao. 2016. 'Role of RAGE in Alzheimer's Disease', *Cellular and Molecular Neurobiology*, 36: 483-95.
- Carvajal, Francisco J., and Nibaldo C. Inestrosa. 2011. 'Interactions of AChE with A β Aggregates in Alzheimer's Brain: Therapeutic Relevance of IDN 5706', *Frontiers in molecular neuroscience*, 4: 19-19.
- Cavedo, E., B. Dubois, O. Colliot, S. Lista, B. Croisile, G. L. Tisserand, J. Touchon, A. Bonafe, P. J. Ousset, O. Rouaud, F. Ricolfi, A. Vighetto, F. Pasquier, S. Galluzzi, C. Delmaire, M. Ceccaldi, N. Girard, S. Lehericy, F. Duveau, M. Chupin, M. Sarazin, D. Dormont, and H. Hampel. 2016. 'Reduced Regional Cortical Thickness Rate of Change in Donepezil-Treated Subjects With Suspected Prodromal Alzheimer's Disease', *J Clin Psychiatry*, 77: e1631-e38.

- Cavedo, Enrica, Michel J. Grothe, Olivier Colliot, Simone Lista, Marie Chupin, Didier Dormont, Marion Houot, Stephane Lehericy, Stefan Teipel, Bruno Dubois, Harald Hampel, Bernard Croisile, Guy Louis Tisserand, Alain Bonafe, Pierre J. Ousset, Olivier Rouaud, Frédéric Ricolfi, Alain Vighetto, Florence Pasquier, Christine Delmaire, Mathieu Ceccaldi, Nadine Girard, Françoise Duveau, Marie Sarazin, and Group Hippocampus Study. 2017. 'Reduced basal forebrain atrophy progression in a randomized Donepezil trial in prodromal Alzheimer's disease', *Sci Rep*, 7: 11706.
- Chakraborty, Ranjita, Vidya Vepuri, Siddhita D. Mhatre, Brie E. Paddock, Sean Miller, Sarah J. Michelson, Radha Delvadia, Arkit Desai, Marianna Vinokur, David J. Melicharek, Suruchi Utreja, Preeti Khandelwal, Sara Ansaloni, Lee E. Goldstein, Robert D. Moir, Jeremy C. Lee, Loni P. Tabb, Aleister J. Saunders, and Daniel R. Marena. 2011. 'Characterization of a Drosophila Alzheimer's disease model: pharmacological rescue of cognitive defects', *PLoS One*, 6: e20799-e99.
- Cheng, Irene H, Jorge J Palop, Luke A Esposito, Nga Bien-Ly, Fengrong Yan, and Lennart Mucke. 2004. 'Aggressive amyloidosis in mice expressing human amyloid peptides with the Arctic mutation', *Nature medicine*, 10: 1190-92.
- Choi, Se Hoon, Young Hye Kim, Matthias Hebesch, Christopher Sliwinski, Seungkyu Lee, Carla D'Avanzo, Hechao Chen, Basavaraj Hooli, Caroline Asselin, Julien Muffat, Justin B. Klee, Can Zhang, Brian J. Wainger, Michael Peitz, Dora M. Kovacs, Clifford J. Woolf, Steven L. Wagner, Rudolph E. Tanzi, and Doo Yeon Kim. 2014. 'A three-dimensional human neural cell culture model of Alzheimer's disease', *Nature*, 515: 274-78.
- Chong, Gao, Hölscher Christian, Liu Yueze, and Li Lin. 2012. 'GSK3: a key target for the development of novel treatments for type 2 diabetes mellitus and Alzheimer disease', *Reviews in the Neurosciences*, 23: 1-11.
- Chu, J., E. Lauretti, and D. Pratico. 2017. 'Caspase-3-dependent cleavage of Akt modulates tau phosphorylation via GSK3beta kinase: implications for Alzheimer's disease', *Mol Psychiatry*, 22: 1002-08.
- Cisse, Moustapha, Ursula Braun, Michael Leitges, Abraham Fisher, Gilles Pages, Frédéric Checler, and Bruno Vincent. 2011. 'ERK1-independent α -secretase cut of β -amyloid precursor protein via M1 muscarinic receptors and PKC α/ϵ ', *Molecular and cellular neurosciences*, 47: 223-32.
- Coleman, Robert A., Christopher Liang, Rima Patel, Sarah Ali, and Jogeshwar Mukherjee. 2017. 'Brain and Brown Adipose Tissue Metabolism in Transgenic Tg2576 Mice Models of Alzheimer Disease Assessed Using 18F-FDG PET Imaging', *Molecular Imaging*, 16: 1536012117704557.
- Combs, Benjamin, Rebecca L. Mueller, Gerardo Morfini, Scott T. Brady, and Nicholas M. Kanaan. 2019. 'Tau and Axonal Transport Misregulation in Tauopathies', *Advances in experimental medicine and biology*, 1184: 81-95.
- Constantinescu, R., A. T. Constantinescu, H. Reichmann, and B. Janetzky. 2007. "Neuronal differentiation and long-term culture of the human neuroblastoma line SH-SY5Y." In, 17-28. Vienna: Springer Vienna.
- Cornelison, G. L., S. A. Levy, T. Jenson, and B. Frost. 2019. 'Tau-induced nuclear envelope invagination causes a toxic accumulation of mRNA in Drosophila', *Aging Cell*, 18: e12847.
- Courtney, C., D. Farrell, R. Gray, R. Hills, L. Lynch, E. Sellwood, S. Edwards, W. Hardyman, J. Raftery, P. Crome, C. Lendon, H. Shaw, and P. Bentham. 2004.

- 'Long-term donepezil treatment in 565 patients with Alzheimer's disease (AD2000): randomised double-blind trial', *Lancet*, 363: 2105-15.
- Cummings, Jeffrey, Garam Lee, Aaron Ritter, Marwan Sabbagh, and Kate Zhong. 2019. 'Alzheimer's disease drug development pipeline: 2019', *Alzheimer's & Dementia: Translational Research & Clinical Interventions*, 5: 272-93.
- . 2020. 'Alzheimer's disease drug development pipeline: 2020', *Alzheimer's & Dementia: Translational Research & Clinical Interventions*, 6: e12050.
- Da Pozzo, Eleonora, Valeria La Pietra, Barbara Cosimelli, Federico Da Settimo, Chiara Giacomelli, Luciana Marinelli, Claudia Martini, Ettore Novellino, Sabrina Taliani, and Giovanni Greco. 2014. 'p53 Functional Inhibitors Behaving Like Pifithrin- β Counteract the Alzheimer Peptide Non- β -amyloid Component Effects in Human SH-SY5Y Cells', *ACS Chemical Neuroscience*, 5: 390-99.
- Dantoine, T., S. Auriacombe, M. Sarazin, H. Becker, J. J. Pere, and I. Bourdeix. 2006. 'Rivastigmine monotherapy and combination therapy with memantine in patients with moderately severe Alzheimer's disease who failed to benefit from previous cholinesterase inhibitor treatment', *Int J Clin Pract*, 60: 110-8.
- Das, Soumyadip, Suresh Ramakrishna, and Kye-Seong Kim. 2020. 'Critical Roles of Deubiquitinating Enzymes in the Nervous System and Neurodegenerative Disorders', *Molecules and cells*, 43: 203-14.
- Davis, J., F. Xu, R. Deane, G. Romanov, M. L. Previti, K. Zeigler, B. V. Zlokovic, and W. E. Van Nostrand. 2004. 'Early-onset and robust cerebral microvascular accumulation of amyloid beta-protein in transgenic mice expressing low levels of a vasculotropic Dutch/Iowa mutant form of amyloid beta-protein precursor', *J Biol Chem*, 279: 20296-306.
- Deane, Rashid, Itender Singh, Abhay P. Sagare, Robert D. Bell, Nathan T. Ross, Barbra LaRue, Rachal Love, Sheldon Perry, Nicole Paquette, Richard J. Deane, Meenakshisundaram Thiyagarajan, Troy Zarcone, Gunter Fritz, Alan E. Friedman, Benjamin L. Miller, and Berislav V. Zlokovic. 2012. 'A multimodal RAGE-specific inhibitor reduces amyloid β -mediated brain disorder in a mouse model of Alzheimer disease', *The Journal of Clinical Investigation*, 122: 1377-92.
- Derakhshankhah, Hossein, Soraya Sajadimajd, Samira Jafari, Zhila Izadi, Sajad Sarvari, Majid Sharifi, Mojtaba Falahati, Faezeh Moakedi, Willis Collins Akeyo Muganda, Mareike Müller, Mohammad Raoufi, and John F. Presley. 2020. 'Novel therapeutic strategies for Alzheimer's disease: Implications from cell-based therapy and nanotherapy', *Nanomedicine: Nanotechnology, Biology and Medicine*, 24: 102149.
- Donahue, John E., Stephanie L. Flaherty, Conrad E. Johanson, John A. Duncan, Gerald D. Silverberg, Miles C. Miller, Rosemarie Tavares, Wentian Yang, Qian Wu, Edmond Sabo, Virginia Hovanesian, and Edward G. Stopa. 2006. 'RAGE, LRP-1, and amyloid-beta protein in Alzheimer's disease', *Acta Neuropathol*, 112: 405-15.
- dos Santos Picanco, Leide C., Priscilla F. Ozela, Maiara de Fatima de Brito Brito, Abraao A. Pinheiro, Elias C. Padilha, Francinaldo S. Braga, Carlos H. T. de Paula da Silva, Cleydson Breno Rodrigues dos Santos, Joaquín M. C. Rosa, and Lorane Izabel da Silva Hage-Melim. 2018. 'Alzheimer's Disease: A Review from the Pathophysiology to Diagnosis, New Perspectives for Pharmacological Treatment', *Current Medicinal Chemistry*, 25: 3141-59.

- Drachman, D. A., and J. Leavitt. 1974. 'Human memory and the cholinergic system. A relationship to aging?', *Arch Neurol*, 30: 113-21.
- Drummond, Eleanor, and Thomas Wisniewski. 2017. 'Alzheimer's disease: experimental models and reality', *Acta Neuropathol*, 133: 155-75.
- Dubey, M., P. Chaudhury, H. Kabiru, and T. B. Shea. 2008. 'Tau inhibits anterograde axonal transport and perturbs stability in growing axonal neurites in part by displacing kinesin cargo: neurofilaments attenuate tau-mediated neurite instability', *Cell Motil Cytoskeleton*, 65: 89-99.
- Duffy, Joseph B. 2002. 'GAL4 system in drosophila: A fly geneticist's swiss army knife', *genesis*, 34: 1-15.
- Duyckaerts, Charles, Marie-Claude Potier, and Benoît Delatour. 2008. 'Alzheimer disease models and human neuropathology: similarities and differences', *Acta Neuropathol*, 115: 5-38.
- Eagger, S. A., R. Levy, and B. J. Sahakian. 1991. 'Tacrine in Alzheimer's disease', *The Lancet*, 337: 989-92.
- El-Hayek, Youssef H., Ryan E. Wiley, Charles P. Khoury, Ritesh P. Daya, Clive Ballard, Alison R. Evans, Michael Karran, José Luis Molinuevo, Matthew Norton, and Alireza Atri. 2019. 'Tip of the Iceberg: Assessing the Global Socioeconomic Costs of Alzheimer's Disease and Related Dementias and Strategic Implications for Stakeholders', *Journal of Alzheimer's Disease*, 70: 323-41.
- Farias, G., A. Cornejo, J. Jimenez, L. Guzman, and R. B. Maccioni. 2011. 'Mechanisms of Tau Self-Aggregation and Neurotoxicity', *Curr Alzheimer Res*, 8: 608-14.
- Farlow, M. R., S. Salloway, P. N. Tariot, J. Yardley, M. L. Moline, Q. Wang, E. Brand-Schieber, H. Zou, T. Hsu, and A. Satlin. 2010. 'Effectiveness and tolerability of high-dose (23 mg/d) versus standard-dose (10 mg/d) donepezil in moderate to severe Alzheimer's disease: A 24-week, randomized, double-blind study', *Clin Ther*, 32: 1234-51.
- Feany, Mel B., and Welcome W. Bender. 2000. 'A Drosophila model of Parkinson's disease', *Nature*, 404: 394-98.
- Field, R. H., A. Gossen, and C. Cunningham. 2012. 'Prior pathology in the basal forebrain cholinergic system predisposes to inflammation-induced working memory deficits: reconciling inflammatory and cholinergic hypotheses of delirium', *J Neurosci*, 32: 6288-94.
- Foidl, Bettina M., and Christian Humpel. 2018. 'Differential Hyperphosphorylation of Tau-S199, -T231 and -S396 in Organotypic Brain Slices of Alzheimer Mice. A Model to Study Early Tau Hyperphosphorylation Using Okadaic Acid', *Frontiers in Aging Neuroscience*, 10.
- Folch, Jaume, Oriol Busquets, Miren Ettcheto, Elena Sánchez-López, Ruben Dario Castro-Torres, Ester Verdaguer, Maria Luisa Garcia, Jordi Olloquequi, Gemma Casadesús, Carlos Beas-Zarate, Carme Pelegri, Jordi Vilaplana, Carme Auladell, and Antoni Camins. 2018. 'Memantine for the Treatment of Dementia: A Review on its Current and Future Applications', *J Alzheimers Dis*, 62: 1223-40.
- Frandemiche, M. L., S. De Seranno, T. Rush, E. Borel, A. Elie, I. Arnal, F. Lanté, and A. Buisson. 2014. 'Activity-dependent tau protein translocation to excitatory synapse is disrupted by exposure to amyloid-beta oligomers', *J Neurosci*, 34: 6084-97.

- Galasko, Douglas, Melville R. Klauber, C. Richard Hofstetter, David P. Salmon, Bruce Lasker, and Leon J. Thal. 1990. 'The Mini-Mental State Examination in the Early Diagnosis of Alzheimer's Disease', *Archives of Neurology*, 47: 49-52.
- Gasparotto, Juciano, Carolina S. Girardi, Nauana Somensi, Camila T. Ribeiro, José C. F. Moreira, Monique Michels, Beatriz Sonai, Mariane Rocha, Amanda V. Steckert, Tatiana Barichello, João Quevedo, Felipe Dal-Pizzol, and Daniel P. Gelain. 2018. 'Receptor for advanced glycation end products mediates sepsis-triggered amyloid- β accumulation, Tau phosphorylation, and cognitive impairment', *Journal of Biological Chemistry*, 293: 226-44.
- Gauthier, S., H. Loft, and J. Cummings. 2008. 'Improvement in behavioural symptoms in patients with moderate to severe Alzheimer's disease by memantine: a pooled data analysis', *Int J Geriatr Psychiatry*, 23: 537-45.
- Giacobini, E. 2000. 'Cholinesterase inhibitors stabilize Alzheimer's disease', *Ann NY Acad Sci*, 920: 321-7.
- Giau, Vo Van, Hyon Lee, Kyu Hwan Shim, Eva Bagyinszky, and Seong Soo A. An. 2018. 'Genome-editing applications of CRISPR-Cas9 to promote in vitro studies of Alzheimer's disease', *Clin Interv Aging*, 13: 221-33.
- Glenner, G. G., and C. W. Wong. 1984. 'Alzheimer's disease: initial report of the purification and characterization of a novel cerebrovascular amyloid protein', *Biochem Biophys Res Commun*, 120: 885-90.
- Goedert, M., and R. Jakes. 1990. 'Expression of separate isoforms of human tau protein: correlation with the tau pattern in brain and effects on tubulin polymerization', *Embo j*, 9: 4225-30.
- Goedert, M., M. G. Spillantini, R. Jakes, D. Rutherford, and R. A. Crowther. 1989. 'Multiple isoforms of human microtubule-associated protein tau: sequences and localization in neurofibrillary tangles of Alzheimer's disease', *Neuron*, 3: 519-26.
- Goedert, M., C. M. Wischik, R. A. Crowther, J. E. Walker, and A. Klug. 1988. 'Cloning and sequencing of the cDNA encoding a core protein of the paired helical filament of Alzheimer disease: identification as the microtubule-associated protein tau', *Proceedings of the National Academy of Sciences of the United States of America*, 85: 4051-55.
- Götz, J., F. Chen, J. van Dorpe, and R. M. Nitsch. 2001. 'Formation of neurofibrillary tangles in P3011 tau transgenic mice induced by A β 42 fibrils', *Science*, 293: 1491-5.
- Götz, Jürgen, Glenda Halliday, and Rebecca M. Nisbet. 2019. 'Molecular Pathogenesis of the Tauopathies', *Annual Review of Pathology: Mechanisms of Disease*, 14: 239-61.
- Gouras, Gunnar K., Claudia G. Almeida, and Reisuke H. Takahashi. 2005. 'Intraneuronal A β accumulation and origin of plaques in Alzheimer's disease', *Neurobiology of Aging*, 26: 1235-44.
- Graham, W. Vallen, Alessandra Bonito-Oliva, and Thomas P. Sakmar. 2017. 'Update on Alzheimer's Disease Therapy and Prevention Strategies', *Annual Review of Medicine*, 68: 413-30.
- Gralle, Matthias, Michelle Gralle Botelho, and Fred S. Wouters. 2009. 'Neuroprotective Secreted Amyloid Precursor Protein Acts by Disrupting Amyloid Precursor Protein Dimers', *Journal of Biological Chemistry*, 284: 15016-25.

- Gratuzé, Maud, Cheryl E. G. Leys, and David M. Holtzman. 2018. 'New insights into the role of TREM2 in Alzheimer's disease', *Molecular Neurodegeneration*, 13: 66.
- Grundke-Iqbal, I., K. Iqbal, Y. C. Tung, M. Quinlan, H. M. Wisniewski, and L. I. Binder. 1986. 'Abnormal phosphorylation of the microtubule-associated protein tau (tau) in Alzheimer cytoskeletal pathology', *Proc. Natl. Acad. Sci. U. S. A.*, 83: 4913.
- Haake, Andrea, Kevin Nguyen, Lauren Friedman, Binu Chakkamparambil, and George T. Grossberg. 2020. 'An update on the utility and safety of cholinesterase inhibitors for the treatment of Alzheimer's disease', *Expert Opinion on Drug Safety*, 19: 147-57.
- Hall, Alicia M., and Erik D. Roberson. 2012. 'Mouse models of Alzheimer's disease', *Brain research bulletin*, 88: 3-12.
- Hempel, H., M. M. Mesulam, A. C. Cuello, M. R. Farlow, E. Giacobini, G. T. Grossberg, A. S. Khachaturian, A. Vergallo, E. Cavedo, P. J. Snyder, and Z. S. Khachaturian. 2018. 'The cholinergic system in the pathophysiology and treatment of Alzheimer's disease', *Brain*, 141: 1917-33.
- Hansen, R. A., G. Gartlehner, A. P. Webb, L. C. Morgan, C. G. Moore, and D. E. Jonas. 2008. 'Efficacy and safety of donepezil, galantamine, and rivastigmine for the treatment of Alzheimer's disease: a systematic review and meta-analysis', *Clin Interv Aging*, 3: 211-25.
- Hardy, J. A., and G. A. Higgins. 1992. 'Alzheimer's disease: the amyloid cascade hypothesis', *Science*, 256: 184-5.
- Heneka, Michael T., Monica J. Carson, Joseph El Khoury, Gary E. Landreth, Frederic Brosseron, Douglas L. Feinstein, Andreas H. Jacobs, Tony Wyss-Coray, Javier Vitorica, Richard M. Ransohoff, Karl Herrup, Sally A. Frautschy, Bente Finsen, Guy C. Brown, Alexei Verkhratsky, Koji Yamanaka, Jari Koistinaho, Eicke Latz, Annett Halle, Gabor C. Petzold, Terrence Town, Dave Morgan, Mari L. Shinohara, V. Hugh Perry, Clive Holmes, Nicolas G. Bazan, David J. Brooks, Stéphane Hunot, Bertrand Joseph, Nikolaus Deigendesch, Olga Garaschuk, Erik Boddeke, Charles A. Dinarello, John C. Breitner, Greg M. Cole, Douglas T. Golenbock, and Markus P. Kummer. 2015. 'Neuroinflammation in Alzheimer's disease', *The Lancet. Neurology*, 14: 388-405.
- Hernández, Félix, Elena Gómez de Barreda, Almudena Fuster-Matanzo, José J. Lucas, and Jesús Avila. 2010. 'GSK3: A possible link between beta amyloid peptide and tau protein', *Experimental Neurology*, 223: 322-25.
- Hernandez, Felix, Jose J. Lucas, and Jesus Avila. 2013. 'GSK3 and Tau: Two Convergence Points in Alzheimer's Disease', *Journal of Alzheimer's Disease*, 33: S141-S44.
- Heron, M. 2019. 'Deaths: Leading Causes for 2017', *Natl Vital Stat Rep*, 68: 1-77.
- Higham, James P., Bilal R. Malik, Edgar Buhl, Jennifer M. Dawson, Anna S. Ogier, Katie Lunnon, and James J. L. Hodge. 2019. 'Alzheimer's Disease Associated Genes Ankyrin and Tau Cause Shortened Lifespan and Memory Loss in *Drosophila*', *Frontiers in cellular neuroscience*, 13: 260-60.
- Himeno, Eri, Yasumasa Ohyagi, Linqing Ma, Norimichi Nakamura, Katsue Miyoshi, Nobutaka Sakae, Kyoko Motomura, Naoko Soejima, Ryo Yamasaki, Tetsuya Hashimoto, Takeshi Tabira, Frank M. LaFerla, and Jun-ichi Kira. 2011. 'Apomorphine treatment in Alzheimer mice promoting amyloid- β degradation', *Ann Neurol*, 69: 248-56.

- Himmler, A., D. Drechsel, M. W. Kirschner, and D. W. Martin, Jr. 1989. 'Tau consists of a set of proteins with repeated C-terminal microtubule-binding domains and variable N-terminal domains', *Mol Cell Biol*, 9: 1381-8.
- Hooper, Claudie, Richard Killick, and Simon Lovestone. 2008. 'The GSK3 hypothesis of Alzheimer's disease', *J Neurochem*, 104: 1433-39.
- Hu, M., J. F. Waring, M. Gopalakrishnan, and J. Li. 2008. 'Role of GSK-3 β activation and $\alpha 7$ nAChRs in A β 1-42-induced tau phosphorylation in PC12 cells', *J. Neurochem.*, 106: 1371.
- Huang, Y., and T. Liu. 2015. 'Amyloid Beta Peptide 1-42 Induces SH-SY5Y Cell Apoptosis via the Promotion of Meg3 Long Noncoding RNA Expression', *Integrative Medicine International*, 2: 73-79.
- Hunter, J. M., J. Kwan, M. Malek-Ahmadi, C. L. Maarouf, T. A. Kokjohn, C. Belden, M. N. Sabbagh, T. G. Beach, and A. E. Roher. 2012. 'Morphological and pathological evolution of the brain microcirculation in aging and Alzheimer's disease', *PLoS One*, 7: e36893.
- Hwang, S., H. Jeong, E. H. Hong, H. M. Joo, K. S. Cho, and S. Y. Nam. 2019. 'Low-dose ionizing radiation alleviates Abeta42-induced cell death via regulating AKT and p38 pathways in Drosophila Alzheimer's disease models', *Biol Open*, 8.
- Inestrosa, N. C., A. Alvarez, C. A. Perez, R. D. Moreno, M. Vicente, C. Linker, O. I. Casanueva, C. Soto, and J. Garrido. 1996. 'Acetylcholinesterase accelerates assembly of amyloid-beta-peptides into Alzheimer's fibrils: possible role of the peripheral site of the enzyme', *Neuron*, 16: 881-91.
- Inestrosa, Nibaldo C., Margarita C. Dinamarca, and Alejandra Alvarez. 2008. 'Amyloid-cholinesterase interactions', *The FEBS Journal*, 275: 625-32.
- Iqbal, K., A. d C. Alonso, S. Chen, M. O. Chohan, E. El-Akkad, C. X. Gong, S. Khatoon, B. Li, F. Liu, and A. Rahman. 2005. 'Tau pathology in Alzheimer disease and other tauopathies', *Biochim. Biophys. Acta, Mol. Basis Dis.*, 1739: 198.
- Isbert, Simone, Katja Wagner, Simone Eggert, Andrea Schweitzer, Gerd Multhaup, Sascha Weggen, Stefan Kins, and Claus U. Pietrzik. 2012. 'APP dimer formation is initiated in the endoplasmic reticulum and differs between APP isoforms', *Cell Mol Life Sci*, 69: 1353-75.
- Ittner, Arne, Sook Wern Chua, Josefina Bertz, Alexander Volkerling, Julia van der Hoven, Amadeus Gladbach, Magdalena Przybyla, Mian Bi, Annika van Hummel, Claire H. Stevens, Stefania Ippati, Lisa S. Suh, Alexander Macmillan, Greg Sutherland, Jillian J. Kril, Ana P. G. Silva, Joel P. Mackay, Anne Poljak, Fabien Delerue, Yazid D. Ke, and Lars M. Ittner. 2016. 'Site-specific phosphorylation of tau inhibits amyloid- β toxicity in Alzheimer's mice', *Science*, 354: 904-08.
- Ittner, L. M., and J. Götz. 2011. 'Amyloid- β and tau--a toxic pas de deux in Alzheimer's disease', *Nat Rev Neurosci*, 12: 65-72.
- Jackson, George R., Martina Wiedau-Pazos, Tzu-Kang Sang, Naveed Wagle, Carlos A. Brown, Sasan Massachi, and Daniel H. Geschwind. 2002. 'Human Wild-Type Tau Interacts with *wingless* Pathway Components and Produces Neurofibrillary Pathology in *Drosophila*', *Neuron*, 34: 509-19.
- Jiang, C. S., Y. X. Ge, Z. Q. Cheng, J. L. Song, Y. Y. Wang, K. Zhu, and H. Zhang. 2019. 'Discovery of new multifunctional selective acetylcholinesterase

- inhibitors: structure-based virtual screening and biological evaluation', *J Comput Aided Mol Des*, 33: 521-30.
- Jiang, S., Y. Li, C. Zhang, Y. Zhao, G. Bu, H. Xu, and Y. W. Zhang. 2014a. 'M1 muscarinic acetylcholine receptor in Alzheimer's disease', *Neuroscience bulletin*, 30: 295-307.
- Jiang, Shangdong, Yanfang Li, Cuilin Zhang, Yingjun Zhao, Guojun Bu, Huaxi Xu, and Yun-Wu Zhang. 2014b. 'M1 muscarinic acetylcholine receptor in Alzheimer's disease', *Neuroscience bulletin*, 30: 295-307.
- Johansson, Ann-Sofi, Fredrik Berglind-Dehlin, Göran Karlsson, Katarina Edwards, Pär Gellerfors, and Lars Lannfelt. 2006. 'Physiochemical characterization of the Alzheimer's disease-related peptides A β 1-42Arctic and A β 1-42wt', *The FEBS Journal*, 273: 2618-30.
- Kadavath, Harindranath, Romina V. Hofele, Jacek Biernat, Satish Kumar, Katharina Tepper, Henning Urlaub, Eckhard Mandelkow, and Markus Zweckstetter. 2015. 'Tau stabilizes microtubules by binding at the interface between tubulin heterodimers', *Proceedings of the National Academy of Sciences of the United States of America*, 112: 7501-06.
- Kalkman, H. O., and D. Feuerbach. 2016. 'Modulatory effects of alpha7 nAChRs on the immune system and its relevance for CNS disorders', *Cell Mol Life Sci*, 73: 2511-30.
- Kamino, K., H. T. Orr, H. Payami, E. M. Wijsman, M. E. Alonso, S. M. Pulst, L. Anderson, S. O'Dahl, E. Nemens, J. A. White, and et al. 1992. 'Linkage and mutational analysis of familial Alzheimer disease kindreds for the APP gene region', *Am J Hum Genet*, 51: 998-1014.
- Kang, Jie, Hans-Georg Lemaire, Axel Unterbeck, J. Michael Salbaum, Colin L. Masters, Karl-Heinz Grzeschik, Gerd Multhaup, Konrad Beyreuther, and Benno Müller-Hill. 1987. 'The precursor of Alzheimer's disease amyloid A4 protein resembles a cell-surface receptor', *Nature*, 325: 733-36.
- Katz, Ben, and Baruch Minke. 2009. 'Drosophila photoreceptors and signaling mechanisms', *Frontiers in cellular neuroscience*, 3: 2-2.
- Khiroug, Serguei S., Patricia C. Harkness, Patricia W. Lamb, Sterling N. Sudweeks, Leonard Khiroug, Neil S. Millar, and Jerrel L. Yakel. 2002. 'Rat nicotinic ACh receptor α 7 and β 2 subunits co-assemble to form functional heteromeric nicotinic receptor channels', *The Journal of Physiology*, 540: 425-34.
- Kizhakke P, Anupama, Shilpa Olakkaran, Anet Antony, Siddanna Tilagul K, and Gurushankara Hunasanahally P. 2019. 'Convolvulus pluricaulis (Shankhapushpi) ameliorates human microtubule-associated protein tau (hMAP τ) induced neurotoxicity in Alzheimer's disease Drosophila model', *Journal of Chemical Neuroanatomy*, 95: 115-22.
- Knapp, M. J., D. S. Knopman, P. R. Solomon, W. W. Pendlebury, C. S. Davis, and S. I. Gracon. 1994. 'A 30-week randomized controlled trial of high-dose tacrine in patients with Alzheimer's disease. The Tacrine Study Group', *Jama*, 271: 985-91.
- Kong, Yanyan, Fushuai Wang, Jiao Wang, Cuiping Liu, Yinping Zhou, Zhengqin Xu, Chencheng Zhang, Bomin Sun, and Yihui Guan. 2020. 'Pathological Mechanisms Linking Diabetes Mellitus and Alzheimer's Disease: the Receptor for Advanced Glycation End Products (RAGE)', *Frontiers in Aging Neuroscience*, 12: 217-17.
- Korecka, Joanna A., Ronald E. van Kesteren, Eva Blaas, Sonia O. Spitzer, Jorke H. Kamstra, August B. Smit, Dick F. Swaab, Joost Verhaagen, and Koen Bossers.

2013. 'Phenotypic Characterization of Retinoic Acid Differentiated SH-SY5Y Cells by Transcriptional Profiling', *PLoS One*, 8: e63862.
- Koriyama, Y., A. Furukawa, M. Muramatsu, J. Takino, and M. Takeuchi. 2015. 'Glyceraldehyde caused Alzheimer's disease-like alterations in diagnostic marker levels in SH-SY5Y human neuroblastoma cells', *Sci Rep*, 5: 13313.
- Krishtal, Jekaterina, Olga Bragina, Kristel Metsla, Peep Palumaa, and Vello Tõugu. 2017. 'In situ fibrillizing amyloid-beta 1-42 induces neurite degeneration and apoptosis of differentiated SH-SY5Y cells', *PLoS One*, 12: e0186636-e36.
- Kwak, Sang Su, Kevin J. Washicosky, Emma Brand, Djuna von Maydell, Jenna Aronson, Susan Kim, Diane E. Capen, Murat Cetinbas, Ruslan Sadreyev, Shen Ning, Enjana Bylykbashi, Weiming Xia, Steven L. Wagner, Se Hoon Choi, Rudolph E. Tanzi, and Doo Yeon Kim. 2020. 'Amyloid- β 42/40 ratio drives tau pathology in 3D human neural cell culture models of Alzheimer's disease', *Nature Communications*, 11: 1377.
- Laurettil, E., J. G. Li, A. Di Meco, and D. Praticò. 2017. 'Glucose deficit triggers tau pathology and synaptic dysfunction in a tauopathy mouse model', *Translational psychiatry*, 7: e1020-e20.
- Leong, Yong Qi, Khuen Yen Ng, Soi Moi Chye, Anna Pick Kiong Ling, and Rhun Yian Koh. 2020. 'Mechanisms of action of amyloid-beta and its precursor protein in neuronal cell death', *Metabolic Brain Disease*, 35: 11-30.
- Leroy, K., K. Ando, V. Laporte, R. Dedecker, V. Suain, M. Authélet, C. Héraud, N. Pierrot, Z. Yilmaz, J. N. Octave, and J. P. Brion. 2012. 'Lack of tau proteins rescues neuronal cell death and decreases amyloidogenic processing of APP in APP/PS1 mice', *Am J Pathol*, 181: 1928-40.
- Lessard, C. B., M. P. Lussier, S. Cayouette, G. Bourque, and G. Boulay. 2005. 'The overexpression of presenilin2 and Alzheimer's-disease-linked presenilin2 variants influences TRPC6-enhanced Ca²⁺ entry into HEK293 cells', *Cell Signal*, 17: 437-45.
- Li, J., D. Liu, L. Sun, Y. Lu, and Z. Zhang. 2012. 'Advanced glycation end products and neurodegenerative diseases: mechanisms and perspective', *J Neurol Sci*, 317: 1-5.
- Li, X. H., B. L. Lv, J. Z. Xie, J. Liu, X. W. Zhou, and J. Z. Wang. 2012a. 'AGEs induce Alzheimer-like tau pathology and memory deficit via RAGE-mediated GSK-3 activation', *Neurobiol. Aging*, 33: 1400.
- Li, Xiao-Hong, Bing-Ling Lv, Jia-Zhao Xie, Jing Liu, Xin-Wen Zhou, and Jian-Zhi Wang. 2012b. 'AGEs induce Alzheimer-like tau pathology and memory deficit via RAGE-mediated GSK-3 activation', *Neurobiology of Aging*, 33: 1400-10.
- Lim, Y. Y., P. Maruff, R. Schindler, B. R. Ott, S. Salloway, D. C. Yoo, R. B. Noto, C. Y. Santos, and P. J. Snyder. 2015. 'Disruption of cholinergic neurotransmission exacerbates A β -related cognitive impairment in preclinical Alzheimer's disease', *Neurobiol Aging*, 36: 2709-15.
- Lipton, S. A. 2005. 'The molecular basis of memantine action in Alzheimer's disease and other neurologic disorders: low-affinity, uncompetitive antagonism', *Curr Alzheimer Res*, 2: 155-65.
- . 2007. 'Pathologically-activated therapeutics for neuroprotection: mechanism of NMDA receptor block by memantine and S-nitrosylation', *Curr Drug Targets*, 8: 621-32.
- Liu, Guoxia, Florence Hui-Ping Tan, Sie-Yik Amy Lau, Mohamad Hafis Jaafar, Fiona Yi-Li Chung, Ghows Azzam, Min-Tze Liong, and Yin Li. 'Lactic acid bacteria feeding reversed the malformed eye structures and ameliorated gut microbiota

- profiles of *Drosophila melanogaster* Alzheimer's Disease model', *Journal of Applied Microbiology*, n/a.
- Llorens-Martín, M., J. Jurado, F. Hernández, and J. Avila. 2014. 'GSK-3 β , a pivotal kinase in Alzheimer disease', *Frontiers in molecular neuroscience*, 7: 46.
- Lovestone, S., M. Boada, B. Dubois, M. Hüll, J. O. Rinne, H. J. Huppertz, M. Calero, M. V. Andrés, B. Gómez-Carrillo, T. León, and T. del Ser. 2015. 'A phase II trial of tideglusib in Alzheimer's disease', *J Alzheimers Dis*, 45: 75-88.
- Lushchekina, Sofya V., Ekaterina D. Kots, Dana A. Novichkova, Konstantin A. Petrov, and Patrick Masson. 2017. 'Role of Acetylcholinesterase in β -Amyloid Aggregation Studied by Accelerated Molecular Dynamics', *BioNanoScience*, 7: 396-402.
- Mandrekar-Colucci, Shweta, and Gary E. Landreth. 2010. 'Microglia and inflammation in Alzheimer's disease', *CNS & neurological disorders drug targets*, 9: 156-67.
- Martin, L., X. Latypova, and F. Terro. 2011. 'Post-translational modifications of tau protein: implications for Alzheimer's disease', *Neurochem Int*, 58: 458-71.
- Martinen, M., M. Takalo, T. Natunen, R. Wittrahm, S. Gabbouj, S. Kemppainen, V. Leinonen, H. Tanila, A. Haapasalo, and M. Hiltunen. 2018. 'Molecular Mechanisms of Synaptotoxicity and Neuroinflammation in Alzheimer's Disease', *Front Neurosci*, 12: 963.
- Merriam, Arnold E., Miriam K. Aronson, Patricia Gaston, Su-Ling Wey, and Ira Katz. 1988. 'The Psychiatric Symptoms of Alzheimer's Disease', *Journal of the American Geriatrics Society*, 36: 7-22.
- Mesulam, M. M. 2013. 'Cholinergic circuitry of the human nucleus basalis and its fate in Alzheimer's disease', *J Comp Neurol*, 521: 4124-44.
- Meyer-Luehmann, Melanie, Tara L. Spires-Jones, Claudia Prada, Monica Garcia-Alloza, Alix de Calignon, Anete Rozkalne, Jessica Koenigsknecht-Talboo, David M. Holtzman, Brian J. Bacskai, and Bradley T. Hyman. 2008. 'Rapid appearance and local toxicity of amyloid- β plaques in a mouse model of Alzheimer's disease', *Nature*, 451: 720-24.
- Mhatre, Siddhita D., Vivek Satyasi, Mark Killen, Brie E. Paddock, Robert D. Moir, Aleister J. Saunders, and Daniel R. Marena. 2014. 'Synaptic abnormalities in a *Drosophila* model of Alzheimer's disease', *Disease Models & Mechanisms*, 7: 373-85.
- Mi, K., and G. V. Johnson. 2006. 'The role of tau phosphorylation in the pathogenesis of Alzheimer's disease', *Curr Alzheimer Res*, 3: 449-63.
- Miyazaki, H., Y. Okamoto, A. Motoi, T. Watanabe, S. Katayama, S. I. Kawahara, H. Makabe, H. Fujii, and S. Yonekura. 2019. 'Adzuki bean (*Vigna angularis*) extract reduces amyloid-beta aggregation and delays cognitive impairment in *Drosophila* models of Alzheimer's disease', *Nutr Res Pract*, 13: 64-69.
- Mondragón-Rodríguez, S., G. Perry, J. Luna-Muñoz, M. C. Acevedo-Aquino, and S. Williams. 2014. 'Phosphorylation of tau protein at sites Ser(396-404) is one of the earliest events in Alzheimer's disease and Down syndrome', *Neuropathol Appl Neurobiol*, 40: 121-35.
- Müller, Ulrike C., Thomas Deller, and Martin Korte. 2017. 'Not just amyloid: physiological functions of the amyloid precursor protein family', *Nature Reviews Neuroscience*, 18: 281-98.
- Nalivaeva, Natalia N., and Anthony J. Turner. 2013. 'The amyloid precursor protein: A biochemical enigma in brain development, function and disease', *FEBS Letters*, 587: 2046-54.

- Nepovimova, E., E. Uliassi, J. Korabecny, L. E. Pena-Altamira, S. Samez, A. Pesaresi, G. E. Garcia, M. Bartolini, V. Andrisano, C. Bergamini, R. Fato, D. Lamba, M. Roberti, K. Kuca, B. Monti, and M. L. Bolognesi. 2014. 'Multitarget drug design strategy: quinone-tacrine hybrids designed to block amyloid-beta aggregation and to exert anticholinesterase and antioxidant effects', *J Med Chem*, 57: 8576-89.
- Newman, Morgan, Esmail Ebrahimie, and Michael Lardelli. 2014. 'Using the zebrafish model for Alzheimer's disease research', *Frontiers in Genetics*, 5.
- Nichols, C. D. 2006. 'Drosophila melanogaster neurobiology, neuropharmacology, and how the fly can inform central nervous system drug discovery', *Pharmacol Ther*, 112: 677-700.
- Nikolac Perkovic, Matea, and Nela Pivac. 2019. 'Genetic Markers of Alzheimer's Disease', *Advances in experimental medicine and biology*, 1192: 27-52.
- Nilsberth, Camilla, Anita Westlind-Danielsson, Christopher B. Eckman, Margaret M. Condron, Karin Axelman, Charlotte Forsell, Charlotte Stenh, Johan Luthman, David B. Teplow, Steven G. Younkin, Jan Näslund, and Lars Lannfelt. 2001. 'The 'Arctic' APP mutation (E693G) causes Alzheimer's disease by enhanced A β protofibril formation', *Nat Neurosci*, 4: 887-93.
- Noh, M. Y., S. H. Koh, Y. Kim, H. Y. Kim, G. W. Cho, and S. H. Kim. 2009. 'Neuroprotective effects of donepezil through inhibition of GSK-3 activity in amyloid-beta-induced neuronal cell death', *J Neurochem*, 108: 1116-25.
- Nordberg, Agneta, and Anne-Lie Svensson. 1998. 'Cholinesterase Inhibitors in the Treatment of Alzheimer's Disease', *Drug Safety*, 19: 465-80.
- Norlin, N., M. Hellberg, A. Filippov, A. A. Sousa, G. Grobner, R. D. Leapman, N. Almqvist, and O. N. Antzutkin. 2012. 'Aggregation and fibril morphology of the Arctic mutation of Alzheimer's A β peptide by CD, TEM, STEM and in situ AFM', *J Struct Biol*, 180: 174-89.
- Norwitz, Nicholas G., Adrian Soto Mota, Sam G. Norwitz, and Kieran Clarke. 2019. 'Multi-Loop Model of Alzheimer Disease: An Integrated Perspective on the Wnt/GSK3 β , α -Synuclein, and Type 3 Diabetes Hypotheses', *Frontiers in Aging Neuroscience*, 11.
- O'Brien, R. J., and P. C. Wong. 2011. 'Amyloid precursor protein processing and Alzheimer's disease', *Annu Rev Neurosci*, 34: 185-204.
- O'Nuallain, Brian, Darragh B. Freir, Andrew J. Nicoll, Emmanuel Risse, Neil Ferguson, Caroline E. Herron, John Collinge, and Dominic M. Walsh. 2010. 'Amyloid β -Protein Dimers Rapidly Form Stable Synaptotoxic Protofibrils', *The Journal of Neuroscience*, 30: 14411-19.
- Ogunsuyi, Opeyemi B., Ganiyu Oboh, Odunayo O. Oluokun, Adedayo O. Ademiluyi, and Omodesola O. Ogunraku. 2020. 'Gallic acid protects against neurochemical alterations in transgenic Drosophila model of Alzheimer's disease', *Advances in Traditional Medicine*, 20: 89-98.
- Oh, E. S., A. V. Savonenko, J. F. King, S. M. Fangmark Tucker, G. L. Rudow, G. Xu, D. R. Borchelt, and J. C. Troncoso. 2009. 'Amyloid precursor protein increases cortical neuron size in transgenic mice', *Neurobiol Aging*, 30: 1238-44.
- Panza, F., V. Solfrizzi, D. Seripa, B. P. Imbimbo, M. Lozupone, A. Santamato, C. Zecca, M. R. Barulli, A. Bellomo, A. Pilotto, A. Daniele, A. Greco, and G. Logroscino. 2016. 'Tau-Centric Targets and Drugs in Clinical Development for the Treatment of Alzheimer's Disease', *Biomed Res Int*, 2016: 3245935.
- Panza, Francesco, Madia Lozupone, Vittorio Dibello, Antonio Greco, Antonio Daniele, Davide Seripa, Giancarlo Logroscino, and Bruno P Imbimbo. 2019.

- 'Are antibodies directed against amyloid- β (A β) oligomers the last call for the A β hypothesis of Alzheimer's disease?', *Immunotherapy*, 11: 3-6.
- Papadimitriou, C., H. Celikkaya, M. I. Cosacak, V. Mashkaryan, L. Bray, P. Bhattarai, K. Brandt, H. Hollak, X. Chen, S. He, C. L. Antos, W. Lin, A. K. Thomas, A. Dahl, T. Kurth, J. Friedrichs, Y. Zhang, U. Freudenberg, C. Werner, and C. Kizil. 2018. '3D Culture Method for Alzheimer's Disease Modeling Reveals Interleukin-4 Rescues A β 42-Induced Loss of Human Neural Stem Cell Plasticity', *Dev Cell*, 46: 85-101.e8.
- Parsons, C. G., W. Danysz, A. Dekundy, and I. Pulte. 2013. 'Memantine and cholinesterase inhibitors: complementary mechanisms in the treatment of Alzheimer's disease', *Neurotox Res*, 24: 358-69.
- Pham, H. M., A. Xu, S. E. Schriener, E. A. Sevrioukov, and M. Jafari. 2018. 'Cinnamaldehyde Improves Lifespan and Healthspan in *Drosophila melanogaster* Models for Alzheimer's Disease', *Biomed Res Int*, 2018: 3570830.
- Pike, C.J., D. Burdick, A.J. Walencewicz, C.G. Glabe, and C.W. Cotman. 1993. 'Neurodegeneration induced by beta-amyloid peptides in vitro: the role of peptide assembly state', *The Journal of Neuroscience*, 13: 1676-87.
- Potter, P. E., P. K. Rauschkolb, Y. Pandya, L. I. Sue, M. N. Sabbagh, D. G. Walker, and T. G. Beach. 2011. 'Pre- and post-synaptic cortical cholinergic deficits are proportional to amyloid plaque presence and density at preclinical stages of Alzheimer's disease', *Acta Neuropathol*, 122: 49-60.
- Presgraves, Steven P., Tariq Ahmed, Sabine Borwege, and Jeffrey N. Joyce. 2003. 'Terminally differentiated SH-SY5Y cells provide a model system for studying neuroprotective effects of dopamine agonists', *Neurotox Res*, 5: 579-98.
- Ramasamy, R., S. J. Vannucci, S. S. D. Yan, K. Herold, S. F. Yan, and A. M. Schmidt. 2005. 'Advanced glycation end products and RAGE: a common thread in aging, diabetes, neurodegeneration, and inflammation', *Glycobiology*, 15: 16R.
- Ramos-Rodriguez, J. J., M. Pacheco-Herrero, D. Thyssen, M. I. Murillo-Carretero, E. Berrocoso, T. L. Spires-Jones, B. J. Bacskai, and M. Garcia-Alloza. 2013. 'Rapid beta-amyloid deposition and cognitive impairment after cholinergic denervation in APP/PS1 mice', *J Neuropathol Exp Neurol*, 72: 272-85.
- Rees, T., P. I. Hammond, H. Soreq, S. Younkin, and S. Brimijoin. 2003. 'Acetylcholinesterase promotes beta-amyloid plaques in cerebral cortex', *Neurobiology of Aging*, 24: 777-87.
- Reisberg, Barry, Rachelle Doody, Albrecht Stöfler, Frederick Schmitt, Steven Ferris, and Hans Jörg Möbius. 2003. 'Memantine in Moderate-to-Severe Alzheimer's Disease', *New England Journal of Medicine*, 348: 1333-41.
- Reiter, Lawrence T., Lorraine Potocki, Sam Chien, Michael Gribskov, and Ethan Bier. 2001. 'A Systematic Analysis of Human Disease-Associated Gene Sequences In *Drosophila melanogaster*', *Genome Research*, 11: 1114-25.
- RIEDEL, G., and K. G. REYMANN. 1996. 'Metabotropic glutamate receptors in hippocampal long-term potentiation and learning and memory', *Acta Physiologica Scandinavica*, 157: 1-19.
- Roberson, E. D., K. Scarce-Levie, J. J. Palop, F. Yan, I. H. Cheng, T. Wu, H. Gerstein, G. Q. Yu, and L. Mucke. 2007. 'Reducing endogenous tau ameliorates amyloid beta-induced deficits in an Alzheimer's disease mouse model', *Science*, 316: 750-4.

- Rudrapatna, Vivek A., Ross L. Cagan, and Tirtha K. Das. 2012. 'Drosophila cancer models', *Developmental dynamics : an official publication of the American Association of Anatomists*, 241: 107-18.
- Rush, Travis, and Alain Buisson. 2014. 'Reciprocal disruption of neuronal signaling and A β production mediated by extrasynaptic NMDA receptors: a downward spiral', *Cell and Tissue Research*, 356: 279-86.
- Sala Frigerio, Carlo, Leen Wolfs, Nicola Fattorelli, Nicola Thrupp, Iryna Voytyuk, Inga Schmidt, Renzo Mancuso, Wei-Ting Chen, Maya E. Woodbury, Gyan Srivastava, Thomas Möller, Eloise Hudry, Sudeshna Das, Takaomi Saido, Eric Karran, Bradley Hyman, V. Hugh Perry, Mark Fiers, and Bart De Strooper. 2019. 'The Major Risk Factors for Alzheimer's Disease: Age, Sex, and Genes Modulate the Microglia Response to A β Plaques', *Cell Reports*, 27: 1293-306.e6.
- Sandin, Linnea, Liza Bergkvist, Sangeeta Nath, Claudia Kielkopf, Camilla Janefjord, Linda Helmfors, Henrik Zetterberg, Kaj Blennow, Hongyun Li, Camilla Nilsberth, Brett Garner, Ann-Christin Brorsson, and Katarina Kågedal. 2016. 'Beneficial effects of increased lysozyme levels in Alzheimer's disease modelled in *Drosophila melanogaster*', *The FEBS Journal*, 283: 3508-22.
- Schröder, H., E. Giacobini, R. G. Struble, K. Zilles, and A. Maelicke. 1991. 'Nicotinic cholinergic neurons of the frontal cortex are reduced in Alzheimer's disease', *Neurobiol Aging*, 12: 259-62.
- Selkoe, D. J. 1991. 'The molecular pathology of Alzheimer's disease', *Neuron*, 6: 487-98.
- Shang, Yu, Mingyuan Liu, Tiantian Wang, Lu Wang, Huixin He, Yufang Zhong, Guangren Qian, Jing An, Tong Zhu, Xinghua Qiu, Jing Shang, and Yingjun Chen. 2019. 'Modifications of autophagy influenced the Alzheimer-like changes in SH-SY5Y cells promoted by ultrafine black carbon', *Environmental Pollution*, 246: 763-71.
- Sharma, Kamlesh. 2019. 'Cholinesterase inhibitors as Alzheimer's therapeutics (Review)', *Mol Med Rep*, 20: 1479-87.
- Shin, J., S. B. Yu, U. Y. Yu, S. A. Jo, and J. H. Ahn. 2010. 'Swedish mutation within amyloid precursor protein modulates global gene expression towards the pathogenesis of Alzheimer's disease', *BMB Rep*, 43: 704-9.
- Shin, Myeongcheol, Quan Feng Liu, Byoungyun Choi, Changmin Shin, Banseok Lee, Chunyu Yuan, You Jin Song, Hye Sup Yun, Im-Soon Lee, Byung-Soo Koo, and Kyoung Sang Cho. 2020. 'Neuroprotective Effects of Limonene (+) against A β 42-Induced Neurotoxicity in a *Drosophila* Model of Alzheimer's Disease', *Biological and Pharmaceutical Bulletin*, 43: 409-17.
- Shin, Yoojin, Se Hoon Choi, Eunhee Kim, Enjana Bylykbashi, Jeong Ah Kim, Seok Chung, Doo Yeon Kim, Roger D. Kamm, and Rudolph E. Tanzi. 2019. 'Blood–Brain Barrier Dysfunction in a 3D In Vitro Model of Alzheimer's Disease', *Advanced Science*, 6: 1900962.
- Shinosaki, Kazuhiro, Takashi Nishikawa, and Masatoshi Takeda. 2000. 'Neurobiological basis of behavioral and psychological symptoms in dementia of the Alzheimer type', *Psychiatry and Clinical Neurosciences*, 54: 611-20.
- Shipley, M. M. 2016. 'Differentiation of the SH-SY5Y Human Neuroblastoma Cell Line', *J Vis Exp*: 53193.
- Shrivastava, S. K., S. K. Sinha, P. Srivastava, P. N. Tripathi, P. Sharma, M. K. Tripathi, A. Tripathi, P. K. Choubey, D. K. Waiker, L. M. Aggarwal, M. Dixit, S. C. Kheruka, S. Gambhir, S. Shankar, and R. K. Srivastava. 2019. 'Design and

- development of novel p-aminobenzoic acid derivatives as potential cholinesterase inhibitors for the treatment of Alzheimer's disease', *Bioorg Chem*, 82: 211-23.
- Silman, I., and J. L. Sussman. 2008. 'Acetylcholinesterase: how is structure related to function?', *Chem Biol Interact*, 175: 3-10.
- Sittironnarit, G., D. Ames, A. I. Bush, N. Faux, L. Flicker, J. Foster, S. Hilmer, N. T. Lautenschlager, P. Maruff, C. L. Masters, R. N. Martins, C. Rowe, C. Szoeki, and K. A. Ellis. 2011. 'Effects of anticholinergic drugs on cognitive function in older Australians: results from the AIBL study', *Dement Geriatr Cogn Disord*, 31: 173-8.
- Sivanantharajah, Lovesha, Amritpal Mudher, and David Shepherd. 2019. 'An evaluation of *Drosophila* as a model system for studying tauopathies such as Alzheimer's disease', *Journal of Neuroscience Methods*, 319: 77-88.
- Smith, M. A., K. Hirai, K. Hsiao, M. A. Pappolla, P. L. Harris, S. L. Siedlak, M. Tabaton, and G. Perry. 1998. 'Amyloid- β Deposition in Alzheimer Transgenic Mice Is Associated with Oxidative Stress', *J. Neurochem.*, 70: 2212.
- Srikanth, Velandai, Annette Maczurek, Thanh Phan, Megan Steele, Bernadette Westcott, Damian Juskiw, and Gerald Münch. 2011. 'Advanced glycation endproducts and their receptor RAGE in Alzheimer's disease', *Neurobiology of Aging*, 32: 763-77.
- Stelzmann, Rainulf A., H. Norman Schnitzlein, and F. Reed Murtagh. 1995. 'An english translation of alzheimer's 1907 paper, "über eine eigenartige erkankung der hirnrinde"', *Clinical Anatomy*, 8: 429-31.
- Strang, Kevin H., Todd E. Golde, and Benoit I. Giasson. 2019. 'MAPT mutations, tauopathy, and mechanisms of neurodegeneration', *Laboratory Investigation*, 99: 912-28.
- Summers, W. K., L. V. Majovski, G. M. Marsh, K. Tachiki, and A. Kling. 1986. 'Oral tetrahydroaminoacridine in long-term treatment of senile dementia, Alzheimer type', *N Engl J Med*, 315: 1241-5.
- Sun, Mingkuan, and Liam Chen. 2015. 'Studying tauopathies in *Drosophila*: A fruitful model', *Experimental Neurology*, 274: 52-57.
- Tackenberg, C., S. Grinschgl, A. Trutzel, A. C. Santucci, M. C. Frey, U. Konietzko, J. Grimm, R. Brandt, and R. M. Nitsch. 2013. 'NMDA receptor subunit composition determines beta-amyloid-induced neurodegeneration and synaptic loss', *Cell Death Dis*, 4: e608.
- Takahashi, Reisuke H., Toshitaka Nagao, and Gunnar K. Gouras. 2017. 'Plaque formation and the intraneuronal accumulation of β -amyloid in Alzheimer's disease', *Pathology International*, 67: 185-93.
- Takuma, K., F. Fang, W. Zhang, S. Yan, E. Fukuzaki, H. Du, A. Sosunov, G. McKhann, Y. Funatsu, and N. Nakamichi. 2009. 'RAGE-mediated signaling contributes to intraneuronal transport of amyloid- β and neuronal dysfunction', *Proc. Natl. Acad. Sci. U. S. A.*, 106: 20021.
- Talarico, G., P. Piscopo, M. Gasparini, E. Salati, M. Pignatelli, S. Pietracupa, L. Malvezzi-Campeggi, A. Crestini, S. Boschi, G. L. Lenzi, A. Confaloni, and G. Bruno. 2010. 'The London APP Mutation (Val717Ile) Associated with Early Shifting Abilities and Behavioral Changes in Two Italian Families with Early-Onset Alzheimer's Disease', *Dementia and Geriatric Cognitive Disorders*, 29: 484-90.

- Tapia-Rojas, Cheril, Fabian Cabezas-Opazo, Carol A. Deaton, Erick H. Vergara, Gail V. W. Johnson, and Rodrigo A. Quintanilla. 2019. 'It's all about tau', *Prog Neurobiol*, 175: 54-76.
- Tariot, P. N., M. R. Farlow, G. T. Grossberg, S. M. Graham, S. McDonald, and I. Gergel. 2004. 'Memantine treatment in patients with moderate to severe Alzheimer disease already receiving donepezil: a randomized controlled trial', *Jama*, 291: 317-24.
- Tayeb, H. O., H. D. Yang, B. H. Price, and F. I. Tarazi. 2012. 'Pharmacotherapies for Alzheimer's disease: beyond cholinesterase inhibitors', *Pharmacol Ther*, 134: 8-25.
- Tiwari, Sneham, Venkata Atluri, Ajeet Kaushik, Adriana Yndart, and Madhavan Nair. 2019. 'Alzheimer's disease: pathogenesis, diagnostics, and therapeutics', *International journal of nanomedicine*, 14: 5541-54.
- Trambauer, Johannes, Akio Fukumori, and Harald Steiner. 2020. 'Pathogenic A β generation in familial Alzheimer's disease: novel mechanistic insights and therapeutic implications', *Current Opinion in Neurobiology*, 61: 73-81.
- Tue, N. T., T. Q. Dat, L. L. Ly, V. D. Anh, and H. Yoshida. 2020. 'Insights from *Drosophila melanogaster* model of Alzheimer's disease', *Front Biosci (Landmark Ed)*, 25: 134-46.
- Van Bulck, Michiel, Ana Sierra-Magro, Jesus Alarcon-Gil, Ana Perez-Castillo, and Jose A. Morales-Garcia. 2019. 'Novel Approaches for the Treatment of Alzheimer's and Parkinson's Disease', *International Journal of Molecular Sciences*, 20: 719.
- Venegas, Carmen, Sathish Kumar, Bernardo S. Franklin, Tobias Dierkes, Rebecca Brinkschulte, Dario Tejera, Ana Vieira-Saecker, Stephanie Schwartz, Francesco Santarelli, Markus P. Kummer, Angelika Griep, Ellen Gelpi, Michael Beilharz, Dietmar Riedel, Douglas T. Golenbock, Matthias Geyer, Jochen Walter, Eicke Latz, and Michael T. Heneka. 2017. 'Microglia-derived ASC specks cross-seed amyloid- β in Alzheimer's disease', *Nature*, 552: 355-61.
- Wagner, U., M. Utton, J.M. Gallo, and C.C. Miller. 1996. 'Cellular phosphorylation of tau by GSK-3 beta influences tau binding to microtubules and microtubule organisation', *Journal of Cell Science*, 109: 1537-43.
- Wang, C., Z. Wu, H. Cai, S. Xu, J. Liu, J. Jiang, H. Yao, X. Wu, and J. Xu. 2015. 'Design, synthesis, biological evaluation and docking study of 4-isochromanone hybrids bearing N-benzyl pyridinium moiety as dual binding site acetylcholinesterase inhibitors', *Bioorg Med Chem Lett*, 25: 5212-6.
- Wang, Hongquan, Yuxia Xu, Jie Yan, Xiaoyan Zhao, Xiaobo Sun, Yanping Zhang, Jingchun Guo, and Cuiqing Zhu. 2009. 'Acteoside protects human neuroblastoma SH-SY5Y cells against β -amyloid-induced cell injury', *Brain research*, 1283: 139-47.
- Wang, Jia, Chaolei Wang, Zheng Wu, Xinnan Li, Shengtao Xu, Jie Liu, Qinying Lan, Zheyang Zhu, and Jinyi Xu. 2018. 'Design, synthesis, biological evaluation, and docking study of 4-isochromanone hybrids bearing N-benzyl pyridinium moiety as dual binding site acetylcholinesterase inhibitors (part II)', *Chemical Biology & Drug Design*, 91: 756-62.
- Wang, Rui, and P. Hemachandra Reddy. 2017. 'Role of Glutamate and NMDA Receptors in Alzheimer's Disease', *J Alzheimers Dis*, 57: 1041-48.
- Wattmo, C., A. K. Wallin, E. Londos, and L. Minthon. 2011. 'Risk factors for nursing home placement in Alzheimer's disease: a longitudinal study of cognition,

- ADL, service utilization, and cholinesterase inhibitor treatment', *Gerontologist*, 51: 17-27.
- Weingarten, M. D., A. H. Lockwood, S. Y. Hwo, and M. W. Kirschner. 1975. 'A protein factor essential for microtubule assembly', *Proceedings of the National Academy of Sciences of the United States of America*, 72: 1858-62.
- Welt, T., L. Kulic, S. E. Hoey, J. McAfoose, C. Späni, A. S. Chadha, A. Fisher, and R. M. Nitsch. 2015. 'Acute Effects of Muscarinic M1 Receptor Modulation on A β PP Metabolism and Amyloid- β Levels in vivo: A Microdialysis Study', *J Alzheimers Dis*, 46: 971-82.
- Whitehouse, P. J., D. L. Price, A. W. Clark, J. T. Coyle, and M. R. DeLong. 1981. 'Alzheimer disease: evidence for selective loss of cholinergic neurons in the nucleus basalis', *Ann Neurol*, 10: 122-6.
- Wilkinson, David G., Paul T. Francis, Elias Schwam, and Jennifer Payne-Parrish. 2004. 'Cholinesterase Inhibitors Used in the Treatment of Alzheimer's Disease', *Drugs & Aging*, 21: 453-78.
- Wolff, T., and D.F. Ready. 1991. 'Cell death in normal and rough eye mutants of *Drosophila*', *Development*, 113: 825-39.
- Xia, Chenjie, Sara J. Makaretz, Christina Caso, Scott McGinnis, Stephen N. Gomperts, Jorge Sepulcre, Teresa Gomez-Isla, Bradley T. Hyman, Aaron Schultz, Neil Vasdev, Keith A. Johnson, and Bradford C. Dickerson. 2017. 'Association of In Vivo [18F]AV-1451 Tau PET Imaging Results With Cortical Atrophy and Symptoms in Typical and Atypical Alzheimer Disease', *JAMA Neurology*, 74: 427-36.
- Xu, C. Shan, Michal Januszewski, Zhiyuan Lu, Shin-ya Takemura, Kenneth J. Hayworth, Gary Huang, Kazunori Shinomiya, Jeremy Maitin-Shepard, David Ackerman, Stuart Berg, Tim Blakely, John Bogovic, Jody Clements, Tom Dolafi, Philip Hubbard, Dagmar Kainmueller, William Katz, Takashi Kawase, Khaled A. Khairy, Laramie Leavitt, Peter H. Li, Larry Lindsey, Nicole Neubarth, Donald J. Olbris, Hideo Otsuna, Eric T. Troutman, Lowell Umayam, Ting Zhao, Masayoshi Ito, Jens Goldammer, Tanya Wolff, Robert Svirskas, Philipp Schlegel, Erika R. Neace, Christopher J. Knecht, Chelsea X. Alvarado, Dennis A. Bailey, Samantha Ballinger, Jolanta A Borycz, Brandon S. Canino, Natasha Cheatham, Michael Cook, Marisa Dreher, Octave Duclos, Bryon Eubanks, Kelli Fairbanks, Samantha Finley, Nora Forknall, Audrey Francis, Gary Patrick Hopkins, Emily M. Joyce, SungJin Kim, Nicole A. Kirk, Julie Kovalyak, Shirley A. Lauchie, Alanna Lohff, Charli Maldonado, Emily A. Manley, Sari McLin, Caroline Mooney, Miatta Ndama, Omotara Ogundeyi, Nneoma Okeoma, Christopher Ordish, Nicholas Padilla, Christopher Patrick, Tyler Paterson, Elliott E. Phillips, Emily M. Phillips, Neha Rampally, Caitlin Ribeiro, Madelaine K Robertson, Jon Thomson Rymer, Sean M. Ryan, Megan Sammons, Anne K. Scott, Ashley L. Scott, Aya Shinomiya, Claire Smith, Kelsey Smith, Natalie L. Smith, Margaret A. Sobeski, Alia Suleiman, Jackie Swift, Satoko Takemura, Iris Talebi, Dorota Tarnogorska, Emily Tenshaw, Temour Tokhi, John J. Walsh, Tansy Yang, Jane Anne Horne, Feng Li, Ruchi Parekh, Patricia K. Rivlin, Vivek Jayaraman, Kei Ito, Stephan Saalfeld, Reed George, Ian Meinertzhagen, Gerald M. Rubin, Harald F. Hess, Louis K. Scheffer, Viren Jain, and Stephen M. Plaza. 2020. 'A Connectome of the Adult *Drosophila* Central Brain', *bioRxiv*: 2020.01.21.911859.
- Yan, S D, X Chen, A M Schmidt, J Brett, G Godman, Y S Zou, C W Scott, C Caputo, T Frappier, and M A Smith. 1994. 'Glycated tau protein in Alzheimer disease:

- a mechanism for induction of oxidant stress', *Proceedings of the National Academy of Sciences*, 91: 7787-91.
- Yan, Shi Du, Xi Chen, Jin Fu, Ming Chen, Huaijie Zhu, Alex Roher, Timothy Slattery, Lei Zhao, Mariko Nagashima, John Morser, Antonio Migheli, Peter Nawroth, David Stern, and Ann Marie Schmidt. 1996. 'RAGE and amyloid- β peptide neurotoxicity in Alzheimer's disease', *Nature*, 382: 685-91.
- Yoshiyama, Y., A. Kojima, C. Ishikawa, and K. Arai. 2010. 'Anti-inflammatory action of donepezil ameliorates tau pathology, synaptic loss, and neurodegeneration in a tauopathy mouse model', *J Alzheimers Dis*, 22: 295-306.
- Zhang, B., Q. Li, X. Chu, S. Sun, and S. Chen. 2016. 'Salidroside reduces tau hyperphosphorylation via up-regulating GSK-3 β phosphorylation in a tau transgenic *Drosophila* model of Alzheimer's disease', *Transl Neurodegener*, 5: 21.
- Zhang, B., Y. Wang, H. Li, R. Xiong, Z. Zhao, X. Chu, Q. Li, S. Sun, and S. Chen. 2016. 'Neuroprotective effects of salidroside through PI3K/Akt pathway activation in Alzheimer's disease models', *Drug Des Devel Ther*, 10: 1335-43.
- Zhang, Dawei, Mari Pekkanen-Mattila, Mansoureh Shahsavani, Anna Falk, Ana I. Teixeira, and Anna Herland. 2014. 'A 3D Alzheimer's disease culture model and the induction of P21-activated kinase mediated sensing in iPSC derived neurons', *Biomaterials*, 35: 1420-28.
- Zhang, Fang, Mary Gannon, Yunjia Chen, Shun Yan, Sixue Zhang, Wendy Feng, Jiahui Tao, Bingdong Sha, Zhenghui Liu, Takashi Saito, Takaomi Saido, C. Dirk Keene, Kai Jiao, Erik D. Roberson, Huaxi Xu, and Qin Wang. 2020. ' β -amyloid redirects norepinephrine signaling to activate the pathogenic GSK3 β /tau cascade', *Science Translational Medicine*, 12: eaay6931.
- Zhang, Li, Huixin Yu, Xincan Zhao, Xiufeng Lin, Chen Tan, Guoxian Cao, and Zhengwu Wang. 2010. 'Neuroprotective effects of salidroside against beta-amyloid-induced oxidative stress in SH-SY5Y human neuroblastoma cells', *Neurochem Int*, 57: 547-55.
- Zhang, Zhang, and James W. Simpkins. 2010. 'Okadaic acid induces tau phosphorylation in SH-SY5Y cells in an estrogen-preventable manner', *Brain research*, 1345: 176-81.
- Zhong, Y., A. Shobo, M. A. Hancock, and G. Multhaup. 2019. 'Label-free distribution of anti-amyloid D-AIP in *Drosophila melanogaster*: prevention of A β 42-induced toxicity without side effects in transgenic flies', *J Neurochem*, 150: 74-87.